Design of Distributed Stand-alone Power Systems using Passivity-Based Control

Rutvika Nandan Manohar

2021

Abstract

This thesis provides a general design framework for stand-alone distributed systems with DC inputs. A complete control methodology is provided to stabilize the system output voltage. Various applicable designs for stand-alone distributed systems are introduced and the mathematical tools needed to design and apply a control strategy based on the energy dynamics of the systems are provided in this dissertation. Across these applications, the results are further validated with numerical simulations which show the successful application of a feedback control regime to guarantee the stabilization of the entire distributed generation network to a desired AC or DC output voltage.

The open loop distributed network is analysed by calculating the duty ratio corresponding to the desired output voltage via steady state analysis. This allows for determination of the behaviour of the system in the absence of a feedback control. It was observed that the open loop system displays undesirable transient behaviour. A key contribution of this dissertation is to develop a control methodology that manages the behaviour of the distributed network in the event of transient changes in the system parameters. Each of the distributed networks is represented by port-controlled Hamiltonian modelling (PCHM), the characteristics of which facilitate the description of the system into well defined matrices indicating dissipation, structure and external inputs. For each distributed network, the feedback control paradigm is set with the energy shaping and damping injection framework of passivity-based control. The structural analysis through zero dynamics dictates that the system retains stability when the feedback is applied through the current through the inductor rather than the output capacitor voltage.

It was found that the feedback control methodology with PBC was successful in damping transient oscillations and achieve a fast convergence in contrast to the open loop for all distributed networks explored in this thesis. In the case of stand-alone networks with an AC output voltage, this control methodology was also used in congruence with phase locked loops to achieve phase and frequency synchronization. In addition, it was proven that PBC can be used for energy functions other than the conventional quadratic function of errors, to suit the solar array-DC/DC converter system's bifurcation characteristics. It was observed that in this case, for a system with multiple equilibrium points, PBC can drive the system to settle at the equilibrium point at a higher power output.

Acknowledgements

First and foremost, I would like to express my deepest gratitude to Prof. Takashi Hikihara of Kyoto University for his patient guidance, invaluable discussion, for pushing me to do better, introducing me to the academic world and for being a constant source of inspiration. I would also like to thank my co-supervisor Prof. Yoshiharu Omura for numerous discussions about my research as well as other general things and for his constant encouragement. I would like to thank Prof. Masayuki Kimura for his invaluable guidance as a co-supervisor and for evaluating this work. I would like to thank Ms. Yoshiko Deguchi for all the assistance she has provided to me during my stay in Japan.

I would also like to take this opportunity to thank my fellow lab mates for their support and their help with my various Japanese language related problems. They have been a family away from home. I would like to thank Mr. Fredrik Raak, Mr. Manueal Sanchez, Mr. Shiu Mochiyama as my seniors, who always guided me during the PhD. I would like to thank Ms. Toko Mannari, Mr. Kazuki Hashimoto and Mr. Songcheol Baek for their support and for tolerating my noisy sighs of exasperation in the PhD room. I would like to thank Mr. Shinya katayama and Mr. Yuma Murakawa for helping me out many times. I am grateful to Mr. Alexander Van-Brunt for helping me survive these three years with constant encouragement and invaluable discussions.

I am very grateful to the Govt. of Japan for funding my education in Kyoto University through the MEXT scholarship. I would also like to extend my thanks to Mitsubishi Electric for the research collaboration and support. It encouraged me to view my research from an industrial point of view.

Finally, I am forever grateful to Ms. Rasika Katakkar, Mr. Mathieu Fevre and to my parents, Mrs. Jyoti Manohar and Mr. Nandan Manohar for being constant pillars of support throughout my time in Japan.

Contents

Abstract **i**

Acknowledgements **iii**

Contents **v**

Acronyms **ix**

1 Introduction **1**
1.1 Distributed Generation . . . 3
1.2 Passivity-based Control . . . 4
1.2.1 Passivity in Systems . . . 4
1.2.2 Dissipative Systems . . . 5
1.2.3 Passive Systems . . . 5
1.2.4 Lyapunov's Theorem . . . 6
1.2.5 Passivity-based Control . . . 6
1.3 Port-controlled Hamiltonian Modelling . . . 7
1.4 Dissertation Objectives . . . 8
1.5 Dissertation Organization . . . 9

2 Basics of Energy Shaping with PBC for Power Converters **11**
2.1 Operating Principle of a Boost Converter . . . 11
2.2 Indirect Stabilization with Inductor Current . . . 13
2.3 PCHM for Boost Converter . . . 15
2.4 PBC for a Boost Converter . . . 16
2.5 Conclusion . . . 17

3 Passivity-based Control for Stand-alone DC/DC Ring-Coupled Converters **19**
3.1 System Design and Modelling . . . 20
3.1.1 Port-controlled Hamiltonian Modelling . . . 21
3.1.2 Steady State Equations of the System: Open Loop Analysis . . . 22
3.2 Application of Passivity-based Control . . . 24
3.2.1 Consideration of Zero Dynamics . . . 24

3.2.2 Energy Shaping in PBC . . . 26
3.3 Numerical Simulations . . . 28
3.3.1 Simulation results for a balanced system . . . 28
3.3.2 Simulation results for an unbalanced system . . . 32
3.3.3 Stabilization to non stationary state . . . 34
3.4 Conclusion . . . 35

4 Phase and Frequency Synchronization for Autonomous AC-Grid System 37
4.1 Buck-type Inverter . . . 39
4.2 System Design . . . 39
4.3 Port-controlled Hamiltonian Modelling . . . 41
4.4 Steady State Analysis : Open loop system . . . 43
4.5 Energy Shaping in PBC . . . 44
4.6 Numerical Simulations . . . 47
4.6.1 Case I: $\Delta\omega_{\mathrm{n}} = 0$, $\theta_{\mathrm{n}} = 0$ . . . 47
4.6.2 Case II: $\Delta\omega = 0$, $\theta_{in} = constant$ . . . 50
4.6.3 Case III: $\Delta\omega \neq 0$, $\theta_{\mathrm{in}} = f(t)$ . . . 53
4.7 Conclusion . . . 54

5 Design Framework for Hybrid Systems 55
5.1 Network Design . . . 55
5.2 Open Loop Controller . . . 58
5.2.1 Steady state analysis for AC Ring . . . 58
5.2.2 Steady state analysis for connection inverters . . . 59
5.2.3 Steady state analysis of DC rings . . . 60
5.3 Port-Controlled Hamiltonian Modelling . . . 60
5.4 Consideration as a network . . . 62
5.5 Application of Feedback through Passivity-based Control . . . 63
5.6 Numerical Simulations . . . 65
5.6.1 Simulation results for a balanced system . . . 65
5.6.2 Simulations for system with disturbance . . . 68
5.7 Discussions . . . 70
5.8 Conclusion . . . 72

6 Application of PBC for Multiple Equilibria 75
6.1 Dual Equilibrium Storage Function . . . 75
6.1.1 Solar Array-DC/DC Converter systems . . . 75
6.2 Design of Multistable Storage Function . . . 77
6.3 PBC for Multistable function . . . 78
6.3.1 Lyapunov Stability of Multistable Storage Function . . . 79
6.3.2 Control Equations . . . 80
6.3.3 Application of Control . . . 81

6.4 Numerical Simulations 83
6.4.1 Flow of Energy through the Ring 83
6.4.2 Application of PBC 83
6.5 Conclusion 85

7 Conclusion **87**
7.1 Conclusion 87
7.2 Future Directions 88

Bibliography **93**

Acronyms

DER	Distributed Energy Resources
PBC	Passivity-based Control
PCHM	Port Controlled Hamiltonian Modelling
DC	Direct Current
AC	Alternate Current
PCHS	Port Controlled Hamiltonian Systems
PWM	Pulse Width Modulation
LC	Inductor Capacitor
LTI	Linear Time Invariant
PLL	Phase Locked Loop
VCO	Voltage COntrolled Oscillator
LPF	Low Pass Filter
PV	Photo Voltaic
THD	Total Harmonic Distortion
CPL	Constant Power Load
IV	Current-Voltage

Chapter 1

Introduction

Renewable energy is derived from natural sources or process that are constantly replenished [1]. Such renewable sources are available abundantly, and in some capacity, everywhere on the planet [2]. Renewable generation produces electricity without the release of carbon dioxide in the atmosphere causing fewer environmental impacts [3, 4]. It also provides fuel diversification and reliable sources of power with a lower risk of fuel spills and reduced necessity for importing fuel. The global focus is thus shifting towards developing innovative methods to harness renewable energy in an increasingly cost-effective and efficient manner [5, 6]. One such method that has attracted interest of governments as well as utility companies worldwide is distributed generation [7–9]. It consists of generation and storage of electricity with the help of various distributed resources (power resources covering a large area) connected in a grid [10].

Distributed stand-alone power systems is an emerging concept wherein the generation of electricity is moved away from centralized power plants and towards individual generator units scattered over towns and villages [11]. It has been discussed widely as an alternative to solve the electrification problem of rural and remote areas by constructing small stand-alone power grids by installing renewable energy generators in multiple households [12]. Such projects have been developing under the umbrellas of local governments as well as the private sector [13, 14]. In remote rural parts of numerous developing countries in Africa and south east Asia, stand-alone systems powered by DC sources such as solar photovoltaic coupled with batteries are gaining popularity [13, 15]. In areas with abundant sunlight, they provide an effective and reliable way to power small irrigation systems as well as for lighting and household use. Towards the goal of rural electrification, various local governments are offering subsidies on installation of photo-voltaic stand-alone systems in remote areas [16, 17]. These systems consist of DC sources like solar panels and batteries that employ voltage conditioning tools like DC/DC converters and inverters to enhance the system efficiency and deliver a stable output voltage [18]. It is imperative to give attention to the control of these power electronic circuits for the design of an effective stand-alone distributed power system [19].

In the last two decades, extensive research has been dedicated to devising control techniques to implement power conditioning, maintain system stability and regulate the

output voltage [20]. To ensure stable operation of a distributed generation system, there is a growing need for a control method which will be able to incorporate the diverse nature of renewable energy resources and increase operational flexibility [21]. As power electronics devices are physical devices that can be mathematically modelled as controlled dynamic systems, it allows for their state variables to be controlled by the application of various control theories [22]. A relatively recent control strategy that has been proposed by [23] for the stabilization of the output voltage of DC/DC converters is passivity-based control (PBC).

PBC was introduced first in [24] to define a control methodology whose objective was to render the closed loop passive. This control method was first employed for the adaptive control of robot manipulators [25]. The energy-shaping plus damping injection methodology used to solve state feedback set point regulation problems in fully actuated robotic systems by Takegaki and Arimoto, has evolved into today's 'passivity-based control' [26]. Along with mechanical systems, this approach is now used to stabilize and control an array of systems that are described by Euler Lagrange or Hamiltonian equations [24]. PBC arises from the theory of passive systems where energy stored in the system is always less than the energy supplied to the system from outside [27]. PBC is applied to passive systems and is performed in two stages. The first stage is the shaping of the potential energy of the system such that the potential energy function has a global and unique minimum at the desired equilibrium. The second stage is to add damping to make the system exponentially stable [24]. Port-controlled Hamiltonian modelling (PCHM) is an indispensable tool for applying PBC to electrical systems that have switching elements and dissipation [28]. It facilitates the description of the system to well defined matrices indicating dissipation, structure and external inputs to the system.

The objective of this thesis is to provide a general design framework for distributed stand-alone systems with DC inputs, and provide a complete control methodology to stabilize the system output voltage. The purpose of this study is to introduce various applicable designs of distributed generation stand-alone systems and to provide the mathematical tools needed to design and apply a control strategy based on energy dynamics. The application of PBC for DC/DC converters was shown in [23]. The application of PBC for parallely connected DC/DC converters was described in detail in [29]. Based on these works, this study extends the application of PBC to three different kinds of stand-alone networks. Firstly, a DC output distributed stand-alone network with multiple DC/DC boost converters connected in a ring formulation is analysed. Extending the scope of this design, a more practical stand-alone network with DC inputs and multiple inverters to obtain AC outputs was introduced. For the AC system, along with stabilization of the output voltages of individual inverters, grid synchronization is a crucial task. The application of PBC with phase-locked loop was shown to be successful to obtain a stable AC output voltage. Integrating these two ideas, a hybrid (DC-AC) stand-alone network is designed. The idea behind this network framework is to introduce a hybrid DC-AC network feasible for small, remotely located areas with stand-alone DC grids, in the vicinity of larger towns requiring a functional AC connection. Finally, based on the conventional application of PBC, we focus on the energy function and tailor it to suit the character-

istics of the system in consideration. This is accomplished for a ring coupled converter system having solar arrays as DC inputs. The current voltage (IV) characteristics for the solar array-DC/DC system as given by [30] are studied and the energy function in PBC is modified to have multiple equilibria to accommodate the system characteristics.

1.1 Distributed Generation

The current model for the generation of electricity, conventional as well as renewable, is through the centralized power plants, requiring transmission and distribution system from the centre to the outlying consumers [31]. The substations are located 10s to 100s of miles away, causing heavy transmission losses [32]. Apart from the energy loss, the construction of a transmission system is a mammoth task, especially for remotely located areas in developing countries [33]. Many of these issues can be solved by distributed generation with renewable energy sources. Distributed generation is defined as the decentralized generation of electricity through small generators located near the end user or the consumer. Distributed generation may serve as a single structure or may be a part of a micro-grid (a smaller grid that is also tied into the larger electricity delivery system), such as at a major industrial facility, a military base, or a large college campus. Distributed generation with renewable resources helps in the supply of clean energy while reducing the distribution and transmission losses. Distributed generation typically employs small photo-voltaic power systems, small wind generators, batteries and diesel generators.

Global distributed energy resource (DER) capacity is expected to grow from 132.4 GW in 2017 to 528.4 GW in 2026 [34]. The introduction of new technology has resulted in the price reduction of solar panels, wind energy, energy from waste and other DER [35]. This in turn has led to the economic viability of DERs and consequently distributed generation has been projected to grow their share in the energy market [36]. There is an increasing interest in decentralised management of DERs due to expected associated risks for over-voltage, under-voltage and grid congestion caused by the penetration of distributed generation. Thus, integration of the distributed energy resources into the grid, and the development of stand-alone microgrids is becoming a widely researched topic.

Stand-alone power systems, which is also referred to as remote-area power supply, is an off-grid electricity system meant for areas that have not yet been included in the traditional utility network [37]. These primarily include remote areas in developing nations, not yet included in the existing distribution network. In remote areas it is more effective to build a off-grid distribution network powered by small generators, typically solar photovoltaic, small wind turbines, and small hydro-power systems depending on the availability in the area. In remote areas, stand-alone systems are proving to be more cost-effective than extending power lines from centralized power plants (which can range from $15,000-$50,000 per mile) [38]. Even though stand-alone distributed generation is an upcoming technology with numerous benefits, it faces various issues such as non-linear loads, voltage instability, output voltage synchronization and fatal transients [11, 14].

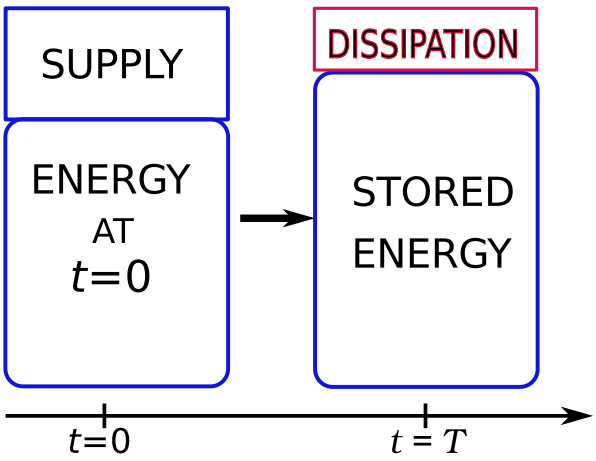

Figure 1.1: Passivity in systems

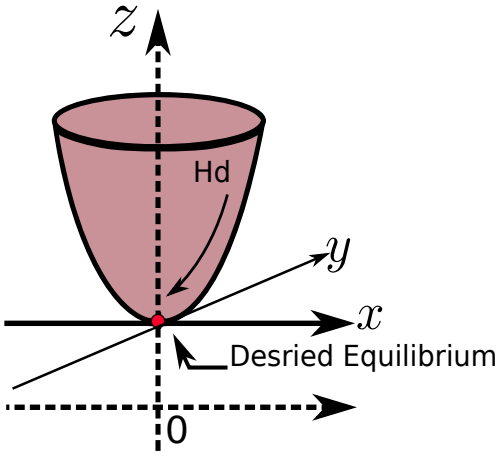

Figure 1.2: Passivity in systems

1.2 Passivity-based Control

1.2.1 Passivity in Systems

Passive systems are a class of dynamical systems in which the energy exchanged with the environment plays a central role. In passive systems the rate at which energy flows in the system is less than or equal to the energy that is supplied from outside. This implies that a passive system cannot store more energy than is supplied to it [24]. Passivity theory is one of the important theories in nonlinear control theories since 1970s. It has also been seen as in important tool for modelling and controlling interconnected systems. The interconnection of passive systems retains the property of passivity [27]. Passivity

is also used in designing various robust control methods. Dissipativity is another basic concept needed in defining passive systems.

The concept of passive systems was first developed in [39] in the context of electrical circuits. If an electrical circuit consists of only passive elements, i.e. resistors, inductors, and capacitors, then it cannot generate energy. The framework of dissipative systems was later developed in [40]. This framework helps to understand the concepts of passive systems and passivity-based control from a dynamical systems point of view.

1.2.2 Dissipative Systems

Consider a system described by Eq. (1.1).

$$\begin{aligned} \frac{\mathrm{d}\boldsymbol{x}}{\mathrm{d}t} &= f(\boldsymbol{x}, \boldsymbol{u}) \\ y &= h(\boldsymbol{x}, \boldsymbol{u}) \end{aligned} \tag{1.1}$$

Here, $\boldsymbol{x} \in X \subset \mathbb{R}^n$, $\boldsymbol{u} \in U \subset \mathbb{R}^m$, $\boldsymbol{y} \in Y \subset \mathbb{R}^m$ are the state, input, and output variables. X, U, and Y are state, input, and output spaces respectively. This system is a dissipative system if there exists a non-negative real function $S(\boldsymbol{x})$, called the storage function (more often than not, it is the energy of the system), such that, for all time $t_1 \geq t_0 \geq 0, \boldsymbol{x_0} \in X \subset \mathbb{R}^n, \boldsymbol{u} \in U \subset \mathbb{R}^m$,

$$S(\boldsymbol{x}) - S(\boldsymbol{x}_0) \leq \int_{t_0}^{t_1} w(t)dt \ , \tag{1.2}$$

where $w(t)$ is the supply rate, a function of the input $\boldsymbol{u}$ and the output $\boldsymbol{y}$. Here the expression $\boldsymbol{x}(t) = \phi(t, t_0, \boldsymbol{x}_0, \boldsymbol{u})$ is used to denote the state at time t reached from initial state $\boldsymbol{x}_0$ at t_0. To put it simply, a dissipative system is the one in which the stored energy is always less than the energy supplied to the system, thus it 'dissipates' energy [27]. Diagrammatic representation of dissipativity in systems is given by Fig. 1.1.

1.2.3 Passive Systems

A passive system is a dissipative system for which the supply rate is a function of the input and output as given by Eq. (1.3) [27, 39].

$$w(\boldsymbol{u}(t), \boldsymbol{y}(t)) = \boldsymbol{u}^{\mathrm{T}}(t)\boldsymbol{y}(t) \tag{1.3}$$

Thus passive systems are systems in which the product of the port variables has units of power, e.g. in case of electrical circuits they are current and voltage [41]. As passive systems come under dissipative systems, passive systems cannot store more energy than is supplied from outside. The difference between the stored and the supplied energy is the dissipated energy.

1.2.4 Lyapunov's Theorem

Stability of the solutions of differential equations describing a dynamical system can be given by a Lyapunov stability criteria [42]. Likewise, to test for the stability of passive systems, the Lyapunov stability criteria is employed.

For a system $\dot{\boldsymbol{x}} = f(\boldsymbol{x})$, having an equilibrium $\boldsymbol{x} = \boldsymbol{x}^*$, consider a function $v(\boldsymbol{x}) : \mathbb{R}^n \rightarrow \mathbb{R}$ with the following three conditions.

(a) $V(\boldsymbol{x}^*) = 0$

(b) $V(\boldsymbol{x}) > 0 \; for \; \boldsymbol{x} \neq \boldsymbol{x}^*$

(c) $\dot{V}(\boldsymbol{x}) \leq 0 \; for \; all \; \boldsymbol{x} \neq 0$

If the first two criteria are satisfied, i.e. $V(\boldsymbol{x})$ is a locally positive definite function, then it is a Lyapunov function. If all three conditions are satisfied, the system is Lyapunov stable. If $\dot{V}(\boldsymbol{x}) < 0$ then the system is asymptotically stable [43]. This determines local stability. For global stability, another property of radial unboundedness has to be satisfied. The function $V(x)$ is analogous to a potential function.

1.2.5 Passivity-based Control

Passivity-based control (PBC) is a method which brings the system to the desired equilibrium state by shaping the energy characteristics of the system. It is done in two steps i.e. energy shaping and damping injection. Energy shaping implies the design of a new 'desired' energy function which has a minimum at the desired equilibrium. The first step entails modifying the potential energy function of the system in such a way that the newly modified energy function has a minimum at the the desired equilibrium. Energy shaping in PBC is represented in Fig. 1.2. The modified storage function has to be shown to be a candidate of a Lyapunov function. The second step is the damping injection stage, where appropriate damping is added to the system to ensure asymptotic stability [44].

Passivity-based control has been traditionally applied to Euler-Lagrange systems [24]. Here, the energy shaping stage accomplishes shaping of the potential energy and keeping the original kinetic energy to satisfy the passivation objective. Addition of the damping reinforces the property of output strict passivity, thus giving asymptotic stability. Lyapunov stability can be confirmed from the input-output stability properties from the output strictly passive map [24].

Thus, a given system needs to be modeled as Hamiltonian or Euler-Lagrange systems of equations for the application of PBC. For electronic systems which consists of non-energy elements like dissipation through resistance and switching elements, Lagrangian formulation is difficult or at times impossible to implement [24]. For systems like these, the kinetic as well as potential energy of the system need to be modified to design a storage function. Considering these resctrictions, instead of Euler-Lagrange modelling, PCHM is used to achieve better results with PBC. The modified storage function has to be shown

to be a candidate of a Lyapunov function. The second step is the damping injection where appropriate damping is added to the system to ensure asymptotic stability [44].

1.3 Port-controlled Hamiltonian Modelling

The concept of energy shaping, formulation of a 'desired' energy function, and making it suitable to be used as a Lyapunov function were introduced in [45]. This lead to the development of a passivity-based control (PBC). For the application of PBC, it is first necessary to model the system mathematically [46]. Generalized Hamiltonian modelling is applied in the case of lossless nonlinear systems with elements that keep the traditional canonical form [24] . In case of electrical systems with resistances and switiching elements, the system is no longer lossless and switching implies a inherent change in the structure of the circuit [44]. In such cases, generalized Hamiltonian modelling is difficult or sometimes even impossible to implement [47].

It is desirable to shape the total energy of the electrical system while considering the physical structure. Port-controlled Hamiltonian modelling (PCHM) is the network representation of systems in interaction with their environment [48, 49]. These systems are called as port-controlled Hamiltonian systems (PCHS). PCHM captures the energy balancing features of the system. It classifies the system neatly into physically well defined interconnection ($\mathbf{J}$), dissipation ($\mathbf{R}$) and external input ($\mathbf{E}$) matrices within a state space framework [24]. The system model using the port-controlled Hamiltonian (PCH) framework is given by Eq. (5.22) and is in the form given in [47].

$$\begin{aligned} \dot{\boldsymbol{x}} &= [\mathbf{J} - \mathbf{R}]\frac{\partial H}{\partial \boldsymbol{x}} + g(\boldsymbol{x})\boldsymbol{u} \\ \boldsymbol{y} &= g^{\mathrm{T}}(\boldsymbol{x})\frac{\partial H}{\partial \boldsymbol{x}} \end{aligned} \tag{1.4}$$

Here, $\boldsymbol{x}$ is a matrix of system variables with dimensions $n \times 1$. $\mathbf{J}$ is the $n \times n$ interconnection matrix satisfying $\mathbf{J}(\boldsymbol{x}) = -\mathbf{J}^{\mathrm{T}}(\boldsymbol{x})$. $\mathbf{R}$ is the dissipation matrix consisting of all the dissipation elements in the system. $\mathbf{R}$ which is a $n \times n$ matrix satisfies $\mathbf{R}(\boldsymbol{x}) = \mathbf{R}^{\mathrm{T}}(\boldsymbol{x})$. $\boldsymbol{u}$ is the input matrix with size $n \times 1$. $\boldsymbol{y}$ is the output of the system. H is the Hamiltonian of the system, which, in this case, is the total energy of the system. In equations described by PCHM the control is applied through the interconnection structure. For example, for a system consisting switching devices, the duty ratio will be included in the interconnection structure.

The energy balance of PCHS can be given by Eq. (1.5). This equation is obtained after evaluating the rate of change of energy.

$$\frac{\mathrm{d}H}{\mathrm{d}t} = -\left[\frac{\partial H}{\partial \boldsymbol{x}}(\boldsymbol{x})\right]\mathbf{R}(\boldsymbol{x})\frac{\partial H}{\partial \boldsymbol{x}}(\boldsymbol{x}) + \boldsymbol{u}^{\mathrm{T}}\boldsymbol{y} \leq \boldsymbol{u}(t)^{\mathrm{T}}\boldsymbol{y}(y) \tag{1.5}$$

Here, the first term represents the dissipation rate (non-positive) due to the dissipative elements like resistances. Thus after integrating Eq. (1.5), the energy balance of the system

can be obtained.

$$\int_0^t \boldsymbol{u}^{\mathrm{T}}(s)\boldsymbol{y}(s)\mathrm{d}s = H[\boldsymbol{x}(t)] - H[\boldsymbol{x}(0)] + \int_0^t \left[\frac{\partial H}{\partial \boldsymbol{x}}[\boldsymbol{x}(s)]\right]^{\mathrm{T}} \mathbf{R}[\boldsymbol{x}(s)]\frac{\partial H}{\partial \boldsymbol{x}}[\boldsymbol{x}(s)]\mathrm{d}s \tag{1.6}$$

In Eq. (1.6), the first term denotes the energy supplied from outside, the second term, the stored energy, and the third term, the dissipated energy (from Eq. (1.5)). It is clear that this equation holds for all $t \geq 0$, so that energy function $H(\boldsymbol{x})$ is bounded from below. The energy balance shows that when a system is modeled with PCH, it retains the property of passivity, given in Eq. (1.3) and Eq. (1.2).

It is thus verified that the system cannot hold more energy than is supplied to it, and the difference between the two is the energy that is dissipated. With Eq. (1.7), it can be understood that any system modeled with PCHM satisfies the property of passivity.

$$\frac{\mathrm{d}H}{\mathrm{d}t} \leq \boldsymbol{u}^{\mathrm{T}}(t)\boldsymbol{y}(t) \tag{1.7}$$

1.4 Dissertation Objectives

The dissertation aims to provide a comprehensive design for stand-alone distributed generation systems with DC inputs. The following are the main tasks performed in this dissertation.

- Circuit design of different types of distributed generation system with DC inputs. These include the stand-alone DC output system, stand-alone AC output system and the hybrid system consisting of both AC and DC systems.

- Proposing a averaged dynamical circuit model described with a system of differential equations and using the port-controlled Hamiltonian modelling to organize the system of equations in matrices neatly describing the structure, inputs and dissipation in the aforementioned stand-alone distributed generation networks.

- Analyse the structural properties of the network to recognize the minimum phase nature of the desired method of feedback to design the control equations through PBC.

- Prove that the shaped energy function for the application of PBC is a candidate of Lyapunov function.

- Formulate a method to stabilize the state variables to a desired state through a feedback control focussing on the energy characteristics of the system (PBC).

- To verify the application of PBC under a variety of conditions with numerical simulations.

- To study the application of PBC for a storage functions other than the conventional quadratic function of errors by proving the Lyapunov stability for the double well potential function.

- To verify with numerical simulation the application of PBC with a dual equilibrium function.

1.5 Dissertation Organization

The thesis is organized as follows. Chapter 2 reviews the application of passivity-based control for a DC/DC boost converter. After the review of the operating principle, the first step is the formulation of the dynamic state model of the converter. The study of the structural properties of the boost converter is an important preliminary step to recognize that PBC applied with feedback through the inductor current guarantees stability, rather than the conventional feedback through the capacitor voltage. The next step is the modelling of the state equations with PCH framework as an indispensable tool for the application of PBC. Finally this chapter reviews the details of the energy shaping and damping injection PBC for a boost converter. This provides a foundation to generalise the application of PBC for more complex networks of converters and inverters as pursued in the later chapters.

Chapter 3 introduces the basic ring-coupled DC network. Here, multiple DC resources with as many DC/DC boost converters are connected in a ring-coupled configuration. This chapter will delve in the design of the circuit as well as the structural stability through zero dynamics before going into details about the steady state analysis and PCHM of the entire network. A control rule with PBC is formulated after proving the Lyapunov stability of the selected desired energy function. Finally, the the effectiveness of PBC is verified through numerical simulations.

Chapter 4 deals introduces an AC output ring coupled network with multiple DC inputs connected to as many buck-type inverters. The buck-type inverter has a H-bridge at the input the invert the polarity to obtain the negative component of the AC output voltage. In order to maintain the stability of the network, synchronization of all the AC outputs is essential. To maintain the phase and frequency synchronization, PLLs are employed in congruence with PBC.

Chapter 5 turns towards a more practical extension of Chapter 2 and Chapter 3, introducing a hybrid network with DC as well as AC outputs. The hybrid network consists of a main AC output ring of multiple inverters connected to multiple DC rings. The network modelling of the system as a whole is discussed. Here, importance of the structure matrix for system extension and analysis of the vulnerable nodes is explored.

Finally, the application of PBC with multiple equilibria for a system of solar arrays and DC/DC converters is investigated in Chapter 6. After examining the bifurcation characteristics of the solar panel-DC/DC converter system, an dual-equilibrium energy function is designed as the desired function. Behaviour of the ring coupled network to

drive the system to the equilibrium with the higher power is studied in detail.

Chapter 7 is the conclusion of the PhD dissertation and indicates the potential future directions of the research presented herein.

Chapter 2

Basics of Energy Shaping with PBC for Power Converters

This chapter introduces the dynamic model of DC-DC boost converter based on Kirchoff's current and Kirchoff's voltage laws. Here, the differential equations of the circuit model are derived for the different switch positions. These derived model equations are combined into a single set of equations parameterized by the switch position function whose value must be co-incide and have the numerical value of either 0 or 1. That is, the numerical values given to the switch function are in the binary set $\{0, 1\}$. This switch model can be interpreted as the 'averaged switch model' with the switching function taking values on the real interval $[0, 1]$. The averaged model discussed below can be used in conjugation with PWM. It will be shown that the averaged model satisfies the energy-balance equation for passive systems. This establishes that the property of 'passivity' for the DC/DC boost converter. Besides this fundamental property, the boost converter also has some structural properties that need to be considered for the application of PBC. This chapter lays out the procedure to obtain the port-controlled Hamiltonian modelling for the boost converter. Taking into consideration the structural properties, PBC is applied with indirect stabilization through the inductor current.

2.1 Operating Principle of a Boost Converter

DC/DC converters are electronic circuits that regulate the flow of energy between two DC systems [50]. A boost converter is a type of DC/DC converter that converts the input voltage to a higher value. At the same time, the current becomes lower while keeping the power between the input and the output. That is, the output voltage of a boost converter is always greater than the input voltage. The circuit diagram of a boost converter is shown in Fig. 2.1.

The boost converter includes two switches, a diode and a controllable transistor switch. When the switch is ON, the diode is reversed biased, thus isolating the output stage. At this time, the input supplies energy to the inductor. When the switch is OFF, the output

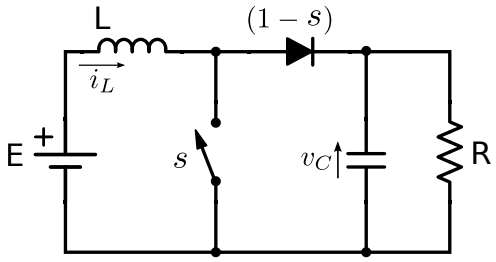

Figure 2.1: Schematic of a boost converter

stage receives energy from the input as well as the inductor [51]. The diode and transistor switch are assumed to be ideal elements, i.e. the transistor has an infinitely fast response and the diode has 0 V threshold voltage. This assumption will be valid throughout this thesis.

The dynamics of a boost converter are formulated in equations based on Kirchhoff's laws in each one of the circuit topologies. The first circuit topology is obtained when the switch position is set to take the numerical value $s = 1$ as shown in Fig. 2.2. In the second topology, the switch takes the numerical value $s = 0$ shown in Fig. 2.3.

When the switch is ON, i.e. $s = 1$, the equations are given by Eq. (2.1).

$$\begin{cases} L\dfrac{\mathrm{d}i_L}{\mathrm{d}t} & = E \\ \\ C\dfrac{\mathrm{d}v_C}{\mathrm{d}t} & = -\dfrac{v}{R} \end{cases} \tag{2.1}$$

When the switch is OFF, i.e. $s = 0$, the equations are as given in Eq. (2.2).

$$\begin{cases} L\dfrac{\mathrm{d}i_L}{\mathrm{d}t} & = -v_C + E \\ \\ C\dfrac{\mathrm{d}v_C}{\mathrm{d}t} & = i_L - \dfrac{v_C}{R} \end{cases} \tag{2.2}$$

Combining these equations, the dynamics of a boost converter are given by Eq. (2.3).

$$\begin{cases} L\dfrac{\mathrm{d}i_L}{\mathrm{d}t} & = -(1-s)v_C + E \\ \\ C\dfrac{\mathrm{d}v_C}{\mathrm{d}t} & = (1-s)i_L - \dfrac{v_C}{R} \end{cases} \tag{2.3}$$

These equations consider the switch position to be either OFF or ON ($s = 0$ or $s = 1$). As the switching is done with PWM or other such methods, if the switching is sufficiently fast, the switching is replaced by averaged states with averaged duty ratio μ between 0 and 1. The averaged model for the boost converter is introduced by replacing s with μ .

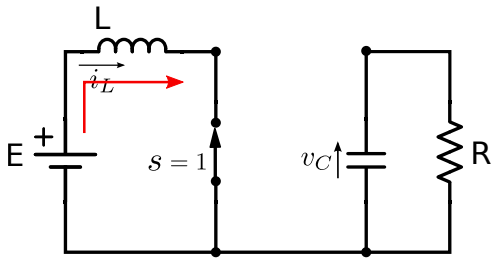

Figure 2.2: Effective circuit for boost converter when switch is ON

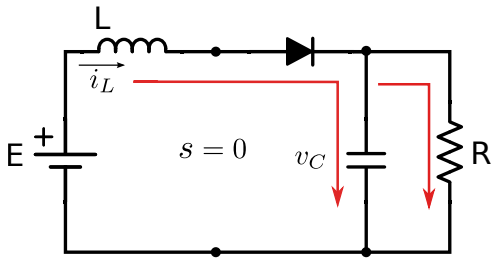

Figure 2.3: Effective circuit for boost converter when switch is OFF

2.2 Indirect Stabilization with Inductor Current

Some structural properties of DC/DC converters have to be taken into consideration before designing PBC. Eq. (2.4) is obtained by eliminating i_L from Eq. (2.3).

$$\ddot{v}_C + \left(\frac{1}{RC} + \frac{\dot{\mu}}{1-\mu}\right) + \frac{1}{LC}\left[(1-\mu)^2) + \frac{L}{R}\frac{\dot{\mu}}{1-\mu}\right]v_C = (1-\mu)\frac{E}{LC} \tag{2.4}$$

The dynamics at an equilibrium point $v_C = v_{Cd}$ are obtained by setting the derivatives to zero. Then the duty ratio μ is obtained by Eq. (2.5).

$$\dot{\mu} = \frac{R(1-\mu)^2}{Lv_{Cd}}\left[E - (1-\mu)v_{Cd}\right] \tag{2.5}$$

The equilibrium points of this equation are given by Eq. (2.6)

$$\mu = 1 \quad ; \quad \mu = 1 - \frac{E}{v_{Cd}} \tag{2.6}$$

Among these, the second one has physical significance. If $v_{Cd} > E$, it is confirmed that the output voltage will always be higher than the input of the converter. However, the phase diagram describes this equilibrium point as unstable, making the system non-minimum phase with respect to the output voltage. This is shown in Fig. 3.4.

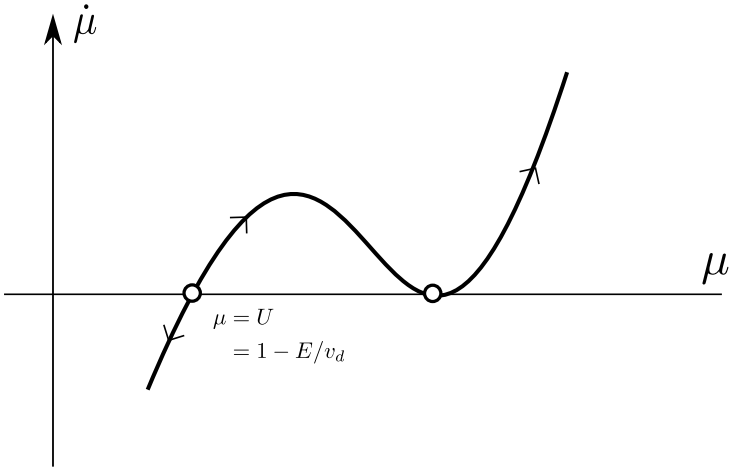

Figure 2.4: Zero dynamics corresponding to constant output voltage

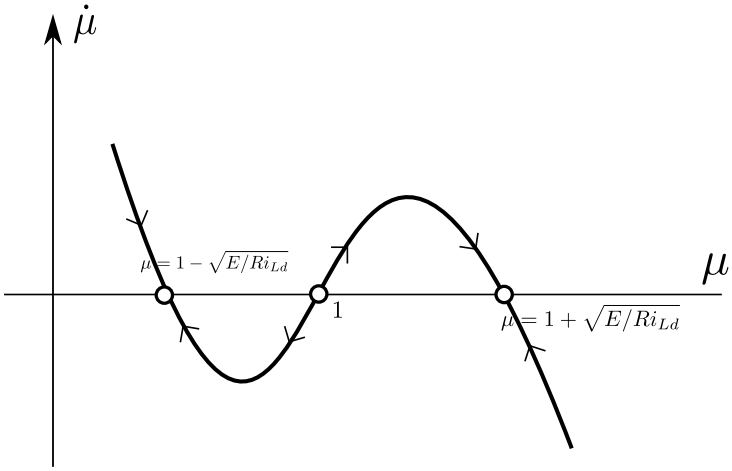

Figure 2.5: Zero dynamics corresponding to constant inductor current

Next, the structural properties of the boost converter with respect to the inductor current will be considered. Writing the boost converter equations in terms of the inductor current, we get Eq. (2.7).

$$\dddot{i}_L + \left(\frac{1}{RC} + \frac{\dot{\mu}}{1-\mu}\right)\ddot{i}_L + \left[(1-\mu)^2\frac{1}{LC}\right]\dot{i}_L = \frac{E}{L}\left(\frac{1}{RC}\frac{\dot{\mu}}{1-\mu}\right) \tag{2.7}$$

Considering the zero dynamics, i.e. by setting the derivatives at zero, for an equilibrium point $i_L = i_{Ld}$, μ takes the following values.

$$\mu = 1; \quad \mu = 1 - \sqrt{\frac{E}{Ri_{Ld}}}; \quad \mu = 1 + \sqrt{\frac{E}{Ri_{Ld}}} \tag{2.8}$$

Plotting the phase diagram of these equilibrium points as given by Fig. 3.3, it is seen that the equilibrium point $\mu = 1 - \sqrt{E/Ri_{Ld}}$ is stable, as long as $Ri_{Ld} > E$. This

again emphasizes the properties of the boost converter, making the system controlled with inductor current a minimum phase system. The inductor current will be used to stabilize the system rather than the output capacitor voltage.

2.3 PCHM for Boost Converter

The Hamiltonian approach allows for the systematic modelling of electrical systems including resistors and switching elements. These non-energetic terms are extracted from the circuit. This leaves the energy conserving LC circuit. These non-energy elements are then introduced into the circuit in the form of 'ports' [48]. This configuration of the LC circuits with ports are represented as a generalized Hamiltonian system with external input variables. This technique is used when modelling DC/DC converters, to allow for the inclusion of power electronic switches and load resistances [29].

The energy of the capacitor plays the role of potential energy and the energy of the inductor plays the role of kinetic energy [44]. These are given by Eqs. (2.9) and (2.10) respectively. U denotes the potential energy and T, the kinetic energy. The total energy is the sum of the kinetic and potential energy and is given by Eq. (2.11). The total energy function is a candidate Hamiltonian function.

$$U = \frac{1}{2} C v_C^2 \tag{2.9}$$

$$T = \frac{1}{2} L i_L^2 \tag{2.10}$$

$$H = \frac{1}{2} C v_C^2 + \frac{1}{2} L i_L^2 \tag{2.11}$$

Considering $\boldsymbol{x}$ as the state vector, consisting of inductor current and capacitance voltage, the total energy is given by Eq. (2.12). Here, $\mathbf{D}$ is a diagonal matrix of inductance and capacitance values corresponding to the current and voltage in $\boldsymbol{x}$.

$$H = \frac{1}{2} [i_L, v_C]^{\mathrm{T}} \begin{bmatrix} L & 0 \\ 0 & C \end{bmatrix} \begin{bmatrix} i_L \\ v_C \end{bmatrix} = \frac{1}{2} \boldsymbol{x}^{\mathrm{T}} \mathbf{D} \boldsymbol{x} \tag{2.12}$$

Eq. (2.3) is obtained by extracting the non energy elements, and representing them as external ports. Thus, the structure of the system is denoted in a separate matrix and so are the dissipation elements. The boost converter equations (Eq. (2.3)) are written in the form of PCH equations (Eq. (5.22)) as given in Eq. (2.13).

$$\begin{bmatrix} L & 0 \\ 0 & C \end{bmatrix} \begin{bmatrix} \dot{i}_L \\ \dot{v}_C \end{bmatrix} = \begin{bmatrix} 0 & -(1-\mu) \\ (1-\mu) & 0 \end{bmatrix} \begin{bmatrix} i_L \\ v_C \end{bmatrix} - \begin{bmatrix} 0 & 0 \\ 0 & R \end{bmatrix} \begin{bmatrix} i_L \\ v_C \end{bmatrix} + \begin{bmatrix} 1 \\ 0 \end{bmatrix} E \tag{2.13}$$

As is seen, the interconnection matrix is skew symmetric and the dissipation matrix is symmetric, and μ denotes the averaged duty ratio. It is obvious from Eq. (2.13) that $\mathbf{J}$ is a function of the duty ratio μ. Hereon, we shall consider $\mathbf{J} = \mathbf{J}(\mu)$. With this, the modelling of a boost converter with PCHM was accomplished.

2.4 PBC for a Boost Converter

With the averaged model of boost converter represented as a port-controlled Hamiltonian system, it is possible to apply passivity-based control. Let us consider the generalized model of the boost converter in the form given by Eq. (2.14) [44].

$$\mathbf{D}\dot{\boldsymbol{x}}(t) = [\mathbf{J}(\mu) - \mathbf{R}]\frac{\partial H}{\partial x} + \mathbf{E} \tag{2.14}$$

Here, $\boldsymbol{x}$ denotes a matrix of system variables consisting of the inductor currents and the capacitance voltages. $\mathbf{J}$ denotes the interconnection matrix and $\mathbf{R}$ denotes the dissipation matrix. The control objective is to follow the desired state trajectory, given by $\boldsymbol{x}^*(t)$. This vector represents the desired values of inductor current and capacitor voltage. We start by choosing a Lyapunov function which preserves the energy characteristics of the system, i.e. the quadratic function of errors. This function is given in Eq. (2.15).

$$H_d = \frac{1}{2}\mathbf{e}^{\mathrm{T}}\mathbf{D}\mathbf{e}, \quad \mathbf{e} = \boldsymbol{x}(t) - \boldsymbol{x}^*(t) \tag{2.15}$$

First, it is necessary to prove that the storage function (H_d) is a candidate of Lyapunov function. By taking the derivative of this function, Eq. (2.17) is obtained.

$$\dot{H}_d = (\boldsymbol{x} - \boldsymbol{x}^*(t))^{\mathrm{T}}\mathbf{D}(\dot{\boldsymbol{x}} - \dot{\boldsymbol{x}}^*(t)) \tag{2.16}$$

$$= (\boldsymbol{x} - \boldsymbol{x}^*(t))^{\mathrm{T}}([\mathbf{J} - \mathbf{R}]\boldsymbol{x} + \mathbf{E} - \mathbf{D}\dot{\boldsymbol{x}}^*(t)) \tag{2.17}$$

By setting the term $\mathbf{D}\dot{\boldsymbol{x}}^*(t)$ as given in Eq. (5.24), the control rule with PBC for boost converters can be formulated.

$$\mathbf{D}\dot{\boldsymbol{x}}^*(t) = (\mathbf{J} - \mathbf{R})\boldsymbol{x}^*(t) + \mathbf{E} + \mathbf{R}_I(\boldsymbol{x} - \boldsymbol{x}^*(t)) \tag{2.18}$$

In Eq. (5.24), $\mathbf{R}_I$ is a symmetric, positively defined matrix which acts as the damping injection, making the system asymptotically stable if $\mathbf{R} + \mathbf{R}_I > 0$. By considering that $\boldsymbol{e}^T\mathbf{J}(\mu)\boldsymbol{e} = 0$ for all values of μ, we get the following condition on the derivative of our chosen Lyapunov function $H_d(\boldsymbol{e})$.

$$\dot{H}_d = \boldsymbol{e}^T(\mathbf{J}(\mu)\boldsymbol{e} - \mathbf{R})\boldsymbol{e} - \mathbf{R}_I\boldsymbol{e} = -\boldsymbol{e}^T(\mathbf{R} + \mathbf{R}_I)\boldsymbol{e} < 0 \tag{2.19}$$

The error $\boldsymbol{e}$ has the origin as the asymptotically stable equilibrium. By satisfying the condition $(\mathbf{R} + \mathbf{R}_I) > 0$, the system becomes exponentially asymptotically stable at the equilibrium point [43]. The derivative of H_d is given in Eq. (3.25).

$$\dot{H}_d(\boldsymbol{e}) = -\boldsymbol{e}^T(\mathbf{R} + \mathbf{R}_I)\boldsymbol{e} \leq -kH_d(\boldsymbol{e}) \tag{2.20}$$

Thus, according to Lyapunov's Theorem, the equilibrium state $\boldsymbol{x}^*$ is asymptotically stable with the control rule given in Eq. (5.24), and exponentially asymptotically stable with the damping injection.

The boost converter equations, written in the form of Eq. (5.24), are given in Eq. (2.21).

$$\begin{bmatrix} L & 0 \\ 0 & C \end{bmatrix} \begin{bmatrix} \dot{i}_{Ld} \\ \dot{v}_{Cd} \end{bmatrix} = \begin{bmatrix} 0 & -(1-u) \\ (1-u) & 0 \end{bmatrix} \begin{bmatrix} i_{Ld} \\ v_{Cd} \end{bmatrix} - \begin{bmatrix} 0 & 0 \\ 0 & R \end{bmatrix} \begin{bmatrix} i_L \\ v_C \end{bmatrix} + \begin{bmatrix} 1 \\ 0 \end{bmatrix} E - \begin{bmatrix} R_1 & 0 \\ 0 & 0 \end{bmatrix} \begin{bmatrix} i_L - i_{Ld} \\ v_C - v_{Cd} \end{bmatrix} \quad (2.21)$$

Here, i_{Ld} is the desired inductor current and v_{Cd} is the desired voltage state, and R_1 is the term in the damping injection matrix R_I. Thus the controller is obtained by solving Eq. (2.21) for the duty ratio, which is the control parameter in Eq. (2.22).

$$\begin{cases} \mu = \dfrac{1}{v_{Cd}} \big[E + R_1 (i_L - i_{Ld}) \big] + 1 \\ \\ C \dot{v}_{Cd} = (1-\mu) i_{Ld} - \left[\dfrac{v_{Cd}}{R} \right] \end{cases} \quad (2.22)$$

The direct output stabilization zero dynamics do not allow for stability in the neighbourhood of the equilibrium point [22, 24]. Thus, indirect control is chosen for the boost converter. Instead of having a constant value for the desired voltage v_{Cd}, it is favourable to have a constant value of the inductor current i_{Ld}.

2.5 Conclusion

This chapter served as an introduction to the ideas that will be explored further in the thesis. Firstly, the definitions of key concepts that will be used in this thesis were explained. These are the concepts of passivity, dissipativity, Lyapunov stability and, PCHM. The boost converter was introduced and was modelled using PCHM. This chapter discussed the structural properties of the boost converter and their effect on the stability properties. Finally, energy shaping for PBC was employed for the boost converter successfully.

Chapter 3

Passivity-based Control for Stand-alone DC/DC Ring-Coupled Converters

Power converters are seen as an important interface to transfer electricity from renewable sources of energy into the power network. Towards designing a distributed generation system,which is autonomous from the conventional power grid, we propose a DC/DC converter system with DC power sources connected in a ring formulation and coupled with dissipation. Ring formulation is proposed to represent one of the ways to realize distributed autonomous systems in small residential areas [52]. The basic idea of such an 'autonomous distributed generation system' is illustrated in Fig. 3.1. This configuration is useful in harnessing energy from DC sources of electricity like solar cells, batteries, fuel cells, and so on.

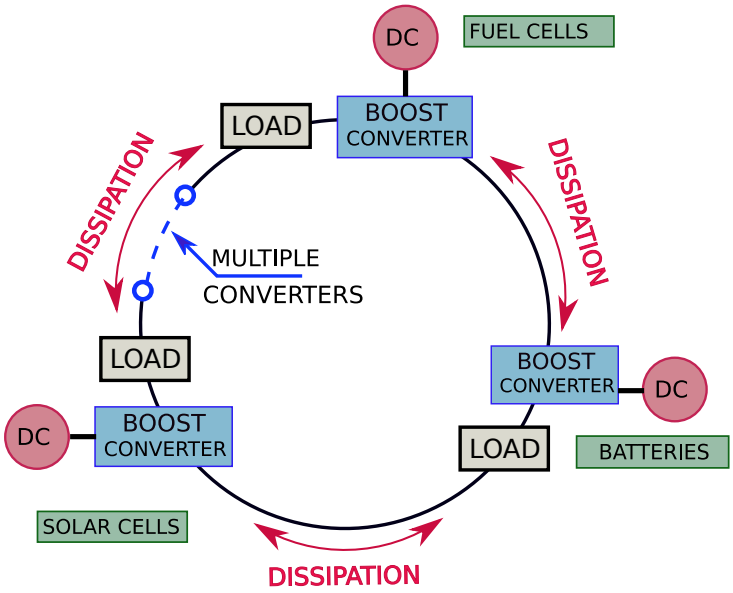

Figure 3.1: System Configuration

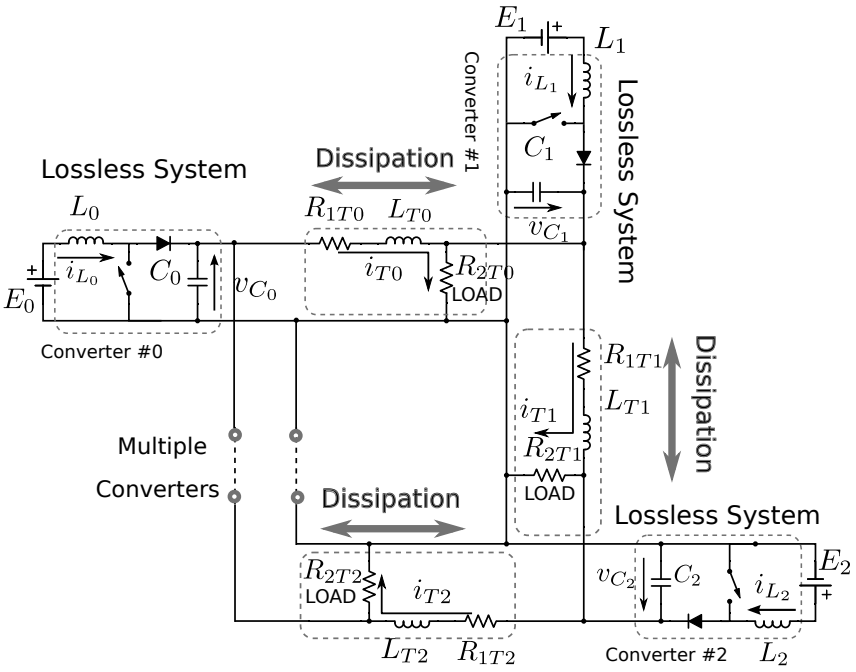

Figure 3.2: Schematic diagram of ring coupled converters.

3.1 System Design and Modelling

For a ring-coupled converter system introduced in this chapter, it is confirmed that the converters keep the property of passivity, individually. In addition, the feedback control is employed with minimizing the energy function of the entire system, as opposed to the individual function of a single DC/DC converter. The energy transfer between the individual converter units governs the dynamic behaviour of the whole ring coupled system. The application of PBC, with 'energy shaping' of the entire system, manifests the property of robustness despite the flow of energy between individual elements. We introduce a system consisting of multiple boost converters with multiple DC input sources. These converters are coupled together with dissipation through inductance and resistance. The coupling through dissipation represents a transmission line model, with inductive and resistive elements [53]. The basic configuration is shown in Fig. 3.1.

The schematic diagram of the circuit is shown in Fig. 3.2. The coupled converters are responsible for the constant voltage output in the ring. Here, load resistances($R_{2T\mathrm{n}}$) are across the output voltages, where as the dissipation elements of line inductor ($L_{T\mathrm{n}}$) and line resistance ($R_{1T\mathrm{n}}$) are in series. The capacitor in the transmission line model is considered as negligible. This is owing to the fact that a parallel capacitor is dominant in the boost converter configuration. The number of converters was set such that it enhances the asymmetry of the system. The number of converters in the ring does not cause any loss of generality. The objective is to apply PBC to the whole system, including the dissipation between the converters.

The system equations are given by Eqs.(3.1)-(3.3). Subscription n denotes the index of the converter. u_{n} denotes the switch position for the #n converter. $u_{\mathrm{n}} = 1$ implies that the switch is ON and $u_{\mathrm{n}} = 0$, that it is OFF. $L_{T\mathrm{n}}$ is the inductance and $R_{1T\mathrm{n}}$ is the dissipation between the #n and #n + 1 converter.

$$L_{\mathrm{n}}\dot{i}_{L\mathrm{n}} = -(1-u_{\mathrm{n}})v_{C\mathrm{n}} + E_{\mathrm{n}} \tag{3.1}$$

$$C_{\mathrm{n}}\dot{v}_{C\mathrm{n}} = (1-u_{\mathrm{n}})i_{L\mathrm{n}} - i_{T\mathrm{n}} + i_{T(\mathrm{n}-1)} - \frac{v_{C\mathrm{n}}}{R_{2T(\mathrm{n}-1)}} \tag{3.2}$$

$$L_{T\mathrm{n}}\dot{i}_{T\mathrm{n}} = v_{C\mathrm{n}} - v_{C(\mathrm{n}+1)} - R_{1T\mathrm{n}}i_{T\mathrm{n}} \tag{3.3}$$

Here, the dot notation represents differentiation with respect to time.

3.1.1 Port-controlled Hamiltonian Modelling

Port-controlled Hamiltonian modeling (PCHM) is the network representation of systems in interaction with their environment [48]. The Hamiltonian approach allows for the systematic modelling of electrical systems including resistors and switching elements. The non-energetic terms are extracted from the circuit. It leaves the energy conserving LC circuit. The non-energy elements are then introduced into the circuit in the form of 'ports' [48]. Such configuration of LC circuits with ports is represented as a generalized Hamiltonian system with external input variables. PCHM technique is used for modeling DC/DC converters was shown in Chapter 2. The same technique will be used to model the distributed generation DC system presented in this chapter.

PCHM classifies the system neatly into physically well defined interconnection ($\mathbf{J}$), dissipation ($\mathbf{R}$) and external input ($\mathbf{E}$) matrices within a state space framework [24]. The system model using the Port Controlled Hamiltonian(PCH) framework is given by Eq.(5.22) as in the form given in [47].

$$\mathbf{D}\dot{\boldsymbol{x}}(t) = [\mathbf{J} - \mathbf{R}]\frac{\partial H}{\partial x} + \mathbf{E} \tag{3.4}$$

For m converters in the configuration, $\boldsymbol{x}$, the state of the system, is a column matrix ((m $\times$ 3) $\times$ 1) of all the inductor currents and capacitance voltages. The matrix $\mathbf{D}$ is a diagonal matrix of the capacitances and inductances of the corresponding currents and voltages. $\mathbf{J}$ gives the interconnection, and $\mathbf{R}$ the dissipation in the system. The interconnection is a function of u_{n}, the switch position of the corresponding boost converters in the ring configuration. $\mathbf{E}$, the input matrix is a column matrix of the input voltages to the respective converters. H is the Hamiltonian, which, in this case, is a quadratic function of $\boldsymbol{x}$, given as $H = \frac{1}{2}\boldsymbol{x}^T\mathbf{A}\boldsymbol{x}$, where $\mathbf{A} = \mathrm{I}_{\mathrm{n}}$.

$$\mathbf{D} = \begin{bmatrix} \mathbf{D}_0 & 0 & \dots & 0 \\ 0 & \mathbf{D}_1 & \dots & 0 \\ \vdots & \vdots & \ddots & \vdots \\ 0 & 0 & \dots & \mathbf{D}_{\mathrm{m}} \end{bmatrix} \mathbf{D}_{\mathrm{n}} \begin{bmatrix} L_{\mathrm{n}} & 0 & 0 \\ 0 & C_{\mathrm{n}} & 0 \\ 0 & 0 & L_{T\mathrm{n}} \end{bmatrix} \tag{3.5}$$

$$\boldsymbol{x} = \begin{bmatrix} \boldsymbol{x}_0 \\ \vdots \\ \boldsymbol{x}_{\mathrm{m}} \end{bmatrix} \quad \boldsymbol{x}_{\mathrm{n}} = \begin{bmatrix} i_{L\mathrm{n}} \\ v_{C\mathrm{n}} \\ i_{T\mathrm{n}} \end{bmatrix} \tag{3.6}$$

$$\mathbf{J} = \begin{bmatrix} \mathbf{A}_0 & -\mathbf{B}^T & 0 & \dots & 0 & \mathbf{B} \\ \mathbf{B} & \mathbf{A}_1 & -\mathbf{B}^T & 0 & \dots & 0 \\ 0 & \mathbf{B} & \ddots & \ddots & \ddots & \vdots \\ \vdots & 0 & \ddots & \ddots & \ddots & 0 \\ 0 & \vdots & \ddots & \ddots & \ddots & -\mathbf{B}^T \\ -\mathbf{B}^T & 0 & \dots & 0 & \mathbf{B} & \mathbf{A}_{\mathrm{m}} \end{bmatrix} \tag{3.7}$$

$$\text{Here, } \mathbf{A}_{\mathrm{n}} = \begin{bmatrix} 0 & -(1-u_{\mathrm{n}}) & 0 \\ (1-u_{\mathrm{n}}) & 0 & -1 \\ 0 & 1 & 0 \end{bmatrix}, \mathbf{B} = \begin{bmatrix} 0 & 0 & 0 \\ 0 & 0 & 1 \\ 0 & 0 & 0 \end{bmatrix} \tag{3.8}$$

$$\mathbf{R} = \begin{bmatrix} \mathbf{R}_0 & 0 & \dots & 0 \\ 0 & \mathbf{R}_1 & \dots & 0 \\ \vdots & \vdots & \ddots & \vdots \\ 0 & 0 & \dots & \mathbf{R}_{\mathrm{m}} \end{bmatrix} \quad \mathbf{R}_{\mathrm{n}} = \begin{bmatrix} 0 & 0 & 0 \\ 0 & \dfrac{1}{R_{2T\mathrm{n}}} & 0 \\ 0 & 0 & R_{1T\mathrm{n}} \end{bmatrix} \tag{3.9}$$

$$\mathbf{E} = \begin{bmatrix} \mathbf{E}_0 \\ \vdots \\ \mathbf{E}_{\mathrm{m}} \end{bmatrix} \quad \mathbf{E}_{\mathrm{n}} = \begin{bmatrix} E_{\mathrm{n}} \\ 0 \\ 0 \end{bmatrix} \tag{3.10}$$

Looking at the adjacency matrix of the interconnection matrix ($\mathbf{J}$), the ring coupled structure is clearly verified. It is seen that $\mathbf{D}$ is a diagonal matrix and $\mathbf{R}$ is a symmetric matrix for m converters. The matrix $\mathbf{J}$ is the interconnection matrix, and shows the coupling between neighbouring converters through dissipation. From Eq.(4.9), it can be verified that $\mathbf{J}$ is a skew-symmetric matrix, with keeping the PCHM structure [47].

3.1.2 Steady State Equations of the System: Open Loop Analysis

Till now the switched model for boost converters, given by [22, 51] has been considered. The control objective is to regulate the average output voltage to a constant reference (e.g DC/DC converters) or a periodic value with frequency much smaller than the switching frequency (inverters). Thus, it is desirable to consider the average value of the voltages

and currents rather than the instantaneous values, given that the ripple and harmonics are sufficiently small.

The averaging of the circuit implies the extracting the DC components of the circuit variables as well as the switching function which governs the switch position. In order to obtain the averaged model of the switching function, we replace the switch position u_{n} in the instantaneous circuit with a modulating signal μ_{n} through averaging. A pulse width modulation (PWM) policy is implemented for switch regulation for the converters. PWM is a method for generating a digital pulse signal to drive the transistor switches in the boost converter circuit from a continuous control input or a modulating signal. If the modulating signal varies slowly in comparison to the switching frequency, it can be shown that the switching function is equal to the modulating signal [51]. As all the other components in the circuit are linear time invariant (LTI), they can be just replaced by their average values without any change of relationship. The only modification necessary is the replacement of the switching function with the modulating signal for the PWM, which will be referred to as the duty ratio. Here after, in this chapter, the state variables $i_{L\mathrm{n}}$, $i_{T\mathrm{n}}$, $v_{C\mathrm{n}}$ will be considered the average values of the instantaneous variables, and μ_{n} as the duty ratio.

Before the application feedback control through PBC, the steady state analysis is provided to gain insight in the open loop system. It is desirable to establish the relationship between the equilibrium values of the average output voltage, the average input current, and the average dissipation current. This analysis provides the constant duty ratios $\mu_{\mathrm{n}} = U_{\mathrm{n}}$ for all the converters, to be implemented to obtain the open loop system. It is clear from Eqs.(3.1)-(3.3) that the equilibrium values of the state variables are given by Eqs.(3.11)-(3.13).

$$\begin{aligned}\bar{i}_{L\mathrm{n}} = &\frac{E_{\mathrm{n}}}{R_{2T(\mathrm{n}-1)}(1-U_{\mathrm{n}})^2} + \frac{1}{R_{1T\mathrm{n}}}\left[\frac{E_{\mathrm{n}}}{(1-U_{\mathrm{n}})^2} - \frac{E_{(\mathrm{n}+1)}}{(1-U_{\mathrm{n}+1})(1-U_{\mathrm{n}})}\right] \\ &- \frac{1}{R_{1T(\mathrm{n}-1)}}\left[\frac{E_{(\mathrm{n}-1)}}{(1-U_{(\mathrm{n}-1)})(1-U_{\mathrm{n}})} - \frac{E_{\mathrm{n}}}{(1-U_{\mathrm{n}})^2}\right]\end{aligned} \tag{3.11}$$

$$\bar{v}_{C\mathrm{n}} = \frac{E_{\mathrm{n}}}{(1-U_{\mathrm{n}})} \tag{3.12}$$

$$\bar{i}_{T_{\mathrm{n}}} = \frac{1}{R_{1T\mathrm{n}}}\left[\frac{E_{\mathrm{n}}}{(1-U_{\mathrm{n}})} - \frac{E_{(\mathrm{n}+1)}}{(1-U_{(\mathrm{n}+1)})}\right] \tag{3.13}$$

Here, $\bar{i}_{L\mathrm{n}}$ denotes steady state inductor current, $\bar{v}_{C\mathrm{n}}$ the steady state output voltage, and $\bar{i}_{T\mathrm{n}}$ the steady state dissipation current for converter #n.

The desired output voltage v_C^* decides the duty ratio. In other words, the duty ratio is used to keep the output in the ring at $\bar{v}_{C\mathrm{n}} = v_C^*$ for all m converters. This is an open loop system. The next section gives the estimation of the open loop system for comparing

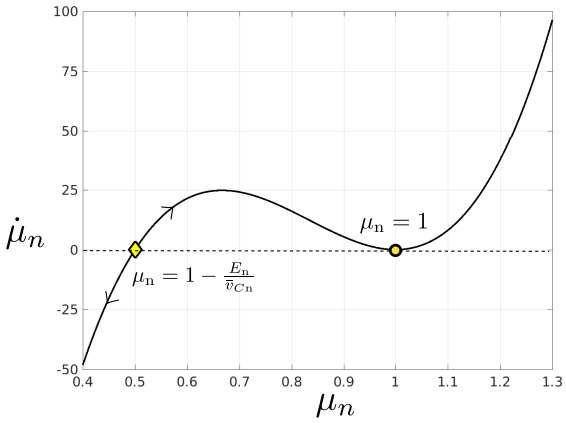

Figure 3.3: Zero dynamics of ring coupled converter system corresponding average output capacitor voltage.

to the results with closed loop system with PBC.

3.2 Application of Passivity-based Control

The control objective for the ring coupled converter system is to regulate the output voltage of the ring towards a desired equilibrium value through faster convergence with a feedback control. First we analyse the structural dynamics of the system and then stabilize the system with a feedback control.

3.2.1 Consideration of Zero Dynamics

In this section we consider the analysis of the averaged ring coupled converter system through to the zero dynamics at the equilibrium points. Zero dynamics are defined as the dynamics that characterizes the internal behaviour of the system once the initial conditions and inputs are chosen, such that the output is identically zero [54]. Here, we consider the 'zero dynamics' associated with the equilibrium points given for the output as the capacitor voltage and the inductor current respectively.

Firstly, the output voltage of the capacitor is regarded as the output of the averaged PWM model of the ring coupled system. Rewriting the equations given by Eqs.(3.1)-(3.3) in terms of $v_{C\rm n}$ the following relation is obtained.

$$C_{\mathrm{n}}\ddot{v}_{C\mathrm{n}} = -\dot{\mu}_{\mathrm{n}} i_{L\mathrm{n}} + (1-\mu_{\mathrm{n}})\dot{i}_{L\mathrm{n}} - \dot{i}_{T\mathrm{n}} + \dot{i}_{T\mathrm{n}} - \frac{\dot{v}_{C\mathrm{n}}}{R_{2T(\mathrm{n}-1)}} \tag{3.14}$$

$$= \frac{-\dot{\mu}_{\mathrm{n}}}{(1-\mu_{\mathrm{n}})}\left[C_{\mathrm{n}}\dot{v}_{C\mathrm{n}} + i_{T\mathrm{n}} - i_{T(\mathrm{n}-1)} + \frac{v_{C\mathrm{n}}}{R_{1T\mathrm{n}}}\right]$$

$$+ \frac{(1-\mu_{\mathrm{n}})}{L_{\mathrm{n}}}\left[E_{\mathrm{n}} - (1-\mu_{\mathrm{n}})\right] - (\dot{i}_{T\mathrm{n}} - \dot{i}_{T(\mathrm{n}-1)}) - \frac{\dot{v}_{C\mathrm{n}}}{R_{2T(\mathrm{n}-1)}} \tag{3.15}$$

The objective for the zero dynamics is to choose the control variable μ_{n} so as to keep the output voltage as well as the dissipation current constrained as: $v_{C\mathrm{n}} = \bar{v}_{C\mathrm{n}}$, $i_{T\mathrm{n}} = \bar{i}_{T\mathrm{n}}$. Then, it can be conferred that $\ddot{v}_C = 0$ and $\dot{v}_{C\mathrm{n}} = 0$ as well as $\dot{i}_{T\mathrm{n}} = 0$ and $\dot{i}_{T(\mathrm{n}-1)} = 0$. Thus, the output is fixed but the control is not, and hence $\dot{\mu}_{\mathrm{n}} \neq 0$. Then, the following relationship is held.

$$\dot{\mu}_{\mathrm{n}} = \frac{(1-\mu_{\mathrm{n}})^2}{L_{\mathrm{n}}[(\bar{i}_{T\mathrm{n}} - \bar{i}_{T(\mathrm{n}-1)}) + \bar{v}_{C\mathrm{n}}/R_{2T(\mathrm{n}-1)}]}\left[E_{\mathrm{n}} - (1-\mu_{\mathrm{n}})\bar{v}_{C\mathrm{n}}\right] \tag{3.16}$$

The equilibrium points of Eq.(3.16) are given at $\mu_{\mathrm{n}} = 1 - E_{\mathrm{n}}/\bar{v}_{C\mathrm{n}}$ and $\mu_{\mathrm{n}} = 1$. Among them, the first has physical significance. If $\bar{v}_{C\mathrm{n}} > E_{\mathrm{n}}$, it is confirmed that the output will be always higher than the input of the converter. However, the phase diagram describes this equilibrium point as unstable, making the system non-minimum phase with respect to the output voltage. The phase diagram is drawn by Fig. 3.3 in accordance with the parameters given in Table. 3.1. Such analysis is possible for single boost converter in [22] and [24].

Next, the analysis of the system corresponding to the zero dynamics with the inductor current as the output of the averaged PWM model is carried out. Rewriting the equations given by Eqs.(3.1)-(3.3) in terms of $i_{L\mathrm{n}}$ the following equation is obtained.

$$L_{\mathrm{n}}\ddot{i}_{L\mathrm{n}} = \dot{\mu}_{\mathrm{n}}\left[\frac{E_{\mathrm{n}} - L_{\mathrm{n}}\dot{i}_{L\mathrm{n}}}{(1-\mu_{\mathrm{n}})}\right] - \frac{(1-\mu_{\mathrm{n}})}{L_{\mathrm{n}}C_{\mathrm{n}}}\left[(1-\mu_{\mathrm{n}})i_{L\mathrm{n}} - i_{T\mathrm{n}} + i_{T(\mathrm{n}-1)} - \frac{E_{\mathrm{n}} - L_{\mathrm{n}}\dot{i}_{L\mathrm{n}}}{(1-\mu_{\mathrm{n}})R_{2T(\mathrm{n}-1)}}\right] \tag{3.17}$$

Same as above, the control variable μ_{n} can be chosen so as to keep the output at a constant value $i_{L\mathrm{n}} = \bar{i}_{L\mathrm{n}}$ which implies that $i_{T\mathrm{n}} = \bar{i}_{T\mathrm{n}}$. It follows that $\ddot{i}_{L\mathrm{n}} = 0$ and $\dot{i}_{L\mathrm{n}} = 0$. The remaining dynamics related to the control variable, i.e the duty ratio μ_{n} are described by Eq.(3.18).

$$n \tag{3.18}$$

The three equilibrium points, $\{\mu_{\mathrm{n,i}}\}_{i=1,2,3}$, corresponding to Eq.(3.18) are obtained as Eq.(3.19).

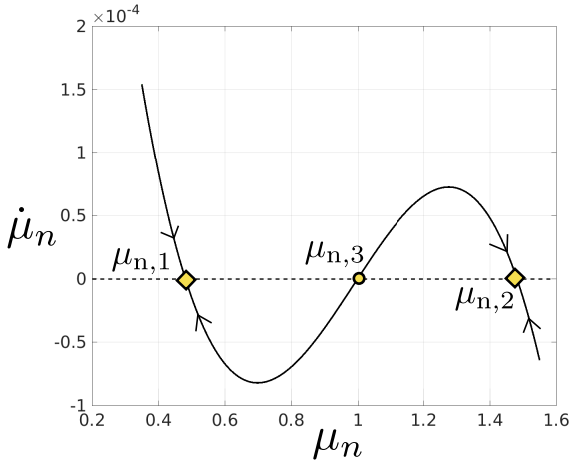

Figure 3.4: Zero dynamics of ring coupled converter system corresponding to average of output inductor current.

$$\mu_{\mathrm{n},1} = 1 - \frac{(\bar{i}_{T\mathrm{n}} - \bar{i}_{T(\mathrm{n}-1)})}{2\bar{i}_{L\mathrm{n}}} - \sqrt{\frac{E_{\mathrm{n}}}{R_{2T(\mathrm{n}-1)} i_{L\mathrm{n}}} - \left[\frac{(\bar{i}_{T\mathrm{n}} - \bar{i}_{T(\mathrm{n}-1)})^2}{4(\bar{i}_{L\mathrm{n}})^2}\right]}$$

$$\mu_{\mathrm{n},2} = 1 - \frac{(\bar{i}_{T\mathrm{n}} - \bar{i}_{T(\mathrm{n}-1)})}{2\bar{i}_{L\mathrm{n}}} + \sqrt{\frac{E_{\mathrm{n}}}{R_{2T(\mathrm{n}-1)} i_{L\mathrm{n}}} - \left[\frac{(\bar{i}_{T\mathrm{n}} - \bar{i}_{T(\mathrm{n}-1)})^2}{4(\bar{i}_{L\mathrm{n}})^2}\right]}$$

$$\mu_{\mathrm{n},3} = 1 \tag{3.19}$$

As $(\bar{i}_{T\mathrm{n}} - \bar{i}_{T(\mathrm{n}-1)})$ is sufficiently small, we can safely neglect it in the squared terms. It can also be established that $(\bar{i}_{T\mathrm{n}} - \bar{i}_{T(\mathrm{n}-1)})/2\bar{i}_{L\mathrm{n}} << \sqrt{E_{\mathrm{n}}/R_{2T\mathrm{n}}}$. Thus, only one equilibrium point satisfies the condition of $0 \leq \mu_{\mathrm{n}} \leq 1$ and is of physical significance. All the equilibrium points are given by Fig. 3.4, in accordance with the parameters specified in Table. 3.1 . It is seen that this equilibrium point is stable, as long as $R_{2T\mathrm{n}}\bar{i}_{L\mathrm{n}} > E_{\mathrm{n}}$. This again emphasizes the properties of the boost converter, making the system controlled with inductor current a minimum phase system. The inductor current will be used to stabilize the system rather than the output capacitor voltage.

3.2.2 Energy Shaping in PBC

We investigate wether it is possible for PBC to be applied to a system of multiple converters coupled with dissipation. The stored energy of a circuit is the sum of the energy in the passive elements, that is the inductors and capacitors. The energy of the multiple converter system is given by Eq.(4.16).

$$H = \frac{1}{2}\boldsymbol{x}^T \mathbf{D} \boldsymbol{x} \tag{3.20}$$

$\boldsymbol{x}$ and $\mathbf{D}$ are as given in Eqs.(4.8) and (3.5), respectively. H, which is the total energy, consisting of the kinetic energy through the inductor and the potential energy stored in the capacitor.

The desired energy function is designed based on the total energy of the system. The formulation is taken to be the quadratic function of errors. It is given by Eq.(4.17).

$$H_d = \frac{1}{2}\boldsymbol{e}^T\mathbf{D}\boldsymbol{e}, \quad \boldsymbol{e} = \boldsymbol{x} - \boldsymbol{x}_d \tag{3.21}$$

Here, $\boldsymbol{x_d} = [\boldsymbol{x}_{1d}\ \boldsymbol{x}_{2d} \ldots \boldsymbol{x}_{\mathrm{md}}]^T$ is the desired trajectory of the state. $\boldsymbol{x}_{\mathrm{nd}} = [\bar{i}_{Ln}\ v_{Cnd}\ i_{Tnd}]^T$, where $\bar{i}_{Ln}$ is a constant, $v_{Cnd}(t)$ and $i_{Tnd}(t)$ are the desired output voltage and line currents. In order to prove that the function given in Eq.(4.17) is a candidate of Lyapunov function, let us check the derivative of the energy function as in Eq.(3.22).

$$\begin{aligned}\dot{H}_d &= (\boldsymbol{x} - \boldsymbol{x}_d(t))^T\mathbf{D}(\dot{\boldsymbol{x}} - \dot{\boldsymbol{x}}_d(t)) \\ &= (\boldsymbol{x} - \boldsymbol{x}_d(t))^T([\mathbf{J} - \mathbf{R}]\boldsymbol{x} + \mathbf{E} - \mathbf{D}\dot{\boldsymbol{x}}_d(t))\end{aligned} \tag{3.22}$$

By setting the term $\mathbf{D}\dot{\boldsymbol{x}}_d(t)$ as given in Eq.(5.24), the control rule with PBC can be formulated for boost converters.

$$\mathbf{D}\dot{\boldsymbol{x}}_d(t) = (\mathbf{J} - \mathbf{R})\boldsymbol{x}_d(t) + \mathbf{E} + \mathbf{R}_I(\boldsymbol{x} - \boldsymbol{x}_d(t)) \tag{3.23}$$

Where, $\mathbf{R}_I$ is a symmetric and positively defined matrix, which acts as the damping injection, making the system asymptotically stable if $\mathbf{R} + \mathbf{R}_I > 0$. The damping is added via the controller, thus helping to determine the duty ratio after feedback. The damping injection compliments the dissipation of the original system [44]. By considering that $\boldsymbol{e}^T\mathbf{J}(\mu)\boldsymbol{e} = 0$ for all values of μ, we obtain the following condition on the derivative of our chosen Lyapunov function $H_d(\boldsymbol{e})$.

$$\dot{H}_d(e) = \boldsymbol{e}^T(\mathbf{J}(\mu)\boldsymbol{e} - \mathbf{R}\boldsymbol{e} - \mathbf{R}_I\boldsymbol{e}) = -\boldsymbol{e}^T(\mathbf{R} + \mathbf{R}_I)\boldsymbol{e} < 0 \tag{3.24}$$

Under the control rule, the error $\boldsymbol{e}$ converges to the origin asymptotically. By satisfying the condition $(\mathbf{R} + \mathbf{R}_I) > 0$, the system becomes exponentially and asymptotically stable at the equilibrium point [43]. Then, the derivative of $H_d(e)$ is given in Eq.(3.25).

$$\dot{H}_d(\boldsymbol{e}) = -\boldsymbol{e}^T(\mathbf{R} + \mathbf{R}_I)\boldsymbol{e} \leq -kH_d(\boldsymbol{e}) \tag{3.25}$$

Hence, it is proved that Lyapunov's Theorem is satisfied. That is, the equilibrium state $\boldsymbol{x}_d$ is asymptotically stable with the control rule given in Eq.(5.24), and exponentially asymptotically stable with the damping injection. $\mathbf{R}_I$ is given in Eq.(4.18). The damping injection is a diagonal matrix of the damping matrices. The damping matrix for the #n converter in the system is represented by $\mathbf{R}_{I\mathrm{n}}$

$$\mathbf{R}_I = \begin{bmatrix} \mathbf{R}_{I0} & 0 & \ldots & 0 \\ 0 & \mathbf{R}_{I1} & \ldots & 0 \\ \vdots & \vdots & \ddots & \vdots \\ 0 & 0 & \ldots & \mathbf{R}_{I\mathrm{m}} \end{bmatrix}, \text{ where } \mathbf{R}_{I\mathrm{n}} = \begin{bmatrix} R_{\mathrm{n}} & 0 & 0 \\ 0 & 0 & 0 \\ 0 & 0 & 0 \end{bmatrix}. \tag{3.26}$$

Then, the control equation is obtained for the given system in Eq.(3.27). The boost converter is controlled with inductor current keeping the minimum phase nature as given by the zero dynamics. The constant desired inductor current ($\bar{i}_{L\mathrm{n}}$) is obtained by solving the steady state Eq.(3.11).

$$\mu_{\mathrm{n}} = \frac{1}{v_{C\mathrm{n}d}}\big[E_{\mathrm{n}} + R_{\mathrm{n}}(i_{L\mathrm{n}} - \bar{i}_{L\mathrm{n}})\big] + 1 \tag{3.27}$$

$$C_{\mathrm{n}}\dot{v}_{C\mathrm{n}d} = (1-\mu_{\mathrm{n}})\bar{i}_{L\mathrm{n}} - i_{T_{\mathrm{n}d}} + i_{T(\mathrm{n}-1)d} - \big[\frac{v_{C\mathrm{n}d}}{R_{2T(\mathrm{n}-1)}}\big] \tag{3.28}$$

$$L_{T_{\mathrm{n}}}\dot{i}_{T\mathrm{n}d} = v_{C\mathrm{n}d} - v_{C((\mathrm{n}+1))d} - R_{1T\mathrm{n}}i_{T\mathrm{n}d} \tag{3.29}$$

The value of the duty ratio μ_{n} is evaluated at every instant t depending on the input, the parameters, and the desired output of the system. That is, μ_{n} depends on time and the state. Hereafter, when PBC is applied to the system, $\mu_{\mathrm{n}}(t)$ is considered as a function of time.

3.3 Numerical Simulations

The desired voltage is set as $\bar{v}_{C\mathrm{n}}$. The duty ratio for open loop system (U_{n}) without feedback control is given by Eq.(3.12). For feedback through PBC, via Eqs.(3.11)-(3.13), the associated desired current $\bar{i}_{L\mathrm{n}}$ is calculated. From this, the corresponding desired trajectory $\boldsymbol{x}_d(t)$ is calculated by solving Eqs.(3.27)- (3.29). When the operator wants to set a desired voltage, only the current via the duty ratio is directly controllable. Hence it is necessary to convert the problem of obtaining the desired voltage, into a control problem of the current. Consequently, in the transient dynamics, the desired voltage, $v_{C\mathrm{n}d}$, will remain fluctuating around $\bar{v}_{C\mathrm{n}}$.

The simulation results obtained for five converters coupled in a ring form are given in this section. The numerical simulations were carried out on ode45 solver Simulink (Version 8.7 R2016a).

3.3.1 Simulation results for a balanced system

Parameters in the ring coupled converter system are set at the same values respectively. This is a balanced case. Additionally, the dissipation between the converters ($L_{T\mathrm{n}}, R_{1T\mathrm{n}}$) as well as the inputs E_{n} are also set at same values for all the converters. This naturally creates an energy balance in the ring. To begin with, numerical simulations are performed for the open loop balanced system without applying any feedback control. The duty cycle was set at a constant value (U_{n}). This value is calculated by Eq.(3.12) for a particular $\bar{v}_C$. Thus, any disturbance in the system will not be acted on but will affect the system output adversely. The parameters for simulation are given in Table. 3.1. Fig. 3.5 shows

Table 3.1: Parameters for Balanced System

Parameter	Value	Unit
E_{n}	15	V
L_{n}	46	mH
C_{n}	100	μF
$L_{T\mathrm{n}}$	15	mH
$R_{1T\mathrm{n}}$	100	Ω
$R_{2T\mathrm{n}}$	170	Ω
$\bar{v}_{C\mathrm{n}}$	40	V

Table 3.2: Different Input Voltages

Parameter	Value	Unit
E_{0-4}	15,13,12,13,15	V
L_{n}	46	mH
C_{n}	100	μF
$L_{T\mathrm{n}}$	15	mH
$R_{1T\mathrm{n}}$	100	Ω
$R_{2T\mathrm{n}}$	170	Ω
$\bar{v}_{C\mathrm{n}}$	40	V

Table 3.3: Different Load Resistances

Parameter	Value	Unit
E_{0-4}	15	V
L_{n}	46	mH
C_{n}	100	μF
$L_{T\mathrm{n}}$	15	mH
$R_{1T\mathrm{n}}$	100	Ω
R_{2T0-4}	130,170,140,170,130	Ω
$\bar{v}_{C\mathrm{n}}$	40	V

the inductor current, dissipation current, output voltage, and duty cycle with respect to time. In the transient, the output voltage and the inductor current shows the transient oscillations. After the transient, the system reaches an equilibrium. The equilibrium value of the output voltage becomes equal to $\bar{v}_C$. As all the boost converters have same inputs and same parameter values, no current flows through the dissipation.

Next we look at simulations results when PBC is applied. PBC results in an output dynamic feedback controller which induces a shaped closed loop energy and enhances the closed loop damping of the system. The damping has the condition $\mathbf{R} + \mathbf{R}_I > 0$. It was set and kept at $\mathbf{R}_{I1} = 15$ for all the simulations. The results, for a balanced case, show faster response and damped oscillations. Feedback is provided by solving Eq.(3.27) to obtain the appropriate duty cycle value to maintain the desired equilibrium voltage. Here, the inductor current is the variable that is measured to provide feedback. The numerical simulation results are shown in Fig. 3.6.

The simulation parameters are set as given in Table. 3.1. Comparing Fig. 3.6 with Fig. 3.5, it is seen that the transient is sufficiently dampened. The time to stabilize the system to the equilibrium is also significantly faster. As all the parameters are the same for all boost converter systems as well as the dissipation, the trajectories on the output voltage and inductor current plane coincide for all five converters. The asymptotic behaviour is clearly observed with a phase plot on the energy sets of H_d. This is shown in Fig. 3.7.

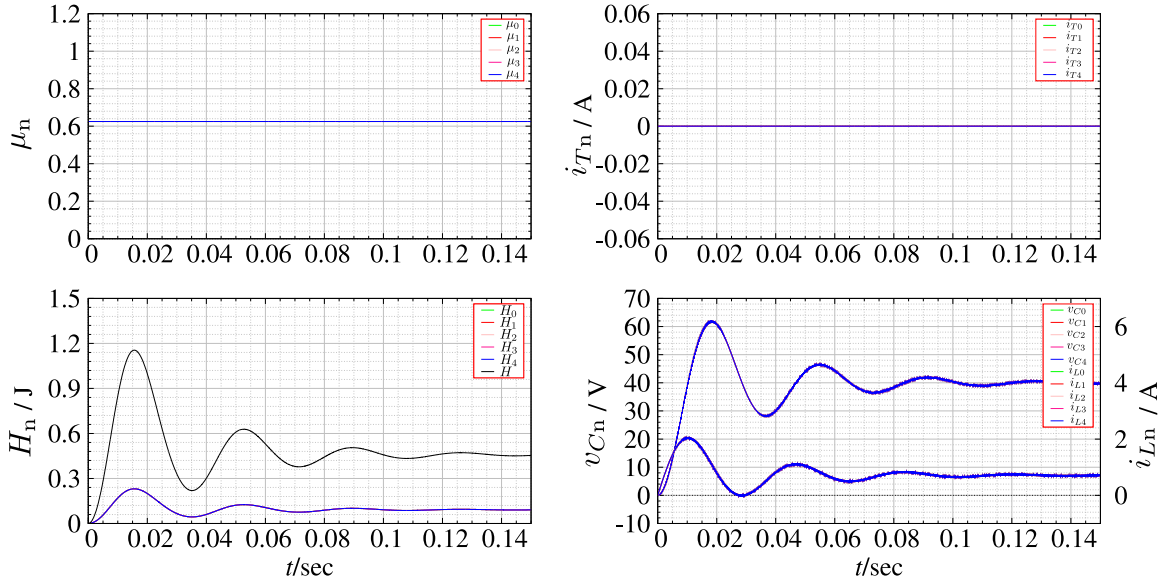

Figure 3.5: Balanced system behaviour of original system with respect to time. Parameters of all converters are set at equal values. The desired output voltage $\bar{v}_C = 40$ V for all 5 converters. The output of all converters coincides through the transient and settles at 40 V.

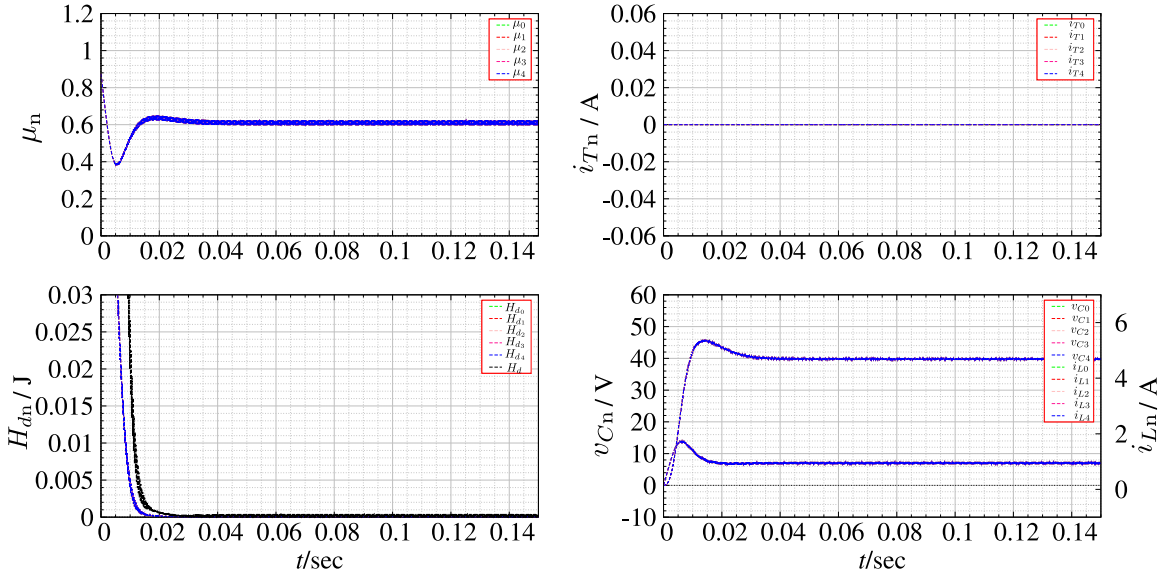

Figure 3.6: Balanced system behaviour with application of PBC to all converters. The energy function H_d goes to zero as system settles to the desired equilibrium. As the system is balanced, all the converters move synchronously. The transient peak is damped and the convergence time is improved.

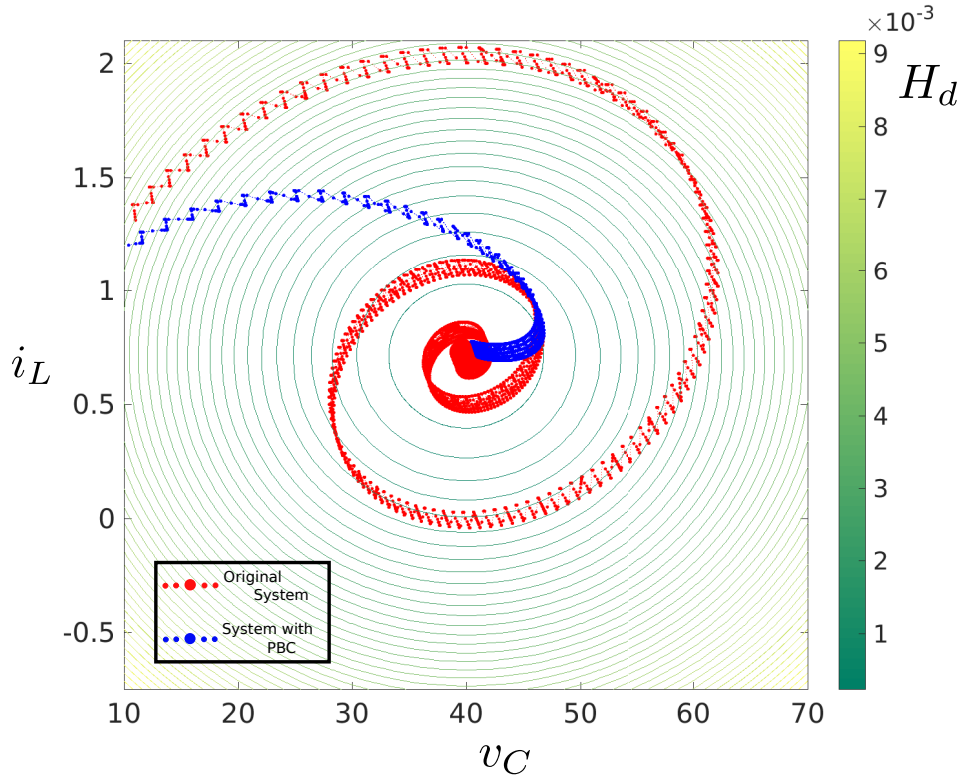

Figure 3.7: Asymptotic behaviour of the original system and system with PBC

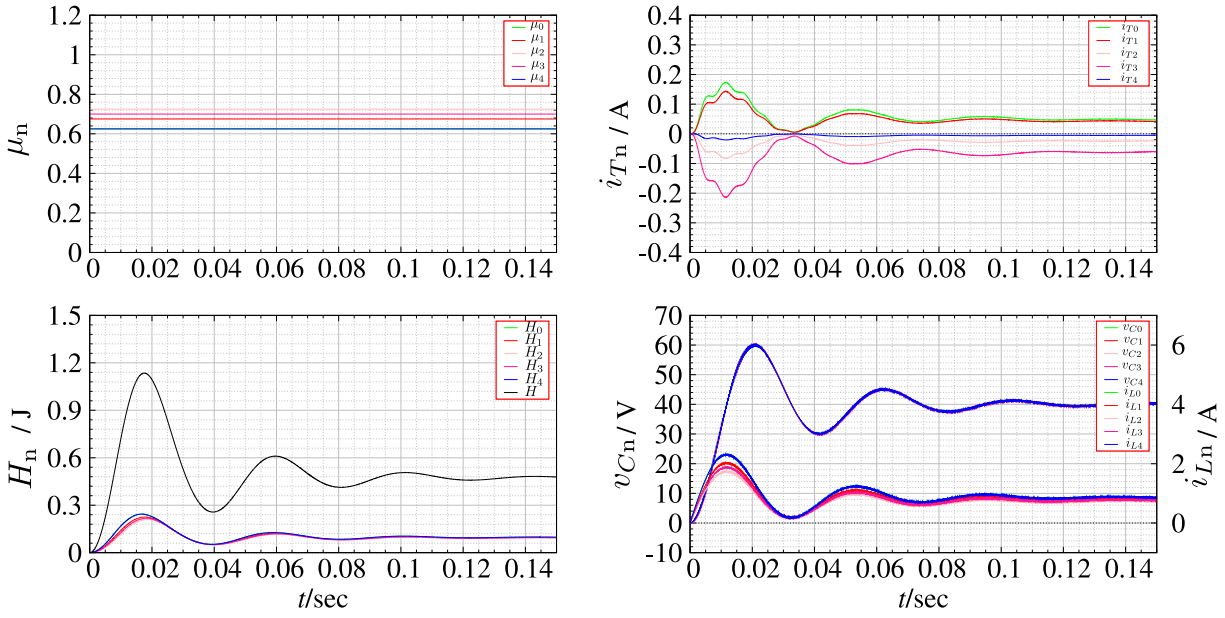

Figure 3.8: Original unbalanced system with different input voltages to the boost converter. Imbalance is created with input values given in Table.3.2.

3.3.2 Simulation results for an unbalanced system

Imbalance occurs in the ring coupled system when converters in the ring and/or the dissipation between two neighbouring converters have different parameter values. In the following simulations we consider imbalance in two different ways: imbalance created with varying input voltage and load resistance values. First, simulations were carried out to see the behaviour of the open loop unbalanced system without application of PBC. The values of the input voltages are varied as given in Table. 3.2.

Fig. 3.8 shows that different input voltages give rise to different current values for the same desired voltage. In this case, all converters have constant but different duty cycles as calculated from Eq.(3.12). Due to the different inputs, it is found that current appears through the dissipation between the coupled converters. The dissipation current is reduced after the transient when the converters converge to the desired voltage.

Figure 3.9 shows simulation results when PBC is applied. The direction of flow of the dissipation current depends on the imbalance created by the different inputs. The duty ratio changes according to the energy function (H_d) and becomes constant as soon as the energy function attains a zero value. The energy function for each of the converter is different for the unbalanced case. It is seen in the results that each energy function becomes zero as the control is applied. This implies that PBC is successfully applied to each converter system as well. Thus, it can be confirmed that interconnection of passive systems is a passive system [27]. Even though energy is exchanged between converter systems during transient period, passivity is retained for each converter, and all converters stabilize at the desired equilibrium.

Next, the load resistances are set differently for each of the converters as given in Table. 3.3. The simulation results for the original system are shown in Fig. 3.10. The different load resistances cause the voltages to settle at slightly different values, this difference is unrecognizable but can be inferred from the continuous flow of dissipation current between the converter systems. This indicates the flow of energy between the converters. The flow of energy is in the direction of the load that consumes the most current, i.e towards the smallest resistance.

Finally, Fig. 3.11 shows the results of PBC applied to the system when the load resistance values are different. As is expected, the results are better than the uncontrolled case. This implies that PBC can successfully regulate the coupled converter systems when the system has different loads. The loads in a realistic system would vary depending on their power demand. Therefore, the successful stabilization of system with PBC with different loads serves as an useful tool for designing practical systems.

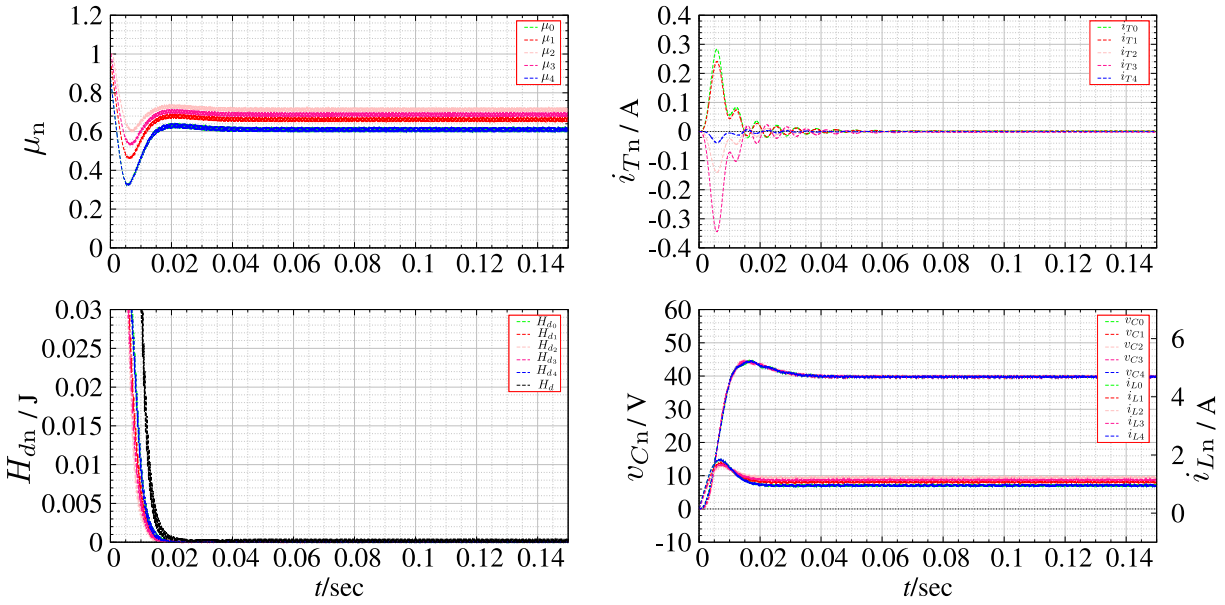

Figure 3.9: Unbalanced system controlled with PBC having different input voltages for the boost converters. Imbalance is created with input values given in Table.3.2.

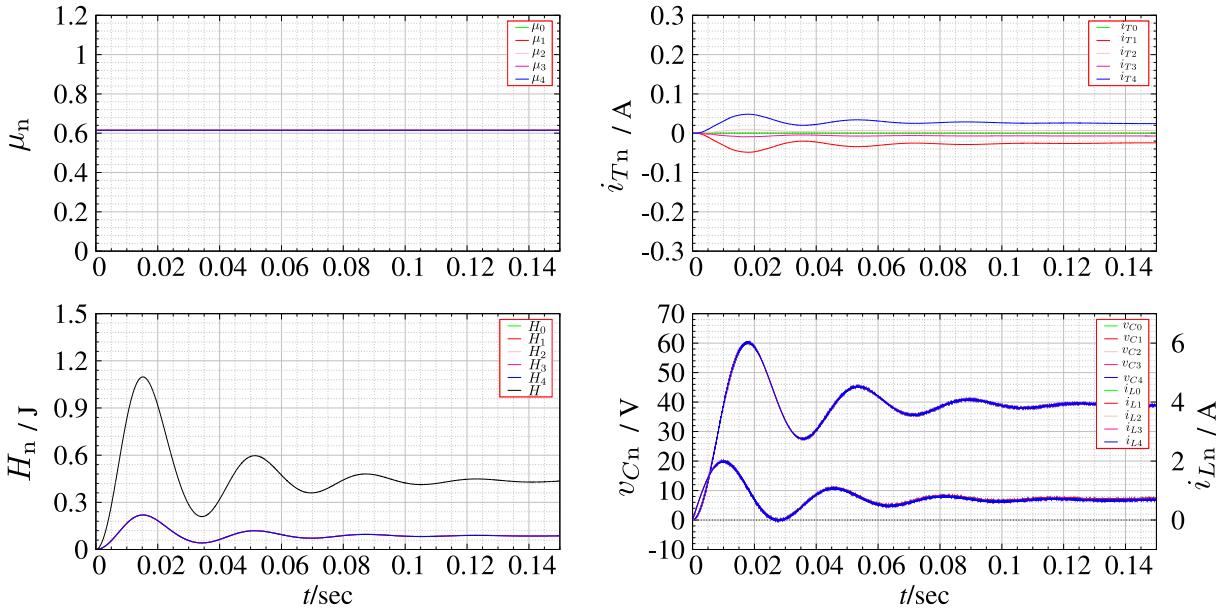

Figure 3.10: Original system with imbalance created with different load resistance values as given in Table.3.3

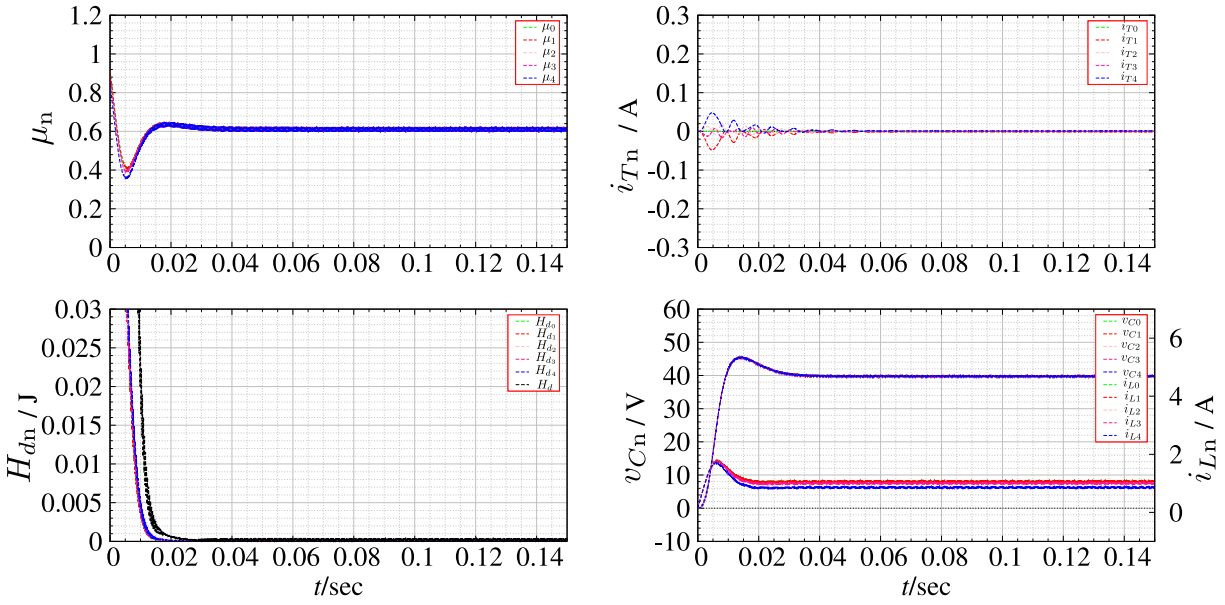

Figure 3.11: Unbalanced system controlled with PBC having different load resistance values as given in Table.3.3.

3.3.3 Stabilization to non stationary state

So far the control has been constructed assuming that the desired state, $v_C^* = \bar{v}_C$ is a constant. We may further extend PBC to the case in which the desired state is not a constant but a function on time. A sinusoidal function with a DC bias is selected as the

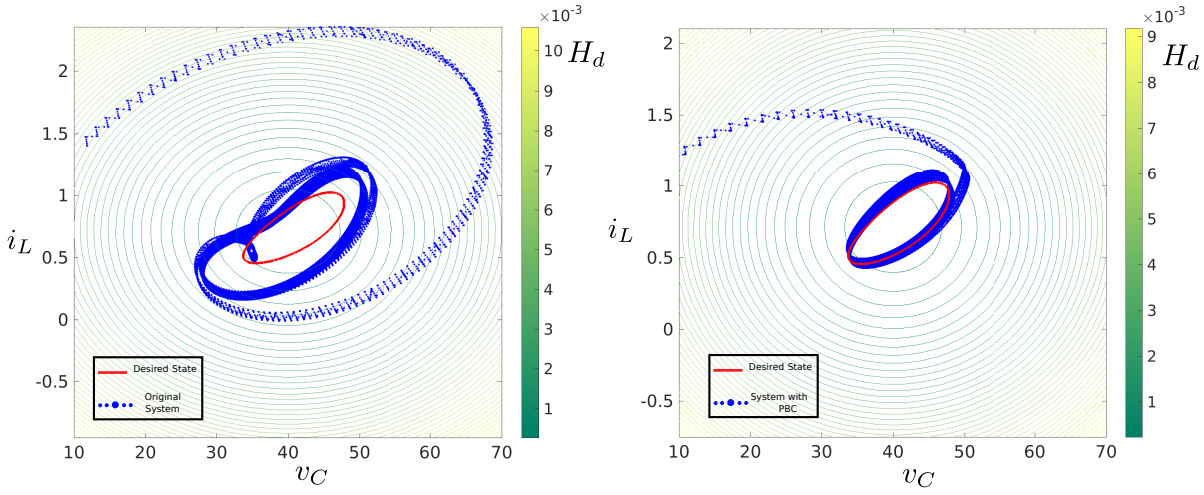

(a) (b)

Figure 3.12: Asymptotic behaviour of system with the desired equilibrium as a function of time: (a) Without application of control (b) With application of PBC

desired state. The desired state is set to be $v_C^* = v_{DC} + A\sin(2\pi ft)$. Here, v_{DC} is the DC bias voltage, A and f are the amplitude and frequency of the sinusoidal voltage. The frequency is much smaller than the switching frequency of the PWM. For simulations we set $v_{DC} = 40$ V, $A = 8$ V, $f = 60$ Hz. Firstly, the simulations were carried out for the original system, where the duty ratio $U_{\rm n}$ is calculated from Eq.(3.12). The results are shown in the form of an energy plot (Fig. 3.12(a)). The other parameters are set as given by Table. 3.1.

Next, simulations were carried out by applying PBC as given by Eqs.(3.27) and (3.29). The results are given in Fig. 3.12(b). Again, the parameters are set as given by Table. 3.1.

It was seen in Sec. 4.5, that the desired function is considered as a function of time. The subsequently obtained control equations for the feedback through the duty cycle also emphasize the fact that it is permissible to have the desired state as a function of time. It implies that PBC is a suitable method of control for such a case. The simulation results confirm the improvement at the application of PBC. The open loop system exhibits an unstable transient and a high transient peak voltage. The system with control settles down to the desired equilibrium relatively faster.

3.4 Conclusion

In this chapter we proposed a method to stabilize a ring coupled converter system, consisting of DC/DC boost converters, to a desired state with the application of feedback control through PBC. PBC, with energy shaping and damping injection was discussed for the quadratic function of errors as the desired storage function. The desired storage function deviates around zero and finally approaches zero as the system attains equilibrium.

Numerical simulations show that PBC can stabilize the output voltage values at the desired state even for a ring coupled configuration of the DC/DC converters. Comparison to the dynamic behaviour of the original open loop system suggests the successful application of PBC during transient operation. Numerical simulations were carried for different initial conditions. This included a balanced condition, where all the boost converters have same parameters, an unbalanced state with different parameters, including the dissipation, and the case in which the desired state is non stationary. PBC was applied for all the three cases. The results for the balanced system show all converters in the ring operating synchronously. There is no energy exchange in the form of dissipation current. Imbalance causes energy imbalance, but the application of PBC restores this imbalance and the entire system stabilizes at the desired state. Practically, the input voltages to the converters as well as the load resistances are not same for all converters in the ring. Even in such imbalanced conditions, the converters co-operate to maintain a stable voltage through the ring coupling. For non stationary desired states, the convergence of the output voltage as well as the inductor current to the desired sinusoidal state is vastly improved under PBC as compared to the original system, with a dampened transient peak.

Chapter 4

Phase and Frequency Synchronization for Autonomous AC-Grid System

In this chapter we focus on renewable DC sources of electricity, and suggest an autonomous grid formulation to utilize the DC electric power. We introduce a ring coupled buck-type inverter system to utilize energy from DC power sources by converting it to AC voltage. The basic design of this grid is shown in Fig. 4.1. In the ring coupled buck-type inverter system, multiple units of inverter circuits are connected in a ring formulation with dissipation in between them. Power inverters play the role of an interface to transfer energy from DC sources of electricity to AC voltage form with a desired frequency [51, 55]. The buck-type inverter circuit employs the circuit configuration of a DC/DC buck converter with the DC input switched using a H-bridge circuit which enables to change the polarity to obtain AC output voltage.

The stabilization of the grid to the desired AC voltage, usually carried out by AVR and governer, is replaced by passivity-based control (PBC). In this chapter we implement PCHM to the autonomous AC grid formulate the feedback control rule using PBC. Conventionally, the objective for PBC has been to stabilize the system to a constant DC voltage. When stabilizing the system to a sinusoidal desired state, the steady state analysis for obtaining the duty ratio of the open loop system is significantly intricate [29,44,56]. This chapter lays out the steady state analysis for the open loop system as well as formulation of the feedback control equations for a sinusoidal desired state.

Another crucial task is that of grid synchronization. Various methods for synchronizing the power from multiple renewable resources to the existing power system are shown in [57]. Here, we focus on synchronizing the multiple AC voltage outputs to the desired state in terms of frequency and phase. It is shown that, if the multiple inverters in the ring coupling have inconsistent phase or frequency, it can prove to be harmful to the system. It is desirable that all the inverters autonomously adjust themselves to the desired sinusoidal state without any phase difference. To achieve this, phase synchronization for all the inverter units in the grid is implemented with attached phase locked loop (PLL) [58].

Finally, the theory is successfully tested with numerical simulations to illustrate the temporal behaviour of the system. Numerical simulations are performed in the SIMULINK

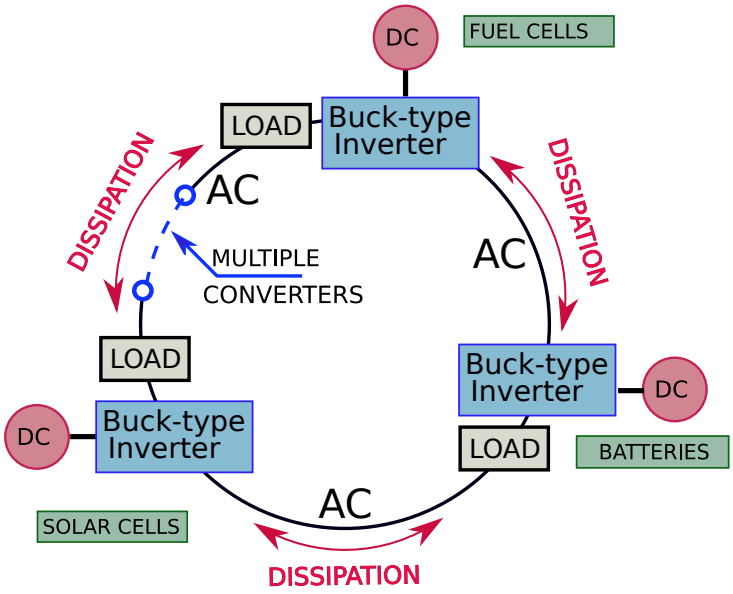

Figure 4.1: Design of a stand-alone distributed autonomous grid

environment on MATLAB R2017.

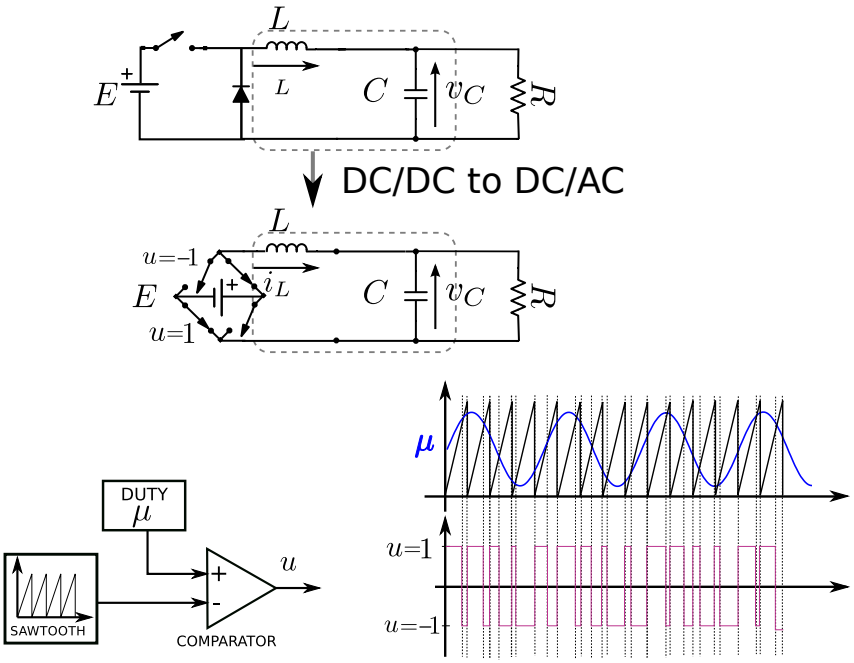

Figure 4.2: Design of a buck-type inverter with a H-bridge

4.1 Buck-type Inverter

The circuit configuration of the buck-type inverter is shown in Fig.4.2. A double bridge is implemented to invert the polarity of the DC source [50]. Here, u represents the instantaneous switch position as shown in the figure. The instantaneous switch position takes the values in the discrete set $\{-1, 0, 1\}$ as shown in the figure. It is seen that the value of u is responsible for changing the polarity of the DC source, thus making it possible to obtain the negative part of the sinusoidal output voltage.

To obtain a constant AC output voltage, the control objective is to regulate the average output voltage to a periodic value with frequency much smaller than the switching frequency (usually 50 or 60 Hz). It is desirable to consider the average value of the voltages and currents rather than the instantaneous values, given that the ripple and harmonics are sufficiently small. To derive an averaged model, it is necessary to average the circuit variables as well as the switching function [51]. Hence, we replace the instantaneous switch position with a modulating signal for the averaged circuit. Hereafter, the modulating function will be referred to with the variable $\mu(t)$.

To implement a PWM policy for switch regulation for generating a digital pulse signal to drive the transistor switches, this modulating function μ acts as the continuous control input. As the modulating signal varies slowly in comparison to the frequency of the switching, it can be shown that the switching function is equal to the modulating signal [51]. We refer to the switching function as the duty ratio.

To obtain the averaged circuit variables, we replace the instantaneous values by the average values. Thus, i_L and v_C are the average the inductor current and capacitor voltage respectively, and μ, the duty ratio. The output voltage of the inverter depends on the duty cycle of the switching [22]. Thus, the averaged control input is takes values in the closed set $[-1, 1]$. The averaged duty cycle will be sinusoidally modulated to achieve a sinusoidal output voltage. The average model of a buck-type inverter is given in Eq.(4.1). Owing to the buck-type configuration, the peak output voltage will be less than the DC input voltage.

$$\begin{aligned} L\dot{i}_L &= -v_C + \mu E \\ C\dot{v}_C &= i_L - v_C/R \end{aligned} \tag{4.1}$$

Here L, C and R represents the inductance, capacitance and load resistance respectively. E is the external DC input. Optimal control of DC/AC inverters with an H-bridge topology has been obtained in [55]. Here, we aim to stabilize the output of the inverter with PBC.

4.2 System Design

The AC grid has multiple DC sources each connected to a buck-type inverter, to invert the DC voltage to AC output, which can be used by the existing household loads. These

inverters are coupled together with dissipation through inductance and resistance.

The schematic diagram of the circuit is shown in Fig. 3.2. The role of the control input, for each buck-type inverter, is to decide the amplitude and frequency of the output voltage. In a ring coupled configuration, it is imperative that the output voltage of each inverter converge to the same value. The voltage in the ring will be maintained at a user-defined desired value.

Here, load resistances(R_{2T}) are across the output voltages whereas the dissipation elements of line inductor (L_t) and line resistance (R_{1T}) are in series. The coupling through dissipation represents a transmission line model, with inductive and resistive elements. The capacitor in the transmission line model is considered as negligible. This is owing to the fact that a parallel capacitor is dominant in the buck-type inverter configuration. The number of inverters in the ring does not cause any loss of generality. Then, the objective is to apply PBC to the whole system, including the dissipation between the inverters.

$$L_{\mathrm{n}}\frac{di_{L_{\mathrm{n}}}}{dt} = -v_{C_{\mathrm{n}}} + \mu_{\mathrm{n}}E_{\mathrm{n}} \tag{4.2}$$

$$C_{\mathrm{n}}\frac{dv_{C_{\mathrm{n}}}}{dt} = i_{L_{\mathrm{n}}} - i_{T\mathrm{n}} + i_{T\mathrm{n}-1} - \frac{v_{C_{\mathrm{n}}}}{R_{2\mathrm{n}-1}} \tag{4.3}$$

$$L_{T\mathrm{n}}\frac{di_{T\mathrm{n}}}{dt} = v_{C_{\mathrm{n}}} - v_{C_{\mathrm{n}+1}} - R_{1\mathrm{n}}i_{T\mathrm{n}} \tag{4.4}$$

The averaged model of the ring coupled buck-type inverter system is given by Eqs.(4.2)-(4.4). Subscription n denotes the index of the inverter. μ_{n} denotes duty ratio function for the #n inverter. $L_{T\mathrm{n}}$ is the inductance and $R_{1T\mathrm{n}}$ in the dissipation between the #0 and #1 inverter.

To ensure phase and frequency synchronization of the ring coupled inverter system, PLLs are added to the basic circuit formulation. Let $\bar{v}_{C\mathrm{n}} = A_n \sin(\Phi_{\mathrm{n}})$ be the desired sinusoidal output voltage. Then, $\sin(\Phi_{\mathrm{n}})$ is the sinusoidal reference, where, $\Phi_{\mathrm{n}} = \omega_d t + \theta_{i\mathrm{n}}(t)$ is the phase. Here ω_d is the centre frequency, and θ_i the phase angle of the input singal. In order to synchronize the phase of the output voltages of ring coupled buck-type inverter systems, any #p inverter can be taken as a reference. The sinusoidal reference for the #p inverter is used as the input signal for the PLL, the output of which is used as the sinusoidal reference of the #p − 1 and #p + 1 inverter. The sinusoidal reference of #p − 1 and #p + 1 is in turn used as the input to PLL, the output of which is used as the sinusoidal reference to #p − 2 and #p + 2, respectively. It ensures minimun time delay in synchronising the phase and frequency of all the inverters in the ring. The connection of the PLL to the system is shown in Fig.4.4.

We consider the centre frequency ω_d to be the same for all the PLLs employed in the ring coupled AC grid. $\theta_i(t)$ incorporates the error in the input frequency (ω_i) from the centre frequency of the VCO. This error is given by $\Delta\omega = \omega_i - \omega_d$. Let the output of the VCO be $r(t, \tilde{\Phi}_{\mathrm{n}}) = V_0 \cos(\omega_d t + \theta_o(t))$, with V_0 as the amplitude and $\tilde{\Phi} = \omega_d t + \theta_o(t)$ as the phase. θ_o represents the phase angle of the output signal. The state equation governing

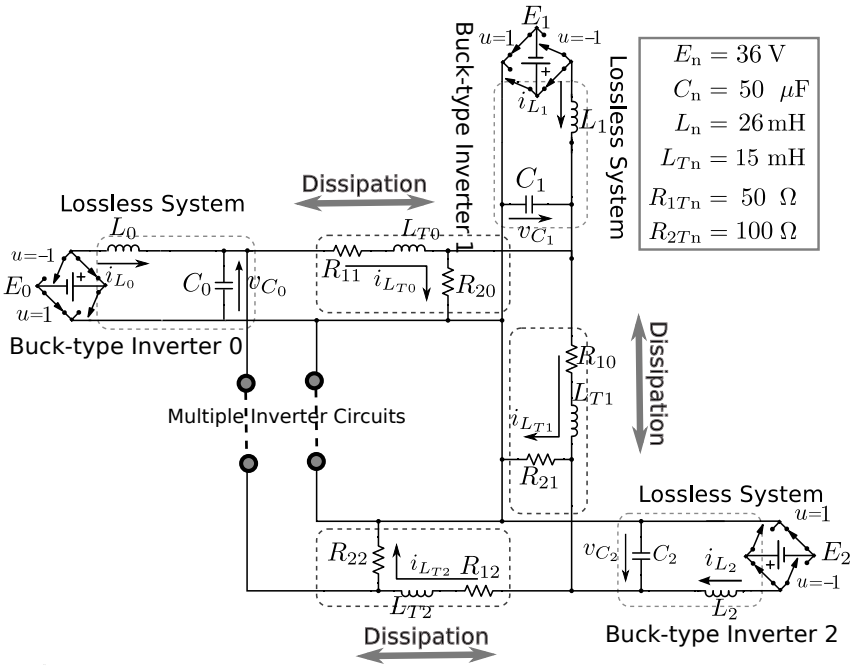

Figure 4.3: Schematic citcuit diagram of ring coupled buck-type inverters.

the change in the phase are given by Eq.(7.7) [59, 60].

$$\frac{d\theta_o}{dt} = K_C[\mathcal{L}^{-1}[F(s)V_{\text{comp}}(s)]K_pA\sin(\theta_e) + v_e] \tag{4.5}$$

Here, $\theta_e = \theta_i - \theta_o$ is the phase error, v_{comp} is the input of the low pass filter, and $V_{\text{comp}}(s)$ is the Laplace transform of v_{comp}. The transfer function of the LPF in the frequency domain is given as $F(s)$ and K_p and K_C are the gains of the phase detector and VCO of the PLL respectively. Lastly, $\mathcal{L}^{-1}$ denotes the Laplace inverse and v_e is the external control voltage. For more details on the working of PLL, please refer to Appendix A.

4.3 Port-controlled Hamiltonian Modelling

PCHM technique is used for modeling the inverter circuit, to allow for the inclusion of power electronic switches and load resistances. PCHM classifies the system neatly into physically well defined interconnection($\mathbf{J}$), dissipation($\mathbf{R}$) and external input($\mathbf{E}$) matrices within a state space framework [24]. The system model using the PCH framework is given by Eq.(5.22) as in the form given in [47].

$$\mathbf{D}\dot{\boldsymbol{x}}(t) = [\mathbf{J} - \mathbf{R}]\frac{\partial H}{\partial x} + \mathbf{G}(\boldsymbol{x})\mathbf{E} \tag{4.6}$$

$$\boldsymbol{y} = \mathbf{G}^T(\boldsymbol{x})\frac{\partial H}{\partial \boldsymbol{x}} \tag{4.7}$$

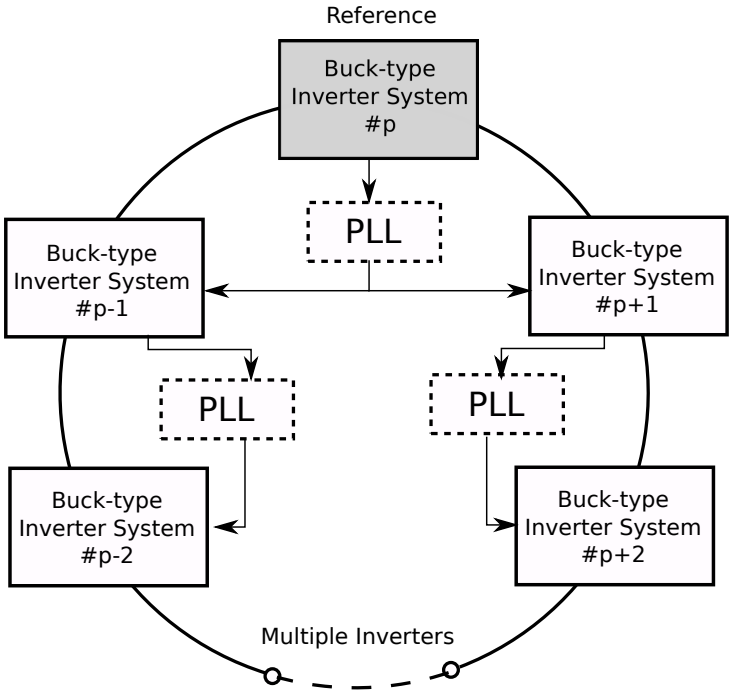

Figure 4.4: System Configuration: Connection of PLL to multiple inverter system.

For m inverters in the configuration, $\boldsymbol{x}$, the state of the system, is a column matrix ((m $\times$ 3) $\times$ 1) of all the inductor currents and capacitance voltages. The matrix $\mathbf{D}$, is a diagonal matrix of the capacitances and inductances of the corresponding currents and voltages. $\mathbf{J}$ and the vector function $\mathbf{G}(\boldsymbol{x})$ gives the interconnection, and $\mathbf{R}$ the dissipation in the system. $\mathbf{G}(\boldsymbol{x})$ is a function of u_{n}, the switch position of the corresponding buck-type inverters in the ring configuration. $\mathbf{E}$, the input matrix is a column matrix of the input voltages to the respective inverters. H is the Hamiltonian, which, in this case, is the total energy of the system.

Here, $\mathbf{D}$, $\mathbf{R}$, $\mathbf{J}$ and $\mathbf{G}$ are ((m $\times$ 3) $\times$ (m $\times$ 3)) matrices, $\mathbf{E}$ is a (m $\times$ 3) $\times$ 1 matrix.

$$\mathbf{D} = \begin{bmatrix} \mathbf{D}_0 & 0 & \dots & 0 \\ 0 & \mathbf{D}_1 & \dots & 0 \\ \vdots & \vdots & \ddots & \vdots \\ 0 & 0 & \dots & \mathbf{D}_{\mathrm{m}} \end{bmatrix} \text{ where , } \mathbf{D}_{\mathrm{n}} \begin{bmatrix} L_{\mathrm{n}} & 0 & 0 \\ 0 & C_{\mathrm{n}} & 0 \\ 0 & 0 & L_{T\mathrm{n}} \end{bmatrix} \text{ , and } \boldsymbol{x} = \begin{bmatrix} \boldsymbol{x}_0 \\ \vdots \\ \boldsymbol{x}_{\mathrm{m}} \end{bmatrix} \text{ where , } \boldsymbol{x}_{\mathrm{n}} = \begin{bmatrix} i_{L\mathrm{n}} \\ v_{C\mathrm{n}} \\ i_{T\mathrm{n}} \end{bmatrix}. \tag{4.8}$$

$$\mathbf{J} = \begin{bmatrix} \mathbf{A}_0 & -\mathbf{B}^T & 0 & \dots & 0 & \mathbf{B} \\ \mathbf{B} & \mathbf{A}_1 & -\mathbf{B}^T & 0 & \dots & 0 \\ 0 & \mathbf{B} & \ddots & \ddots & \ddots & \vdots \\ \vdots & 0 & \ddots & \ddots & \ddots & 0 \\ 0 & \vdots & \ddots & \ddots & \ddots & -\mathbf{B}^T \\ -\mathbf{B}^T & 0 & \dots & 0 & \mathbf{B} & \mathbf{A}_\mathrm{m} \end{bmatrix} \text{ where, } \mathbf{A}_\mathrm{n} = \begin{bmatrix} 0 & -1 & 0 \\ 1 & 0 & -1 \\ 0 & 1 & 0 \end{bmatrix}, \mathbf{B} = \begin{bmatrix} 0 & 0 & 0 \\ 0 & 0 & 1 \\ 0 & 0 & 0 \end{bmatrix}. \tag{4.9}$$

$$\mathbf{R} = \begin{bmatrix} \mathbf{R}_0 & 0 & \dots & 0 \\ 0 & \mathbf{R}_1 & \dots & 0 \\ \vdots & \vdots & \ddots & \vdots \\ 0 & 0 & \dots & \mathbf{R}_\mathrm{m} \end{bmatrix}, \text{ where } \mathbf{R}_\mathrm{n} = \begin{bmatrix} 0 & 0 & 0 \\ 0 & \dfrac{1}{R_{2T\mathrm{n}}} & 0 \\ 0 & 0 & R_{1T\mathrm{n}} \end{bmatrix}. \tag{4.10}$$

$$\mathbf{G} = \begin{bmatrix} \mathbf{G}_0 & 0 & \dots & 0 \\ 0 & \mathbf{G}_1 & \dots & 0 \\ \vdots & \vdots & \ddots & \vdots \\ 0 & 0 & \dots & \mathbf{G}_\mathrm{m} \end{bmatrix}, \text{ where } \mathbf{G}_\mathrm{n} = \begin{bmatrix} \mu_\mathrm{n} & 0 & 0 \\ 0 & 0 & 0 \\ 0 & 0 & 0 \end{bmatrix}, \text{ and } \mathbf{E} = \begin{bmatrix} \mathbf{E}_0 \\ \vdots \\ \mathbf{E}_\mathrm{m} \end{bmatrix} \text{ where , } \mathbf{E}_\mathrm{n} = \begin{bmatrix} E_\mathrm{n} \\ 0 \\ 0 \end{bmatrix}. \tag{4.11}$$

Looking at the adjacency matrix of the interconnection matrix ($\mathbf{J}$), the ring coupled structure is clearly verified. It is seen that $\mathbf{D}$ is a diagonal matrix and $\mathbf{R}$ is a symmetric matrix for m inverters. The matrix $\mathbf{J}$ is the interconnection matrix, and shows the coupling between neighbouring inverters through dissipation. From Eq.(4.9), it can be verified that $\mathbf{J}$ is a skew-symmetric matrix, with keeping the PCHM structure [47].

4.4 Steady State Analysis : Open loop system

As it was shown in Chapter 3, steady state analysis is provided to obtain the open loop system. In the case of the AC system described above, the steady state values are sinusoidal. A sinusoidal duty ratio can be implemented to obtain the desired output voltage for the open loop system. It is analogous to setting a constant average duty ratio for the switching for DC/DC converters. This constitues the open loop system, without a feedback control.

For the #n buck-type inverter in the, the desired voltage is a AC waveform in the form $\bar{v}_{C\mathrm{n}} = \sin(2\pi f_\mathrm{n} t) = A_\mathrm{n} \sin(\Phi_\mathrm{n})$. $\Phi_\mathrm{n} = 2\pi f_\mathrm{n} t + \theta_{i\mathrm{n}}$ with angular frequency $\omega_{d\mathrm{n}} = 2\pi f_\mathrm{n}$. For steady state analysis, $\theta_{i\mathrm{n}}$ is a constant, i.e the angular frequency does not change with time.

Eqs.(4.2)-(4.4) give the mathematical description of the system for any #n buck-type inverter system. Steady sate analysis is employed to formulate the equilibrium values for

the desired inductor current ($\bar{i}_{L\mathrm{n}}$) and the desired disspiation current ($\bar{i}_{T\mathrm{n}}$) for a given desired voltage $v_{C\mathrm{n}} = \bar{v}_{C\mathrm{n}}$. Then, it will be possible to formulate the sinusoidal duty ratio U.

It is possible to analytically solve the linear differential equation Eq.(4.4), by employing the known values of $v_{C\mathrm{n}} = \bar{v}_{C\mathrm{n}}$, $v_{C\mathrm{n+1}} = \bar{v}_{C\mathrm{n+1}}$. The solution to the equation is given by Eq.(4.14).

$$\begin{aligned}\bar{i}_{T\mathrm{n}} =& \frac{R_{1\mathrm{n}}A_n}{R_{1\mathrm{n}}^2 + L_{T\mathrm{n}}^2\omega_{d\mathrm{n}}}(\sin\Phi_{\mathrm{n}} - \frac{\omega_{\mathrm{n}}L_{T\mathrm{n}}}{R_{1\mathrm{n}}}\cos\Phi_{\mathrm{n}}) \\ &+ \frac{R_{1\mathrm{n}}A_{n+1}}{R_{1\mathrm{n}}^2 + L_{T\mathrm{n}}^2\omega_{d\mathrm{n+1}}}(\sin\Phi_{\mathrm{n+1}} - \frac{\omega_{d\mathrm{n+1}}L_{T\mathrm{n}}}{R_{1\mathrm{n}}}\cos\Phi_{\mathrm{n+1}}) + ke^{-(R_{1\mathrm{n}}/L_{\mathrm{n}})t} \end{aligned} \tag{4.12}$$

Here, k is the constant of integration. The value of k is obtained by applying the initial condition $i_{Td}(0) = 0$.

$$k = \frac{A_{\mathrm{n}}\omega_{\mathrm{n}}L_{T\mathrm{n}}}{R_{1\mathrm{n}}^2 + L_{\mathrm{n}}^2\omega_{d\mathrm{n}}} - \frac{A_{\mathrm{n+1}}\omega_{d\mathrm{n+1}}L_{T\mathrm{n}}}{R_{1\mathrm{n}}^2 + L_{\mathrm{n}}^2\omega_{d\mathrm{n+1}}} \tag{4.13}$$

The equilibrium value of $i_{L\mathrm{n}}$ can be obtained by solving Eq.(4.2) with $i_{T\mathrm{n}} = \bar{i}_{T\mathrm{n}}$.

$$\bar{i}_{L\mathrm{n}} = C_{\mathrm{n}}\dot{\bar{v}}_C - \bar{i}_{T\mathrm{n}} + \bar{i}_{T\mathrm{n-1}} + \frac{\bar{v}_C}{R_{2T\mathrm{n-1}}} \tag{4.14}$$

Finally, the open loop duty ratio $U_{\mathrm{n}}$to obtain from Eq.(4.3) by substituting $i_{L\mathrm{n}} = \bar{i}_{L\mathrm{n}}$and given in (5.17).

$$U_{\mathrm{n}} = \frac{L_{\mathrm{n}}}{E_{\mathrm{n}}}[C_{\mathrm{n}}\ddot{\bar{v}}_{C\mathrm{n}} - \dot{i}_{Td\mathrm{n}} + \dot{\bar{i}}_{T\mathrm{n-1}} + \frac{\dot{\bar{v}}_C}{R_{2T\mathrm{n-1}}}] + \frac{\bar{v}_C}{E_{\mathrm{n}}} \tag{4.15}$$

Here, $\bar{x}$ denotes the desired averaged value, $\dot{x}$ denotes $\frac{\mathrm{d}x}{\mathrm{d}t}$, and $\ddot{x}$ denotes $\frac{\mathrm{d}^2x}{\mathrm{d}t^2}$.

4.5 Energy Shaping in PBC

We investigate whether it is possible for PBC to be applied to a system of multiple inverters coupled with dissipation. The stored energy of a circuit is the sum of the energy in the passive elements, that is the inductors and capacitors. The energy of the multiple inverter system is given by Eq.(4.16).

$$H = \frac{1}{2}\boldsymbol{x}^T\mathbf{D}\boldsymbol{x} \tag{4.16}$$

$\boldsymbol{x}$ and $\mathbf{D}$ are as given in Eqs.(4.8). H, which is the total energy, is also considered to be the Hamiltonian of the system.

The modified energy function is based on the Hamiltonian. The formulation is taken to be the quadratic function of errors. It is given by Eq.(4.17).

$$H_d = \frac{1}{2}\boldsymbol{e}^T\mathbf{D}\boldsymbol{e}, \quad \boldsymbol{e} = \boldsymbol{x} - \boldsymbol{x}_d \tag{4.17}$$

Here, $\boldsymbol{x_d}$ is the desired trajectory of the state. It was proven in Chapter 2 that Lyapunov's Theorem is satisfied for this desired storage function. That is, the equilibrium state $\boldsymbol{x}_d$ is asymptotically stable with the control rule given in Eq.(5.24), and exponentially asymptotically stable with the damping injection. $\mathbf{R}_I$ is given in Eq.(4.18).

$$\mathbf{R_I} = \begin{bmatrix} \mathbf{R_{I0}} & 0 & \dots & 0 \\ 0 & \mathbf{R_{I1}} & \dots & 0 \\ \vdots & \vdots & \ddots & \vdots \\ 0 & 0 & \dots & \mathbf{R_{In}} \end{bmatrix}, \text{ where } \mathbf{R_{In}} = \begin{bmatrix} R_{\alpha \mathrm{n}} & 0 & 0 \\ 0 & 0 & 0 \\ 0 & 0 & 0 \end{bmatrix}. \tag{4.18}$$

For a buck-type inverter system, an indirect output stabilization is ensured by setting the current ($\bar{i}_L$) to a constant sinusoidal value, depending on the desired output voltage amplitude and frequency. The zero dynamics of the buck-type inverter with respect to the output capacitor voltage being unstable, a feedback control is considered through current (indirect stabilization) as was shown in Chapter.3 [22]. Thus, we set a constant desired current, and then formulate the desired state values for the output voltage and dissipation current. The desired current ($\bar{i}_{L\mathrm{n}}$) is obtained from the steady state analysis given by Eq.(4.14). The control equations are formulated based on the PBC equation Eq.(4.19)-(4.21).

$$\mu_{\mathrm{n}} = [L_{\mathrm{n}} \dot{\bar{i}}_{L\mathrm{n}} + \tilde{v}_{C\mathrm{n}} - R_\alpha (i_{L\mathrm{n}} - \bar{i}_{L\mathrm{n}})] \tag{4.19}$$

$$C_{\mathrm{n}} \dot{\tilde{v}}_{C\mathrm{n}} = \bar{i}_{L\mathrm{n}} - \tilde{i}_{T\mathrm{n}} + \tilde{i}_{T\mathrm{n}-1} - \left[\frac{\tilde{v}_{C\mathrm{n}}}{R_{2\mathrm{n}-1}}\right] \tag{4.20}$$

$$L_{T\mathrm{n}} \dot{\tilde{i}}_{T\mathrm{n}} = \tilde{v}_{C\mathrm{n}} - \tilde{v}_{C\mathrm{n}+1} - R_{1\mathrm{n}} \tilde{i}_{T\mathrm{n}} \tag{4.21}$$

Here, $\boldsymbol{x}_d = [\bar{i}_L \ \tilde{v}_C \ \tilde{i}_{LT}]^{\mathrm{T}}$ is the desired dynamic state vector for the controller, and μ is the feedback duty ratio.

For the feedback control through PBC, value of the duty ratio μ is evaluated atevery instant t depending on the input, the parameters, and the desired output of the system. That is, μ depends on time and the state. Hereafter, when PBC is applied to the system, μ is considered as a function of time and state of the system.

To synchronize the phase of the output voltages of ring coupled buck-type inverter systems, the #p inverter is taken as a reference. The sinusoidal reference for the #p inverter is used as the input signal for the PLL, the output of which is used as the external frequency input for the sinusoidal reference of the #p $-$ 1 and #p $+$ 1 inverter. The sinusoidal reference of #p $-$ 1 and #p $+$ 1 is in turn used as the input to PLL, the output of which is used as the external frequency to #p $-$ 2 and #p $+$ 2 respectively. For odd number of inverters in the system, it ensures minimun time delay in synchronising the phase and frequency of all the inverters in the ring. The connection of the PLL to the system is shown in Fig.4.4.

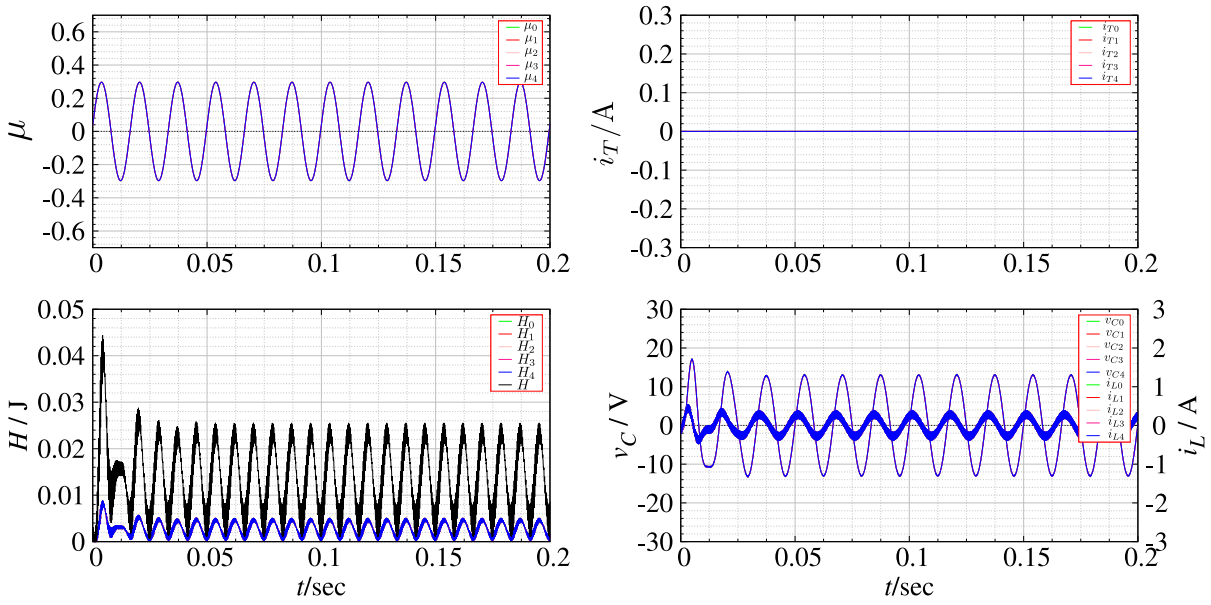

Figure 4.5: Time evolution of original AC grid system without control. Here, $\bar{v}_{C\mathrm{n}}$ is set with parameters $A_{\mathrm{n}} = 13$, $f_{\mathrm{n}} = 60$ Hz.

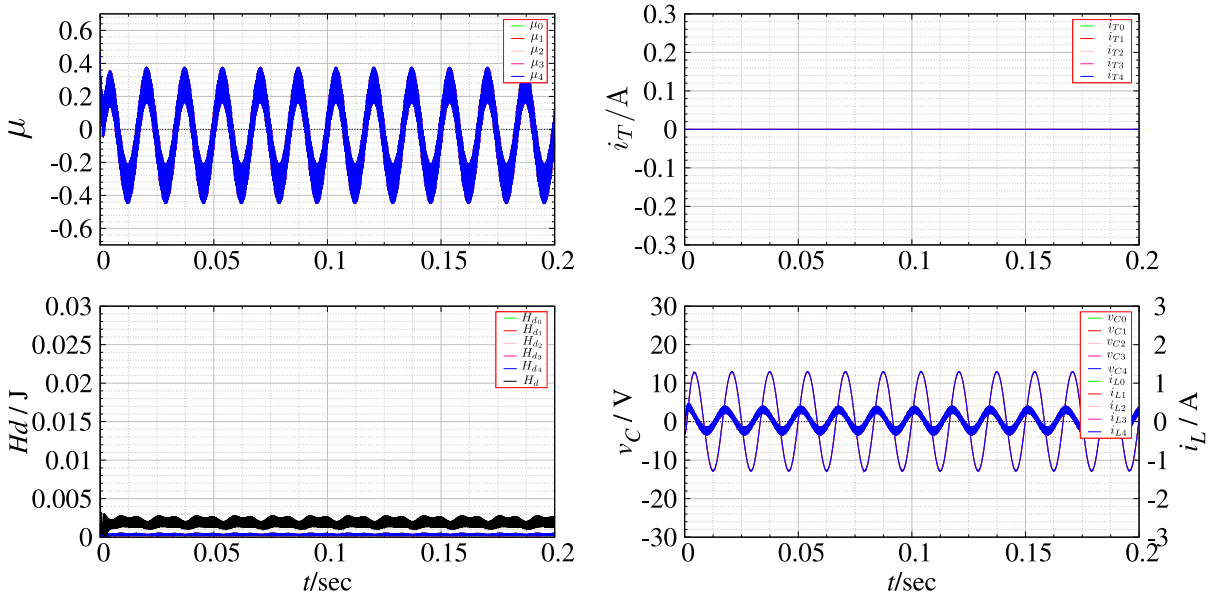

Figure 4.6: Time evolution of AC grid with PBC. Here, $\bar{v}_{C\mathrm{n}}$ is set with parameters $A_{\mathrm{n}} = 13$, $f_{\mathrm{n}} = 60$ Hz.

4.6 Numerical Simulations

The simulation results are obtained for five inverters coupled in a ring form are given in this section. The numerical simulations were carried out on ode45 solver Simulink (Version 8.7 R2016a). The numerical simulations are performed in three cases depending on the phase angle and frequency of the inverters in the ring.

4.6.1 Case I: $\Delta\omega_{\mathrm{n}} = 0$, $\theta_{\mathrm{n}} = 0$

In Case I we test the effectiveness of the original open loop system as well as the system with feedback through PBC under balance and unbalanced conditions. There is no phase diference between the output of the inverter systems and the desired frequency remains constant at the centre frequency of the VCO. Thus $\omega_{i\mathrm{n}} = \omega_{d\mathrm{n}} = \omega_d$. This implies the output frequency of all inverters stays constant at a particular value. The simulations were proceeded for a ring-coupled system consisting of 5 buck-type inverters to enhance the asymmetry in the system. Firstly, we investigate the effectiveness of the application of a sinusoidal averaged duty cycle to the switches through PWM to achieve AC voltage for the open loop system. Fig.4.5 shows system behaviour with the steady state analysis as given in Eq.(5.17). The steady state analysis is applied to a balanced ring coupled inverter system. A balanced system implies that the parameters of all inverter systems are set to be the equal. The parameters are given in Fig.4.3.

It is seen in Fig.4.5 that AC output voltage is generated in all five inverters for the open loop system, and due to the condition of balance, all inverters synchronize with each other. The energy of the entire system is the sum of the energy in the inductors (analogous to kinetic energy in mechanical systems) and the energy in the capacitors (analogous to the potential energy in mechanical systems). The energy of the system depends on the inductor currents and capacitor voltage, it oscillates with twice the frequency as the output voltage frequency. As all the inverter system and the dissipation between them is balanced, there is no flow of energy between the coupled inverters.

Next, the system behaviour with the application of feedback through PBC is shown in Fig.4.6. The results show a marked improvement in the transient period of the dynamic behaviour, with a smaller transient peak amplitude and a faster convergence to the desired state. The behaviour of the designed energy function (H_d) is also shown. The system achieves control when the value of the energy function drops down to zero. As the system output is not constant with time, the energy function oscillates around the zero value.

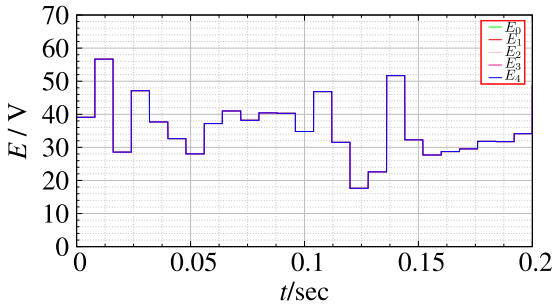

Figure 4.7: Variation of the input voltage with respect to time

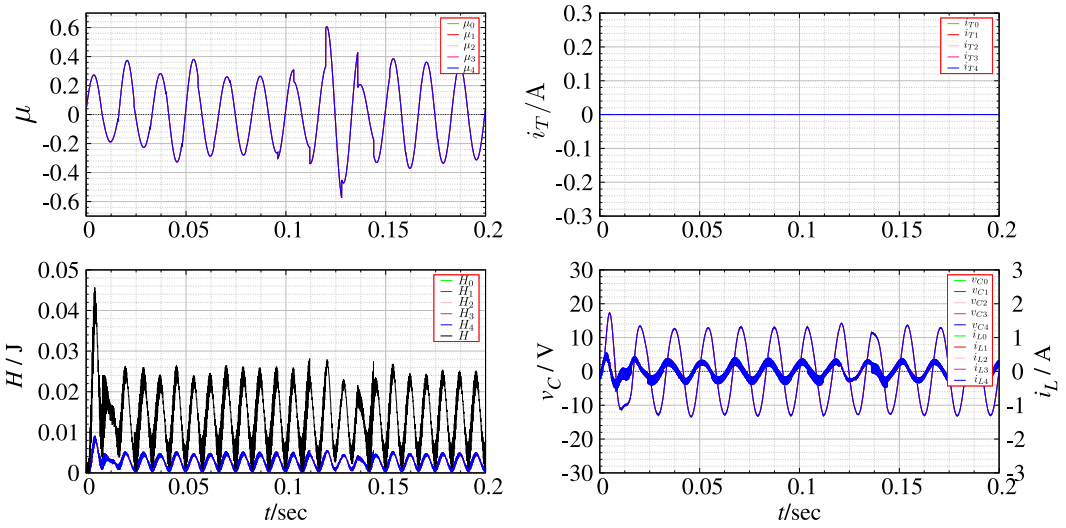

Figure 4.8: Behaviour of unbalanced open loop AC-grid with varying input voltages without PBC

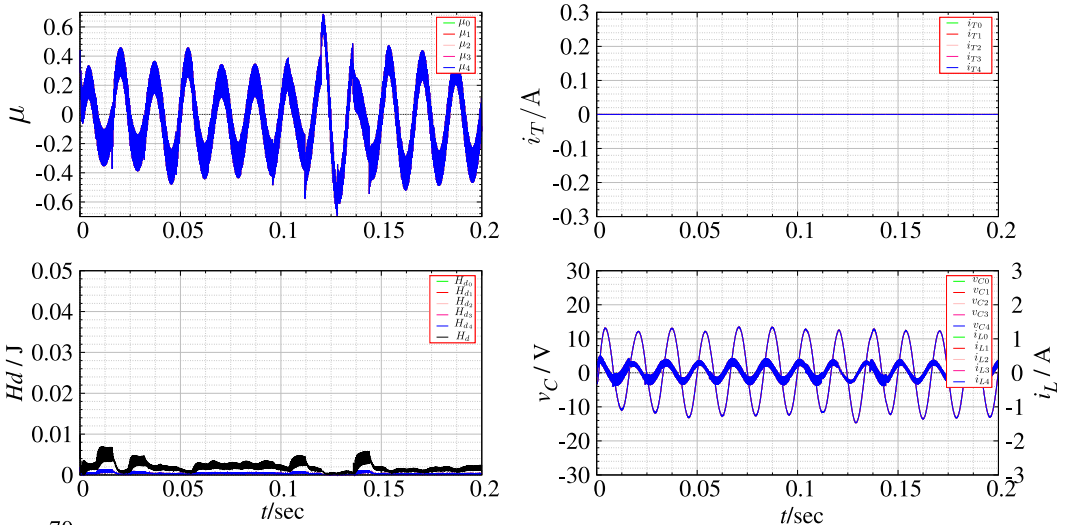

Figure 4.9: Behaviour of unbalanced AC-grid with varying input voltages with PBC

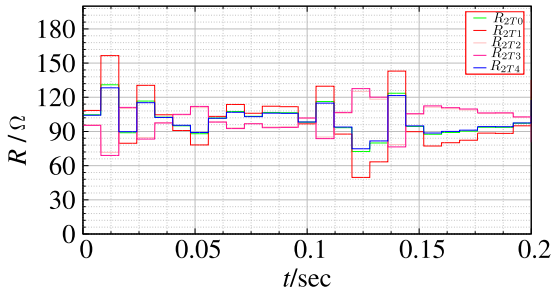

Figure 4.10: Variation of the load resistances with respect to time

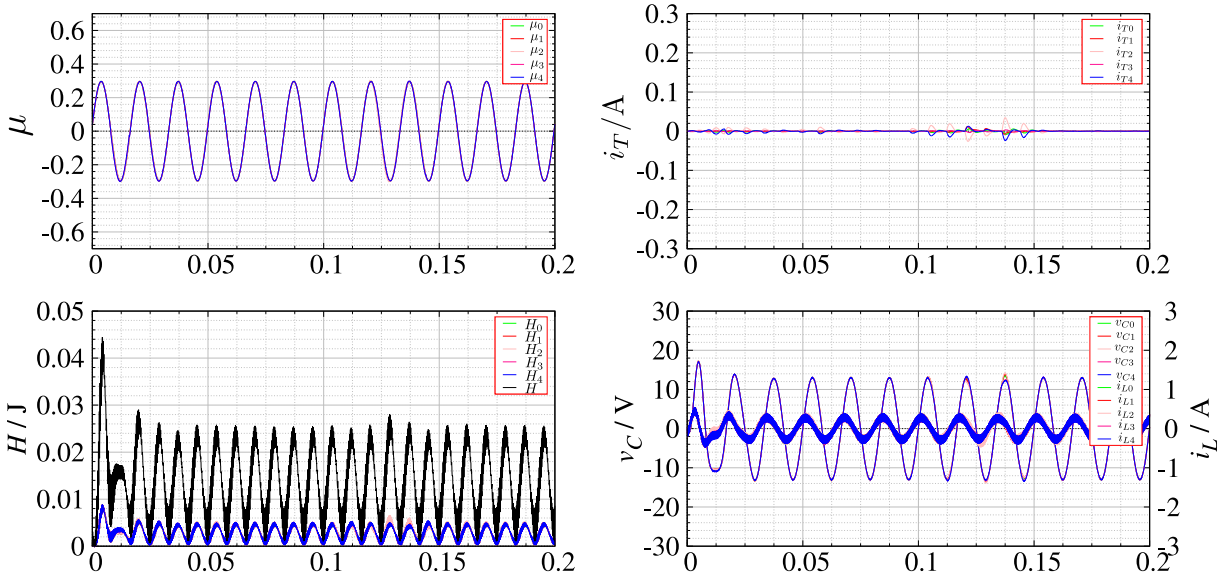

Figure 4.11: Behaviour of unbalanced open loop AC-grid with varying load resistances without PBC

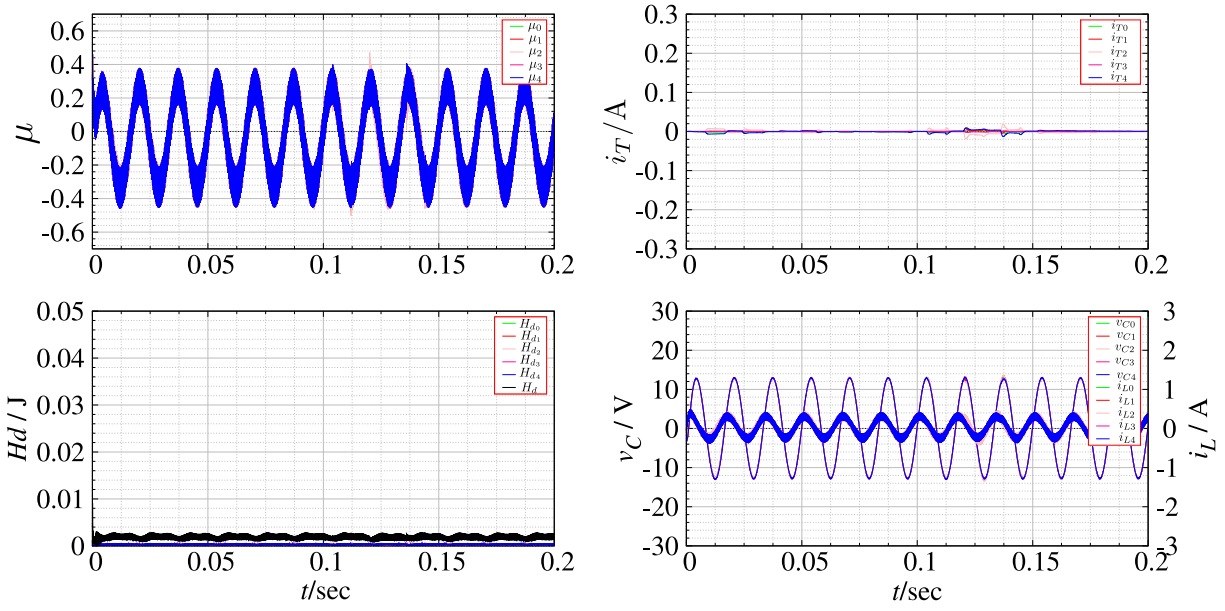

Figure 4.12: Behaviour of unbalanced AC-grid with varying load resistances under PBC

Imbalance appears in the system by setting different parameters for the coupled inverters. For practical cases where the input comes from PV arrays, imbalance occurs at the change of input voltage for each inverter system, depending on the irradiation. Therefore, next, we check the effectiveness of PBC by applying extreme noise to the input voltage. Fig.4.7 shows the change in the input voltages for all the inputs. This will create high imbalance conditions, as the input voltage for each inverter will change separately from the others. The parameters other than the input voltage are balanced. First, the results without PBC (i.e open loop system) are shown in Fig.4.8. Here, at every transient change, the output shows deviation from the desired sinusoidal wave. The application of PBC to such an unbalanced system is shown in Fig.4.9. It can be seen that despite extreme variation of the input voltage from the balanced voltage, the output is fairly sinusoidal. he transient expected at the sudden change in the input voltage is dampened and the output is kept fairly constant at the desired sinusoidal voltage. The second case with imbalance is when the load resistances are varied as shown in Fig.4.10. The open loop system output without PBC is shown in Fig.4.11 and with the application of PBC in Fig.4.12. Even though both outputs are fairly similar, the application of PBC helps to dampen the transient to obtain a smoother output voltage.For both cases, frequency as well as the phase is maintained. Imbalance occurring in the ring coupled inverter system creates a difference in the output voltage of the inverters, inducing the flow of dissipation current between the inverters.

4.6.2 Case II: $\Delta\omega = 0$, $\theta_{i\mathrm{n}} = constant$

In the numerical simulations shown in Sec.4.6.1, the frequency and phase of the output voltages was same for all the inverters. It was assumed that the sinusoidal reference for the PWM for all the inverters has the same frequency and is switched ON at the same time, resulting in zero phase difference between the outputs. Even though all the sinusoidal references can be provided with an external frequency, it is not fair to assume that all the sinusoidal references will start at the exact same moment. Thus, it is possible that there might be a phase difference between the sinusoidal references, and as a consequence, between the output voltages themselves. The sinusoidal inputs to the switches, shown by x_{n}, for the five converters are given in Fig.4.13.

Figures 4.14 and 4.15 show the output voltage and input currents of all 5 inverter systems for the open loop system and with PBC respectively. The origin of the temporal axis is when all the input voltages are switched ON. For the numerical simulations #0 is used as the reference inverter. The proportional gain (K_p) of the PLL is set at 180. To emulate a practical case, all the sinusoidal signals start at different times. Without PLL, it would create a constant phase difference in the outputs, leading to an undesirable output voltage. Here, # 0 is considered as the reference inverter. The phase of this reference is as $\Phi = \omega_d t + 0.6$, with an arbitarary constant phase angle $\theta_i = 0.6$ rad. It is observed that until all the sinusoidal references are switched ON, the output in unstable. As the reference signals are switched ON, the PLL achieves the lock-in condition and the system output settles down to the desired state. The centre frequency is $\omega_d = 377$rad/sec

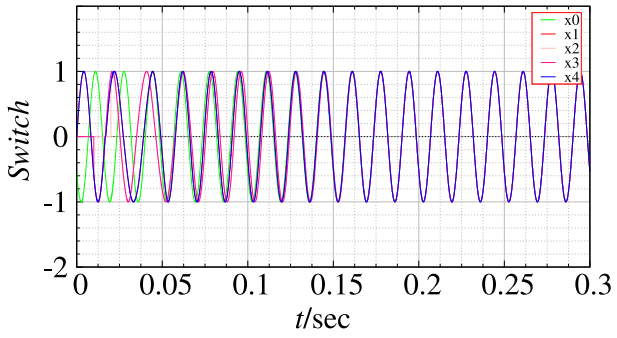

Figure 4.13: Inverter input when the switches start at different times.

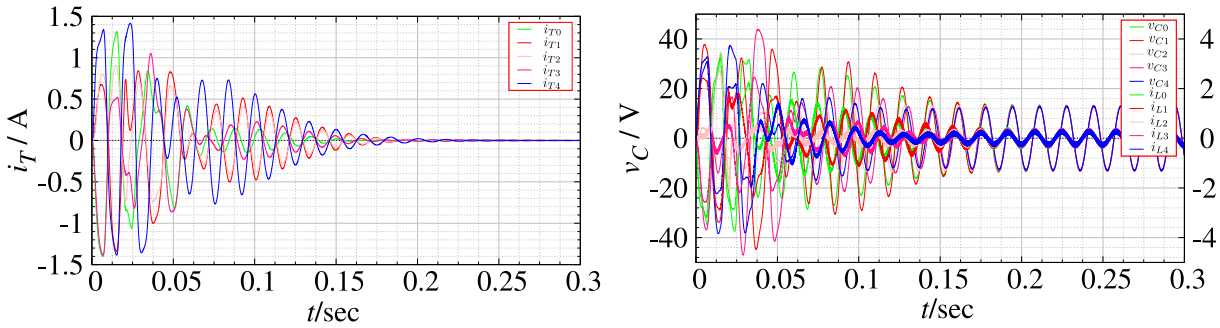

Figure 4.14: Phase synchronization with PLL applied to autonomous AC grid of ring coupled buck-type inverter without PBC.

(60 Hz).

Comparing the two figures, it is seen that the inverter output is more synchronized when PBC is applied, which is indicated by the dissipation current($i_{T\mathrm{n}}$) flowing between the inverters. The dissipation current for the original open loop system is almost three times higher than when PBC is applied. The output settles down to the desired state faster with PBC, and the dissipation current goes to zero for all inverters. With PBC, the duty ratio governing the output voltage dynamically changes to drive the energy function to the minimum value. The dynamic change in the duty ratio ensures a smaller deviation from the desired state due to the thorough consideration of the energy characteristics of the system through PBC. In both cases, the PLL shows the phase synchronization of all the inverters to that of the reference inverter.

Effect of Ripple and Harmonics

As mentioned before, the ripple and the harmonics have been considered negligible. To obtain negligible ripple, the inductor values have been chosen as specified in [61]. Reducing the harmonic effects of the AC output port is recognized as one of the most difficult challenges in a DC/AD inverter design. The ratio of the switching frequency to the output frequency is finite, as opposed to infinite for the DC/DC converters. For low

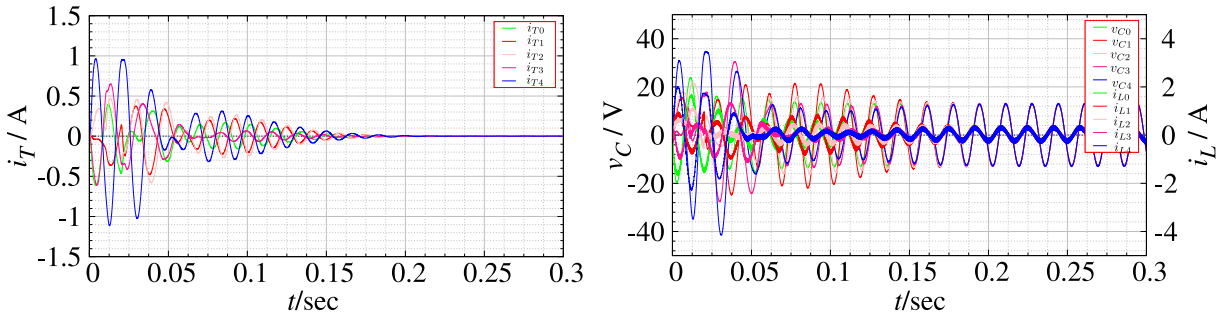

Figure 4.15: Phase synchronization with PLL applied to autonomous AC grid of ring coupled buck-type inverter with PBC.

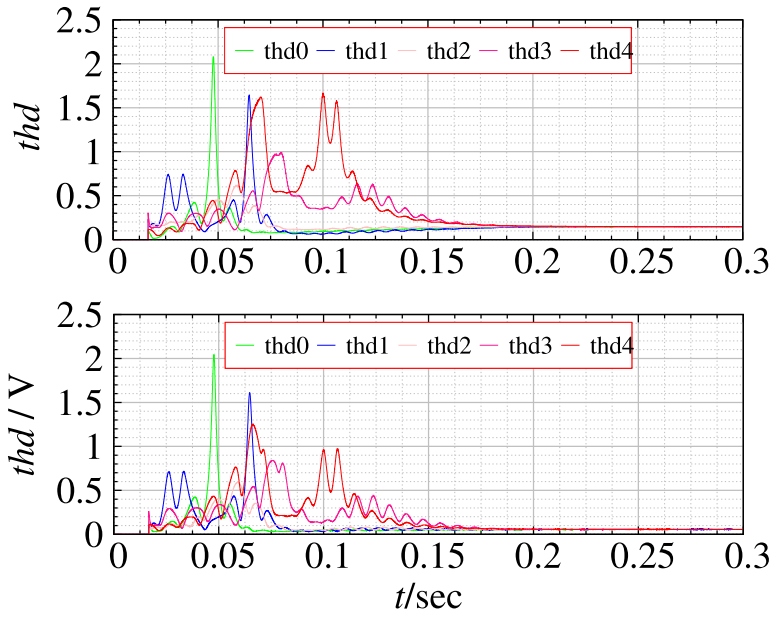

Figure 4.16: THD variations for results in Fig.4.15 for PWM frequency 3 kHz and 10 kHz respectively

frequency switching, methods like harmonic elimination and harmonic cancellation are employed citekassakian2000principles. In this research we employ PWM, rendering the harmonics to higher frequencies, and thus, easy to eliminate with smaller components. Total harmonic distortion is the measure of the harmonic distortion present in the signal. The higher the frequency of switching, the lower is the THD. The variation of the current THD for the system with PBC in Figs.4.15 is shown in Fig.4.16. For a switching frequency of 3 kHz the THD settles on 0.3 and settles to as low as 0.1 for PWM switching frequency 10 kHz.

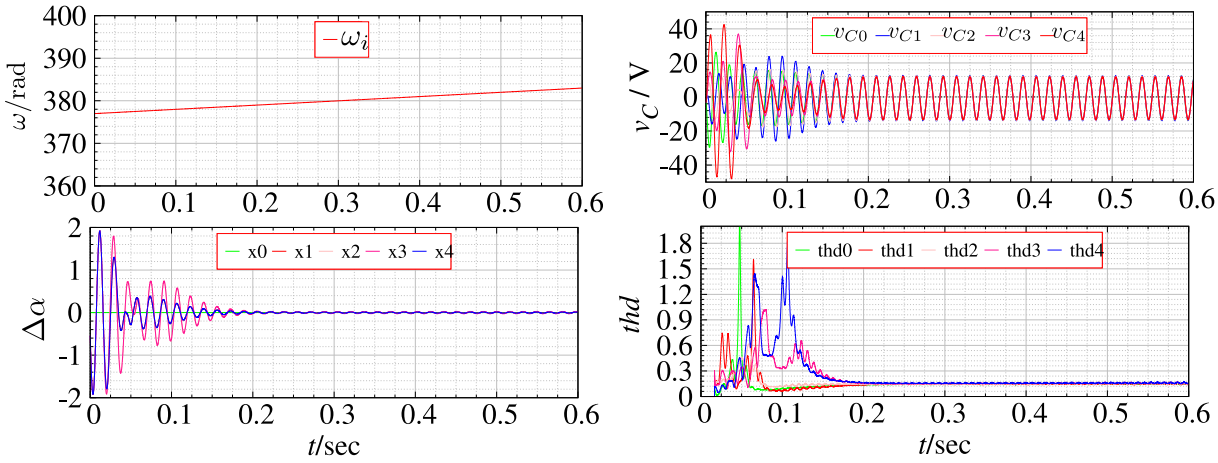

Figure 4.17: Linear change in the frequency of the sinusoidal PWM reference.

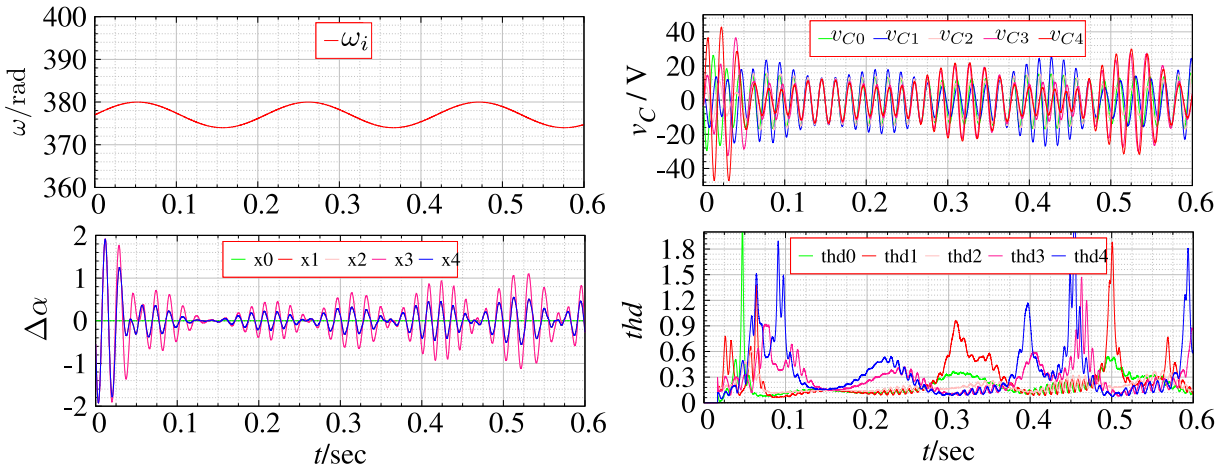

Figure 4.18: Sinusoidal change in the frequency of the sinusoidal PWM reference.

4.6.3 Case III: $\Delta\omega \neq 0$, $\theta_{\text{in}} = f(t)$

Next we vary the desired frequency from the centre frequency of the oscillator frequency creating an error frequency $\Delta\omega = \omega_i - \omega_d$. The tracking of the PLL is observed for changes in frequency. The frequency is varied in two ways. First, the frequency of this input is set to be different than the centre frequency of the VCO. For a VCO centre frequency of 377 rad/sec, we set the initial input frequency to be 396 rad/sec. Then, the frequency is varied linearly as a function of time with $\Delta\omega = 10t$. The results for these two cases is shown in Fig.4.17 . Here, $\Delta\alpha$ is the difference between the sinusoidal signal of the reference inverter and the other inverters in the ring. Thus, $\Delta\alpha$ indicates the deviation of the PLL output from the desired sinusoidal reference. Note that $v_e = 0$ for the purpose of numerical simulations.

The PLL achieves a phase lock in when the frequency is set at a different value from

the centre frequency. After initial transient oscillations of different phase, the output steadies at the input frequency. For the linear change in frequency, the PLL is able to keep the locked-in conditions even when the frequency is slowly increasing. The PLL maintains the hold-in conditions for the linearly increasing input frequency and retains all inverter systems at the input frequency. Thus, the PLL is successful in tracking the input successfully for these two cases of frequency change.

For cases where the frequency changes sinusoidally, the output shows an interference effect and the PLL may not be able to synchronize all the inverter outputs at the desired frequency. The results for this case are shown in Fig.4.18. Thus a sinusoidal change in the frequency poses as a limitation of the synchronization with PLL.

4.7 Conclusion

In this chapter we introduced an autonomous distributed generation AC grid to harness renewable DC sources of electricity. System stabilization for the grid to the desired output voltage is achieved through PBC. PBC with its energy shaping and damping injection techniques was discussed through a modified energy function based on the quadratic function of errors. The modified function approaches zero as the system reaches equilibrium.

A buck-type inverter was introduced to obtain a AC voltage with the desired amplitude and frequency by alternating the polarity of the DC input with the help of power electronic switches. Analysing the steady state behaviour for the open loop system, the necessary switching is determined via the sinusoidal duty ratio. The control of the output voltage in a ring coupled inverter system was attained with the focus on the energy characteristics of the system with the application of PBC. The control equations were obtained by proving the desired energy function as a Lyapunov function. The convergence to the desired steady state were verified by numerical simulations as well as the effectiveness of PBC. The system was studied under conditions of imbalance. Numerical simulations indicate that PBC proves to remain an effective method of control under imbalance conditions.

It was found that phase differences between the output voltage of different inverter systems leads to unstable output voltage for the entire system. PBC causes the system to converge to a desired state, but even small inconsistencies in frequency can prove to be detrimental. In order to avoid such instabilities we implemented frequency and phase angle synchronization to the entire system through PLL. Application of PLL was achieved through mathematical modelling, and then studied through numerical simulations. It was seen that the PLL successfully tracks the input reference for frequencies other than the centre frequency for the VCO as well as a linear change in the input frequency. Thus, a PLL, along with PBC, proves to be an efficient method to attain phase synchronization in an autonomous grid with ring coupled buck-type inverters.

Chapter 5

Design Framework for Hybrid Systems

In this chapter we propose a model for a stand-alone hybrid distributed generation system. In this model, the input sources are distributed DC sources like solar panels or batteries. The idea behind this network framework is to introduce a hybrid DC-AC network feasible for small, remotely located areas with stand-alone DC grids, in the vicinity of larger towns requiring a functional single-phase AC connection. The open loop system is obtained by providing the open loop duty ratio through the steady state analysis. The network is mathematically represented with port-controlled Hamiltonian modelling. Network stabilization to the desired voltage, both AC as well as DC, is attained with nonlinear passivity-based control taking into consideration not only the energy characteristics but also the inherent physical structure.

5.1 Network Design

Distributed generation is defined as the decentralized generation of electricity through small generators located near the end user or the consumer [10, 11]. It is an emerging concept wherein the generation of electricity is moved away from centralized power plants and towards individual generator units scattered over towns and villages [62]. Distributed generation has been discussed widely as an alternative to solve the electrification problem of rural and remote areas by constructing small stand-alone power grids by installing renewable energy generators in multiple households [63]. Such projects have been developing under the umbrellas of local governments as well as the private sector [64–67].

Of late, several ideas for stand-alone renewable energy grids have been previously proposed for rural areas [68–71]. In this chapter we introduce a hybrid stand-alone, off-grid distributed generation network aimed at employing solar panels or other DC sources as the primary inputs. The control of the DC stand alone grid with passivity-based control was proposed in Chapter 3 and the AC grid in Chapter 4. In other research works various designs of DC as well as hybrid microgrids have been proposed. A theoretical resut for the DC stand alone microgrid has been proposed in [72, 73]. A passivity-based approach for a hybrid DC/AC grid-tied microgird has been porposed in [74] where a well-defined

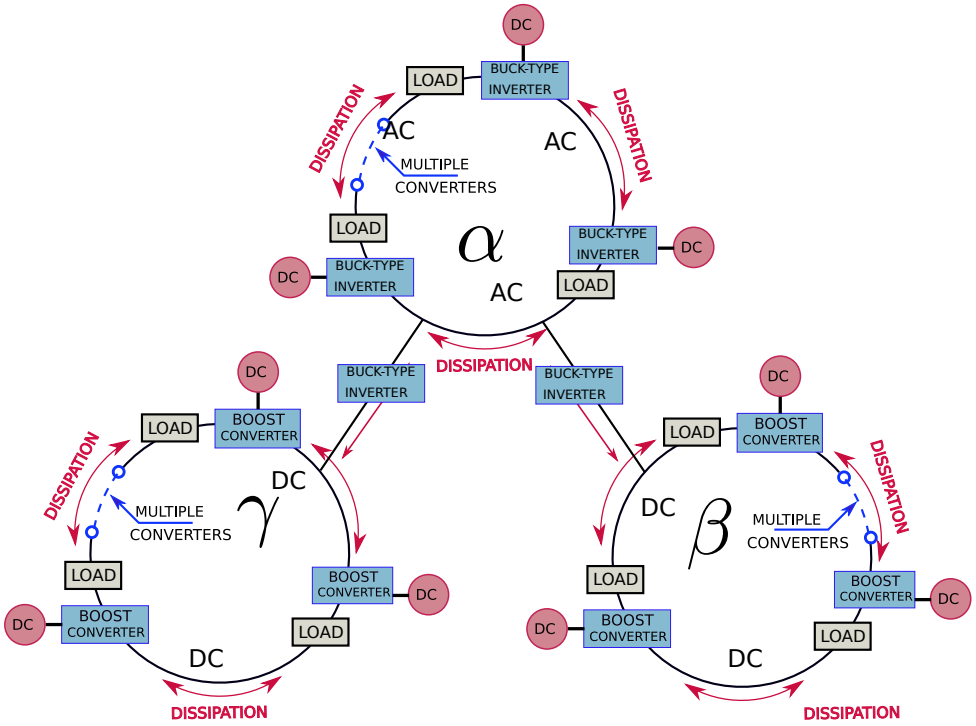

Figure 5.1: Network Configuration

hybrid network connected to the grid is considered and the control is porposed through PBC. The network presented in this chapter, in contrast, is a stand-alone network, and

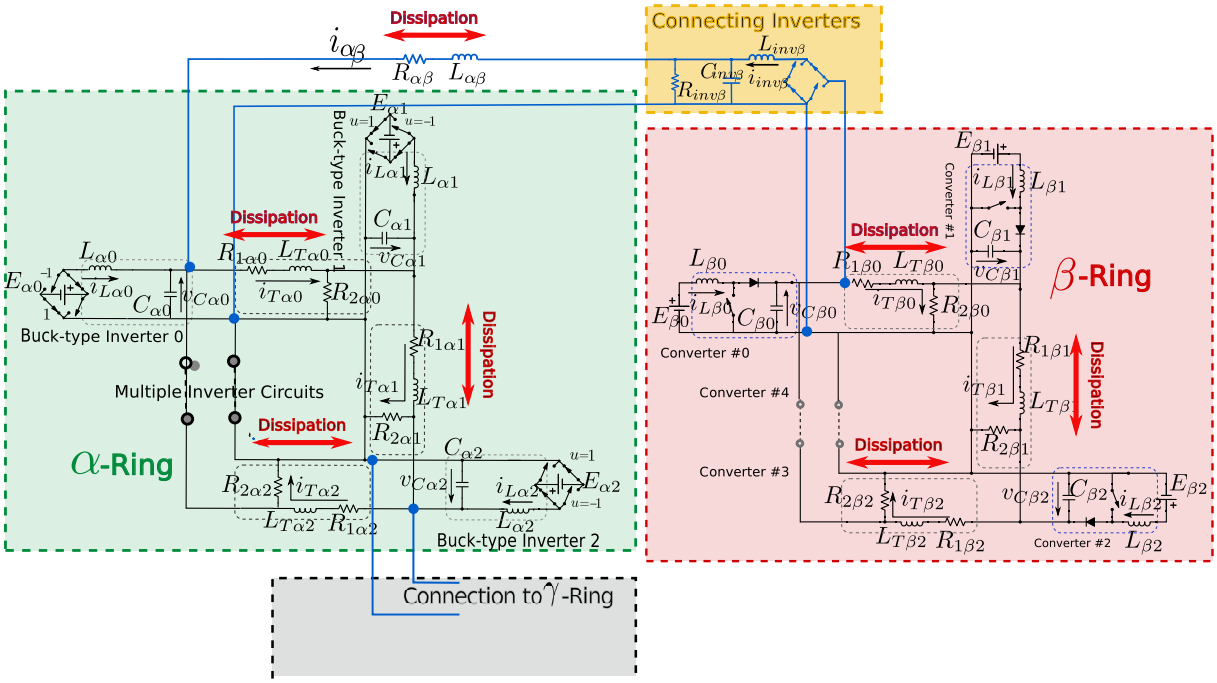

Figure 5.2: Schematic diagram of connection of AC and DC ring

the application of the open loop system as well as the system with PBC is proposed for a generalized system with multiple inverters for the AC network, and multiple DC links. The structure of the proposed hybrid DC-AC network is as described by Fig.5.1. The network configuration shows multiple connected rings, with the α ring comprising of multiple DC inputs accompanied with buck-type inverters to obtain an AC output. The α ring is connected to multiple DC rings (β and γ), with DC inputs which are conditioned with multiple DC/DC boost converters. The idea behind this network framework is to introduce a hybrid DC-AC network feasible for small, remotely located areas with stand-alone DC grids, in the vicinity of larger towns requiring a functional AC connection.

To achieve the stable operation of the entire network, we implement nonlinear passivity-based control. Here, the goal is to attain the desired output voltage by rendering the entire network passive along with its AC as well as DC components. For ring-coupled converters, it is confirmed that the converters keep the property of passivity individually as well as in the entire ring by minimizing an energy function [75]. In the context of a hybrid network, consideration has to be given to coupled converters as well as inverters operating concurrently. We define an energy function such that its minimum corresponds to the desired equilibrium of the entire network. The energy transfer between individual converter/inverter units in a particular ring, as well as that between the rings themselves, governs the the dynamic behaviour of the hybrid dispersed generation network.

Figure 5.2 shows a schematic diagram for the connection of the α-β rings. The connection of the α-γ ring is assumed to be similar. The coupled converter/inverter units in the ring are responsible for keeping the constant voltage in the ring. The system equations are given below and are divided into three parts. First, for the α ring, subscription n denotes the #n inverter in the ring. The equations for the α ring are given by Eqs.(5.1)-(5.3). The control task is to regulate the average output voltage for all the converters/inverters. As the output voltages are either DC, or AC with frequency (usually 50 or 60 Hz) much lower then the switching frequency of the power electronic switches, it is desirable to consider the averaged circuit variables rather than the instantaneous ones. It is assumed that the ripples and harmonics are sufficiently small. Then, the instantaneous switch position will be replaced by a modulating function μ. The averaged circuit variables will be replaced by their instantaneous values.

$$L_{\alpha \mathrm{n}} \frac{di_{L\alpha \mathrm{n}}}{dt} = - v_{C\alpha \mathrm{n}} + \mu_{\alpha \mathrm{n}} E_{\alpha \mathrm{n}} \tag{5.1}$$

$$C_{\alpha \mathrm{n}} \frac{dv_{C\alpha \mathrm{n}}}{dt} = i_{L\alpha \mathrm{n}} - i_{T\alpha \mathrm{n}} + i_{T\alpha \mathrm{n}-1} - \frac{v_{C_{\alpha \mathrm{n}}}}{R_{2\alpha \mathrm{n}-1}} + \eta i_{\alpha\beta} + \zeta i_{\alpha\gamma} \tag{5.2}$$

$$L_{T\alpha \mathrm{n}} \frac{di_{T\alpha \mathrm{n}}}{dt} = v_{C_{\alpha \mathrm{n}}} - v_{C_{\alpha \mathrm{n}+1}} - R_{1\alpha \mathrm{n}} i_{T\alpha \mathrm{n}} \tag{5.3}$$

Here, $\eta = 1$ for the inverter #n of which the output is connected to the DC ring β and $\zeta = 1$ for the inverter connected to the DC ring γ. $i_{\alpha\beta}$ and $i_{\alpha\gamma}$ are the currents flowing in

the dissipation between the α-β rings and α-γ rings respectively.

Equations for the connecting inverter between the rings α and β and the dissipation current between these rings are given by Eqs.(5.4)-(5.6).

$$L_{\text{inv}\beta}\frac{di_{\text{inv}\beta}}{dt} = -v_{\text{inv}\beta} + \mu_{\text{inv}\beta}v_{C\beta\text{q}} \tag{5.4}$$

$$C_{\text{inv}\beta}\frac{dv_{\text{inv}\beta}}{dt} = i_{\text{inv}\beta} - \frac{v_{\text{inv}\beta}}{R_{\text{inv}\beta}} - i_{\alpha\beta} \tag{5.5}$$

$$L_{\alpha\beta}\frac{di_{\alpha\beta}}{dt} = v_{\text{inv}\beta} - v_{C\alpha\eta} - R_{\alpha\beta}i_{\alpha\beta} \tag{5.6}$$

Here #q is the converter where the DC ring β is connected to the AC ring α. The equations for the inverter connecting the α-γ rings assume a similar form. Let #s be the converter of the DC ring γ connected to the α ring. $\mu_{\text{inv}\beta}$ is the duty ratio of the inverter between β and α ring.

For the DC Rings β and γ the format of the equations is the same. Eq.5.7-5.9 give the system equations for the β ring. The subscription p denotes the #p converter in the β ring.

$$L_{\beta\text{p}}\frac{di_{L\beta\text{p}}}{dt} = -(1-u_{\beta\text{p}})v_{C\beta\text{p}} + E_{\beta\text{p}} \tag{5.7}$$

$$C_{\beta\text{p}}\frac{v_{C\beta\text{p}}}{dt} = (1-u_{\beta\text{p}})i_{\beta\text{p}} - i_{T\beta\text{p}} + i_{T\beta(\text{p}-1)} - \frac{v_{C\beta\text{p}}}{R_{2T\beta\text{p}}} - \nu\mu_{\text{inv}\beta}i_{\text{inv}\beta} \tag{5.8}$$

$$L_{T\beta\text{p}}\dot{i}_{T\beta\text{p}} = v_{C\beta\text{p}} - v_{C\beta(\text{p}+1)} - R_{1T\beta\text{p}}i_{T\beta\text{p}} \tag{5.9}$$

Here, $\nu = 1$ for the converter $\#p$ which is connected to the AC ring α.

5.2 Open Loop Controller

This section will explore the design of the open loop system by applying the steady state analysis to the AC ring, the DC ring as well as the connecting inverters. The open loop duty ratio can be obtained by fixing the desired output voltages for the α ring, the β, γ rings and the connecting inverters. The application of the open loop duty ratio, gives the behaviour of the system without feedback through the nonlinear PBC.

5.2.1 Steady state analysis for AC Ring

For the #n buck-type inverter in the α ring, the desired voltage is a AC waveform in the form $\bar{v}_{C\alpha\text{n}} = A_{\alpha\text{n}}\sin(2\pi f_{\alpha\text{n}}t)$ Here, the angular frequency $\omega_{\alpha\text{n}} = 2\pi f_{\alpha\text{n}}$.

Eqs.(5.1)-(5.3) give the mathematical description of the system for any #n buck-type inverter system. Steady sate analysis is employed to formulate the equilibrium values for the desired inductor current ($\bar{i}_{L\alpha n}$) and the desired disspiation current ($\bar{i}_{T\alpha n}$) for a given desired voltage $v_{C\alpha n} = \bar{v}_{C\alpha n}$. Then, it will be possible to formulate the sinusoidal duty ratio $U_{\alpha n}$.

It is possible to analytically solve the linear differential equation Eq.(5.3), by employing the known values of $v_{C\alpha n} = \bar{v}_{C\alpha n}$, $v_{C\alpha n+1} = \bar{v}_{C\alpha n+1}$. The solution is given by Eq.(5.10).

$$\begin{aligned}\bar{i}_{T\alpha n} =& \frac{R_{1\alpha n}A_{\alpha n}}{R_{1\alpha n}^2 + L_{T\alpha n}^2\omega_{d\alpha n}}(\sin(\omega_{\alpha n}t) - \frac{\omega_{\alpha n}L_{T\alpha n}}{R_{1\alpha n}}\cos(\omega_{\alpha n}t)) \\ &+ \frac{R_{1\alpha n}A_{\alpha n+1}}{R_{1\alpha n}^2 + L_{T\alpha n}^2\omega_{\alpha n+1}}(\sin(\omega_{\alpha n+1}t) - \frac{\omega_{\alpha n+1}L_{T\alpha n}}{R_{1\alpha n}}\cos(\omega_{\alpha n+1}t)) + k_\alpha e^{-(R_{1\alpha n}/L_{\alpha n})t}\end{aligned} \tag{5.10}$$

Here, k_α is the constant of integration. The value of k_α is obtained by applying the initial condition $i_{Td}(0) = 0$.

$$k_\alpha = \frac{A_{\alpha n}\omega_{\alpha n}L_{T\alpha n}}{R_{1\alpha n}^2 + L_{\alpha n}^2\omega_{\alpha n}} - \frac{A_{\alpha n+1}\omega_{\alpha n+1}L_{T\alpha n}}{R_{1\alpha n}^2 + L_{\alpha n}^2\omega_{\alpha n+1}} \tag{5.11}$$

Then, the equilibrium value of $i_{L\alpha n}$ can be obtained by solving Eq.(5.1) with $i_{T\alpha n} = \bar{i}_{T\alpha n}$.

$$\bar{i}_{L\alpha n} = C_{\alpha n}\dot{\bar{v}}_{C\alpha n} - \bar{i}_{T\alpha n} + \bar{i}_{T\alpha n-1} + \frac{\bar{v}_{C\alpha n}}{R_{2\alpha n-1}} + \eta\bar{i}_{\alpha\beta} + \nu\bar{i}_{\alpha\gamma} \tag{5.12}$$

Finally, the open loop duty ratio $U_{\alpha n}$ is obtained from Eq.(5.2) by substituting $i_{L\alpha n} = \bar{i}_{L\alpha n}$ and given in Eq.(5.17).

$$U_{\alpha n} = \frac{L_{\alpha n}}{E_{\alpha n}}[C_{\alpha n}\ddot{\bar{v}}_{C\alpha n} - \dot{\bar{i}}_{T\alpha n} + \dot{\bar{i}}_{T\alpha n-1} + \frac{\dot{\bar{v}}_{C\alpha n}}{R_{2\alpha n-1}}] + \frac{\bar{v}_{C\alpha n}}{E_{\rm n}} + \eta\ddot{\bar{i}}_{\alpha\beta} + \nu\ddot{\bar{i}}_{\alpha\gamma} \tag{5.13}$$

5.2.2 Steady state analysis for connection inverters

As the setting for the AC ring, the steady state analysis can be applied to the inverters between the rings. The desired voltage is set to be the same as the instantaneous desired voltage of the AC ring: $v_{{\rm inv}\beta} = A_\beta \sin(\omega_\beta t)$. Then, by analytically solving Eq.(5.6), we can get the following.

$$\begin{aligned}\bar{i}_{\alpha\beta} =& \frac{R_{\alpha\beta}A_\beta}{R_{\alpha\beta}^2 + L_{\alpha\beta}^2\omega_\beta}(\sin(\omega_\beta t) - \frac{\omega_\beta L_{\alpha\beta}}{R_{\alpha\beta}}\cos(\omega_\beta t)) - \frac{R_{\alpha\beta}A_{\alpha 0}}{R_{\alpha\beta}^2 + L_{\alpha\beta}^2\omega_{\alpha 0}}(\sin(\omega_{\alpha 0}) \\ &- \frac{\omega_{\alpha 0}L_{\alpha\beta}}{R_{\alpha\beta}}\cos(\omega_{\alpha 0})) + k_{\alpha\beta}e^{-(R_{\alpha\beta}/L_{\alpha\beta})t}\end{aligned} \tag{5.14}$$

$$k_{\alpha\beta} = \frac{A_\beta\omega_\beta L_{\alpha\beta}}{R_{\alpha\beta}^2 + L_{\alpha\beta}^2\omega_\beta} - \frac{A_{\alpha 0}\omega_{\alpha 0}L_{\alpha\beta}}{R_{\alpha\beta}^2 + L_{\alpha\beta}^2\omega_{\alpha 0}} \tag{5.15}$$

The other state variables are given as follows.

$$\bar{i}_{\text{inv}\beta} = C_{\alpha\beta}\dot{\bar{v}}_{\text{inv}\beta} - \bar{i}_{\alpha\beta} + \frac{\bar{v}_{\text{inv}\beta}}{R_{\text{inv}\beta}} \tag{5.16}$$

$$U_{\alpha\beta} = \frac{L_{\alpha\beta}}{\bar{v}_{C\beta\text{q}}}[C_{\alpha\beta}\ddot{\bar{v}}_{\text{inv}\beta} + \dot{\bar{i}}_{\alpha\beta} + \frac{\dot{\bar{v}}_{\text{inv}\beta}}{R_{\text{inv}\beta}}] + \frac{\bar{v}_{\text{inv}\beta}}{\bar{v}_{C\beta\text{q}}} \tag{5.17}$$

5.2.3 Steady state analysis of DC rings

The desired steady state of the DC outputs is constant, thus the derivative of the state variables become zero. Thus, the steady state variables for the β ring are given as below. Here the open loop duty ratio ($U_{\beta\text{p}}$) can be easily obtained from Eq.5.19.

$$\begin{aligned}\bar{i}_{L\beta\text{p}} = &\frac{E_{\beta\text{p}}}{R_{2T_{\beta\text{p}-1}}(1-U_{\beta\text{p}})^2} + \frac{1}{R_{1T_{\beta\text{p}}}}\left[\frac{E_{\beta\text{p}}}{(1-U_{\beta\text{p}})^2} - \frac{E_{\beta\text{p}+1}}{(1-U_{\beta\text{p}+1})(1-U_{\beta\text{p}})}\right] \\ &- \frac{1}{R_{1T_{\beta\text{p}-1}}}\left[\frac{E_{\beta\text{p}-1}}{(1-U_{\beta\text{p}-1})(1-U_{\beta\text{p}})} - \frac{E_{\beta\text{p}}}{(1-U_{\beta\text{p}})^2}\right]\end{aligned} \tag{5.18}$$

$$\bar{v}_{C\beta\text{p}} = \frac{E_{\beta\text{p}}}{(1-U_{\beta\text{p}})} \tag{5.19}$$

$$\bar{i}_{T_{\beta\text{p}}} = \frac{1}{R_{1T_{\beta\text{p}}}}\left[\frac{E_{\beta\text{p}}}{(1-U_{\beta\text{p}})} - \frac{E_{\beta\text{p}+1}}{(1-U_{\beta\text{p}+1})}\right] \tag{5.20}$$

The steady state analysis for the γ ring can be obtained similarly.

5.3 Port-Controlled Hamiltonian Modelling

The system model using the PCH framework is given by Eq.(5.22) as in the form given in [47].

$$\mathbf{D}\dot{\boldsymbol{x}}(t) = [\mathbf{J} - \mathbf{R}]\frac{\partial H}{\partial x} + \mathbf{G}(\boldsymbol{x})\mathbf{E} \tag{5.21}$$

$$\boldsymbol{y} = \mathbf{G}^T(\boldsymbol{x})\frac{\partial H}{\partial \boldsymbol{x}} \tag{5.22}$$

For total m inverters/converters in the ring network, $\boldsymbol{x}$, the state of the system, is a $((\text{m} \times 3) \times 1)$ column matrix of all the inductance currents and capacitance voltages. The matrix $\mathbf{D}$ is a diagonal matrix of the capacitance and inductance values of the corresponding currents and voltages. The structure matrix, $\mathbf{J}$, is a $((\text{m} \times 3) \times (\text{m} \times 3))$

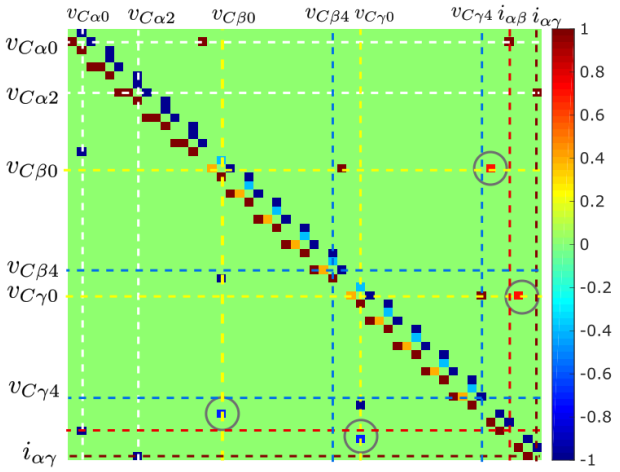

Figure 5.3: Structure matrix as a function of time: $\mu_{\text{inv}\beta}$, $\mu_{\text{inv}\gamma} = -0.7$.

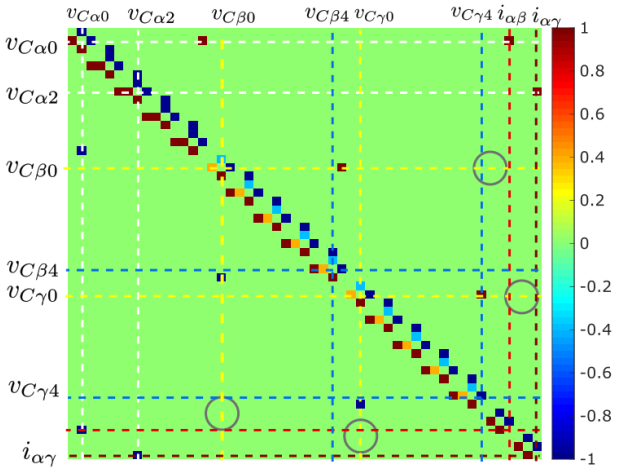

Figure 5.4: Structure matrix as a function of time: $\mu_{\text{inv}\beta}$, $\mu_{\text{inv}\gamma} = 0$.

skew-symmetric matrix. As the input voltage to the connecting inverters is the output voltage of inverter #q of ring β and converter #r of ring γ, the structure matrix $\mathbf{J}$ is a function of $\mu_{\text{inv}\beta}$ and $\mu_{\text{inv}\gamma}$ as well as the DC-DC converter duty ratios $\mu_{\beta\text{p}}$ and $\mu_{\gamma\text{s}}$. A $((\text{m} \times 3) \times (\text{m} \times 3))$ diagonal matrix, $\mathbf{G}$, is a function of $\mu_{\alpha\text{n}}$. $\mathbf{J}$ and $\mathbf{G}$ are determined from the structure as per Kirchoff's law. $\mathbf{E}$ is a $((\text{m} \times 3) \times 1)$ matrix of the external DC inputs to the corresponding inverters. $\mathbf{R}$, the dissipation martix, is $((\text{m} \times 3) \times (\text{m} \times 3))$ a diagonal matrix, with resistance elements. Finally, H is the Hamiltonian of the system which, corresponds to the energy of the system.

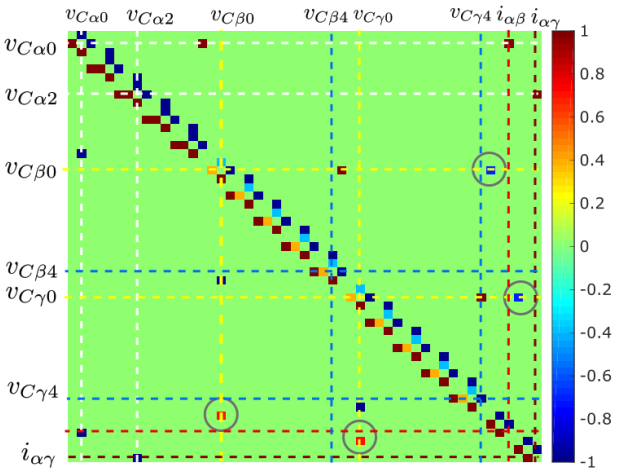

Figure 5.5: Structure matrix as a function of time: $\mu_{\text{inv}\beta}$, $\mu_{\text{inv}\gamma} = 0.7$.

5.4 Consideration as a network

As the structure matrix, **J** is the function of the sinusoidal duty ratio of the inverters, it is a function of time. The structure matrix represents the connection of all the state variables. It indicates whether a pair of state variables are connected to each other. Figs.5.5-5.3 give a graphical representation of the structure matrix of the proposed distributed generation system. It visualizes the structure of the matrix. Here, for Figs.5.5-5.3 $\mu_{\beta\text{p}}$ and $\mu_{\gamma\text{s}}$= 0.6. As $\mu_{\text{inv}\beta}$ and $\mu_{\text{inv}\gamma}$ are sinusoidal, the structure matrix is shown for three values of $\mu_{\text{inv}\beta}$ and $\mu_{\text{inv}\gamma}$.

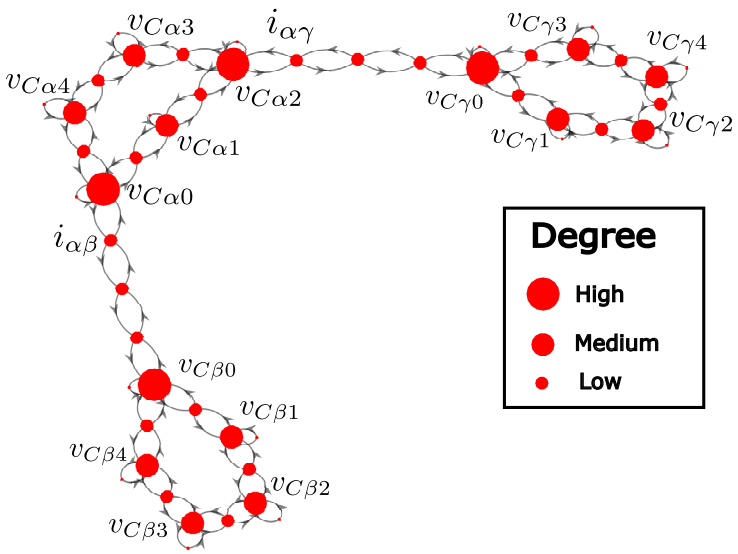

Figure 5.6: Graph representation with degree centrality analysis

As the proposed network comprises of multiple converter/inverters units, it is desirable to know the connection properties to identify the most important units of the entire network. For a smaller system with fewer number of units, the important units are evident, but for larger systems, not necessarily in ring coupled formulation, such analysis is important to figure out the weak areas of the network. For the proposed AC-DC distributed generation system, the centrality of the network is shown in the graph representation shown in Fig.5.6. Here, the state variables are represented as nodes of the graph. The size of the nodes is proportional to the degree centrality of the node, indicating that the biggest nodes are the ones with the highest degree. Failure of the higher degree nodes is more likely to result in the failure of the network as a whole [76]. Thus, this information helps to make the network more robust by safeguarding the vulnerable nodes [77].

5.5 Application of Feedback through Passivity-based Control

We investigate whether it is possible for PBC to be applied to the distributed generation system with AC and DC voltage output. As shown in Chapters 3 and 4, the quadratic function of errors, given again for reference in Eq.5.23

$$H_d = \frac{1}{2}\boldsymbol{e}^T\mathbf{D}\boldsymbol{e}, \quad \boldsymbol{e} = \boldsymbol{x} - \boldsymbol{x}_d \tag{5.23}$$

Then, the control rule with nonlinear PBC can be formulated for the entire network as given below.

$$\mathbf{D}\dot{\boldsymbol{x}}_d(t) = (\mathbf{J} - \mathbf{R})\boldsymbol{x}_d(t) + \mathbf{E} + \mathbf{R}_I(\boldsymbol{x} - \boldsymbol{x}_d(t)) \tag{5.24}$$

The damping injection, $\mathbf{R}_I$ has the same properties as stated in Chapter 3 and Chapter 4. For stabilization through non-linear PBC we take into consideration the zero dynamics of the system to confirm the structural properties in addition to the mathematical analysis mentioned above, to apply feedback control. The zero dynamics analysis indicates that the distributed generation network system is a non-minimum phase system with respect to the output voltage, but a minimum phase system with respect to the input inductor current. Thus, the chosen method of feedback is with the inductor current rather than the output voltage.

The nonlinear control equations are obtained from the exogenous control system given in Eq.(5.24). They play the role of a reference model with a stronger dissipation structure than the original system underscored by the added damping. The control equations are obtained separately for the AC ring, the DC rings and the connecting inverters as was done for the steady state analysis. The control equations for the AC ring are given in Eqs. (5.25)-(5.27).

$$\mu_{\alpha \mathrm{n}} = [L_{\mathrm{n}} \dot{\bar{i}}_{L\mathrm{n}} + \tilde{v}_{C\mathrm{n}} - R_{\alpha \mathrm{n}k}(i_{L\mathrm{n}} - \bar{i}_{L\mathrm{n}})]/E_{\alpha \mathrm{n}} \tag{5.25}$$

$$C_{\alpha \mathrm{n}} \dot{\tilde{v}}_{C\alpha \mathrm{n}} = \bar{i}_{L\alpha \mathrm{n}} - \tilde{i}_{T\alpha \mathrm{n}} + \tilde{i}_{T\alpha \mathrm{n}-1} - \big[\frac{\tilde{v}_{C\alpha \mathrm{n}}}{R_{2\alpha \mathrm{n}-1}}\big] + \eta \tilde{i}_{\alpha\beta} + \zeta \tilde{i}_{\alpha\gamma} \tag{5.26}$$

$$L_{T\alpha \mathrm{n}} \dot{\tilde{i}}_{T\alpha \mathrm{n}} = \tilde{v}_{C\alpha \mathrm{n}} - \tilde{v}_{C\alpha \mathrm{n}+1} - R_{1\alpha \mathrm{n}} \tilde{i}_{T\alpha \mathrm{n}} \tag{5.27}$$

Here $\boldsymbol{x}_{d\alpha \mathrm{n}} = [\bar{i}_L \ \tilde{v}_C \ \tilde{i}_{LT}]^{\mathrm{T}}$ is the desired dynamic state vector of the controller for the inverters in the AC ring and $\mu_{\alpha \mathrm{n}}$ is the feedback duty cycle. Next, the control equations for the inverters are obtained as follows.

$$\mu_{\mathrm{inv}\beta} = [L_{\mathrm{inv}\beta} \dot{\bar{i}}_{L\mathrm{inv}\beta} + \tilde{v}_{C\mathrm{inv}\beta} - R_{\alpha\beta k}(i_{L\mathrm{inv}\beta} - \bar{i}_{L\mathrm{inv}\beta})]/\bar{v}_{C\beta \mathrm{q}} \tag{5.28}$$

$$C_{\mathrm{inv}\beta} \dot{\tilde{v}}_{C\mathrm{inv}\beta} = \bar{i}_{L\mathrm{inv}\beta} - \big[\frac{\tilde{v}_{C\mathrm{inv}\beta}}{R_{2\mathrm{n}-1}}\big] \tag{5.29}$$

$$L_{\alpha\beta} \dot{\tilde{i}}_{T\alpha\beta} = \tilde{v}_{\mathrm{inv}\beta} - \tilde{v}_{C\alpha \mathrm{n}} - R_{\alpha\beta} \tilde{i}_{\alpha\beta} \tag{5.30}$$

For the connecting inverter control equations, the DC input is given by the steady state voltage of the corresponding DC/DC converter of the DC ring, in this case given by #q. The equations for the connecting inverter between $\gamma - \alpha$ rings can be obtained in a similar manner. Finally, the control rule for the DC rings is given by Eqs.(5.31)-(5.33).

$$\mu_{\beta \mathrm{p}} = \frac{1}{\tilde{v}_{C\beta \mathrm{p}}} \big[E_{\beta \mathrm{p}} + R_{\beta \mathrm{p}k}(i_{L\beta \mathrm{p}} - \bar{i}_{L\beta \mathrm{p}})\big] + 1 \tag{5.31}$$

$$C_{\beta \mathrm{p}} \dot{\tilde{v}}_{C\beta \mathrm{p}} = (1 - \mu_{\beta \mathrm{p}}) \bar{i}_{L\beta \mathrm{p}} - \tilde{i}_{T\beta \mathrm{p}} + \tilde{i}_{T\beta \mathrm{p}-1} - \big[\frac{\tilde{v}_{C\beta \mathrm{p}}}{R_{2\beta \mathrm{p}-1}}\big] - \mu_{\mathrm{inv}\beta} \bar{i}_{\mathrm{inv}\beta} \tag{5.32}$$

$$L_{T\beta \mathrm{p}} \dot{\tilde{i}}_{T\beta \mathrm{p}} = \tilde{v}_{C\beta \mathrm{p}} - \tilde{v}_{C\beta \mathrm{p}+1} - R_{1\beta \mathrm{p}} \tilde{i}_{T\beta \mathrm{p}} \tag{5.33}$$

The constant desired inductor current $\bar{i}_{L\alpha \mathrm{n}}$, $\bar{i}_{L\mathrm{inv}\beta}$, $\bar{i}_{L\mathrm{inv}\gamma}$, $\bar{i}_{L\beta \mathrm{p}}$ and $\bar{i}_{L\gamma \mathrm{s}}$ are obtained from the steady state analysis. The state inductor current for all converter/inverter units is used for feedback control with corresponding damping $R_{\alpha \mathrm{n}k}$, $R_{\mathrm{inv}\beta k}$, $R_{\mathrm{inv}\gamma k}$, $R_{\beta \mathrm{p}k}$ and $R_{\gamma \mathrm{s}k}$.

With the application of nonlinear PBC, the value of the duty ratio μ is evaluated at every instant t depending on the input, the system parameters, and the desired output of the system. That is, μ depends on time and the state.

Table 5.1: Parameters for α-ring

Parameter	Value	Unit
Parameter	Value	Unit
$E_{\alpha \mathrm{n}}$	36	V
$L_{\alpha \mathrm{n}}$	46	mH
$C_{\alpha \mathrm{n}}$	100	μF
$L_{T\alpha \mathrm{n}}$	15	mH
$R_{1\alpha \mathrm{n}}$	50	Ω
$R_{2\alpha \mathrm{n}}$	100	Ω
$\bar{v}_{C\alpha \mathrm{n}}$ $(A_{\mathrm{n}} = 13)$	$13\sin(376 * t)$	V

Table 5.2: Connecting Inverters

Parameter	Value	Unit
Parameter	Value	Unit
$L_{\mathrm{inv}\beta}$	16	mH
$C_{\mathrm{inv}\beta}$	100	μF
$R_{\mathrm{inv}\beta}$	100	Ω
$R_{\alpha\beta}$	10	Ω
$L_{\alpha\beta}$	16	mH

Table 5.3: Parameters for β, γ-ring

Parameter	Value	Unit
$E_{\beta \mathrm{p}}$	18	V
$L_{\beta \mathrm{p}}$	46	mH
$C_{\beta \mathrm{p}}$	100	μF
$L_{T\beta \mathrm{p}}$	15	mH
$R_{1\beta \mathrm{p}}$	50	Ω
$R_{2\beta \mathrm{p}}$	100	Ω
$\tilde{v}_{C\beta \mathrm{p}}$	40	V

5.6 Numerical Simulations

The simulation results are obtained for five converters coupled in a ring form are given in this section. The numerical simulations were carried out on ode45 solver Simulink (Version 8.7 R2016a).

5.6.1 Simulation results for a balanced system

In this section, results are presented for numerical simulations performed first, for the open loop balanced system and then for the balanced system with feedback through PBC. A balanced state is when the parameters for all converters/inverters in each ring are set at the same values respectively. Additionally, the dissipation between the converters/inverters (L_T) and the input voltage (E) are also set at the same value for each ring respectively. This creates a natural balance within each ring, but not necessarily between the rings. These values are set as given in Table. 5.1-5.3 for α, β, γ rings and the connecting inverters.

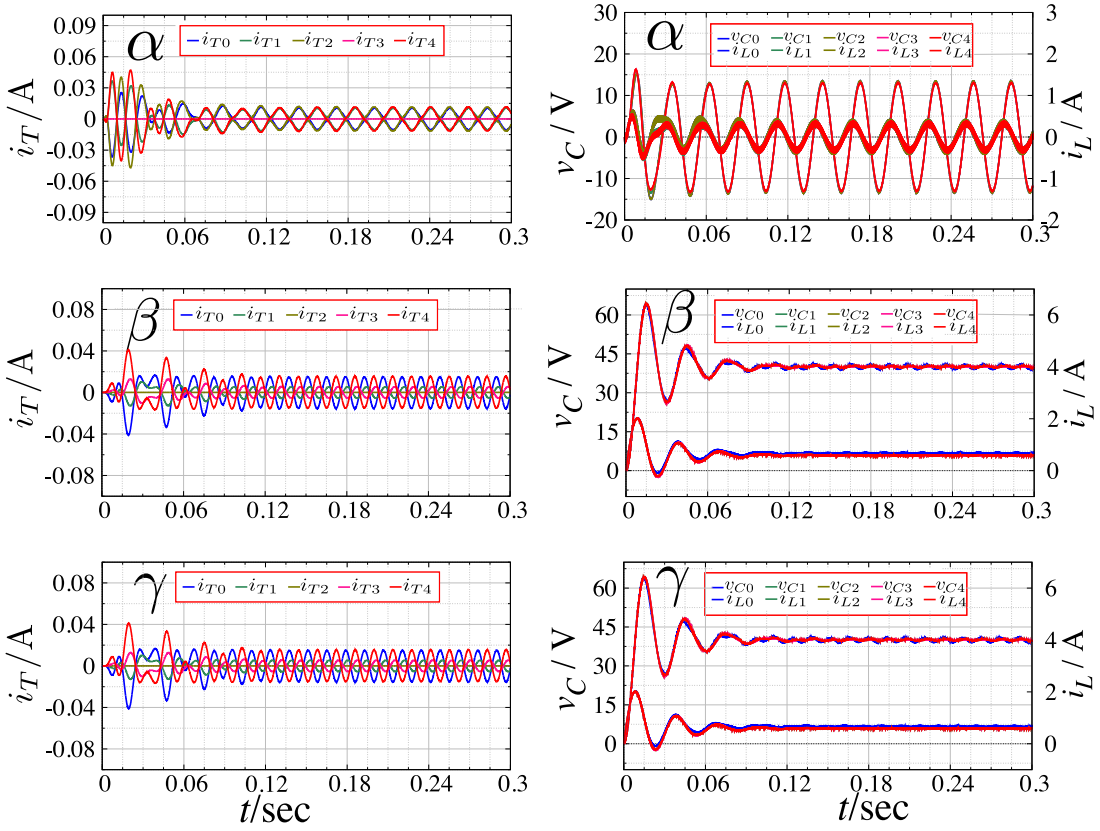

Figure 5.7: Numerical Simulation for balanced open loop system without the applicaiton of PBC.

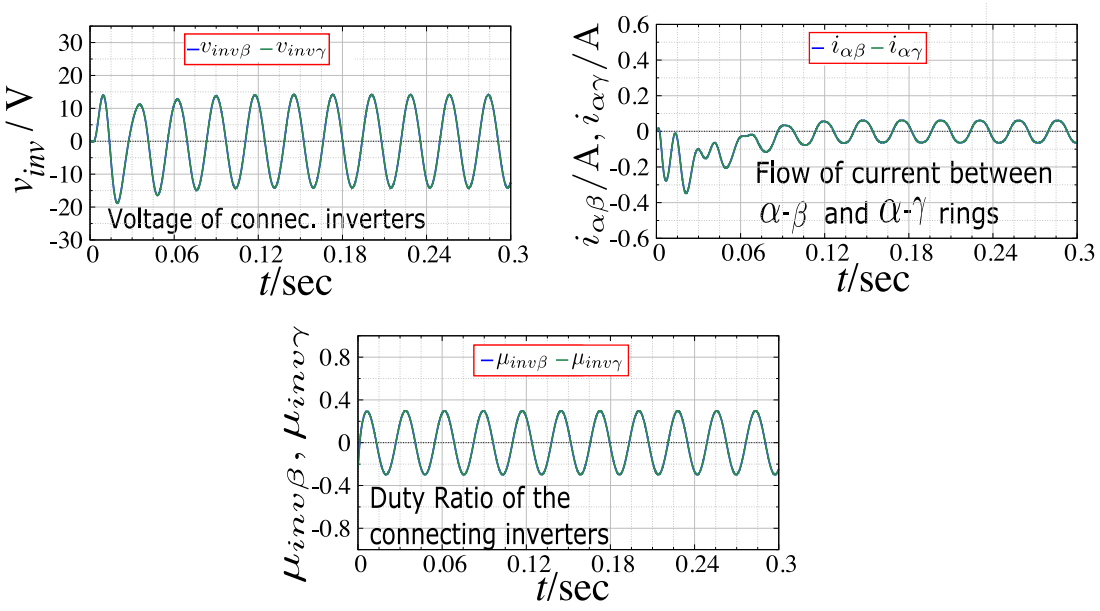

Figure 5.8: Numerical Simulation for balanced open loop system system without the applicaiton of PBC.

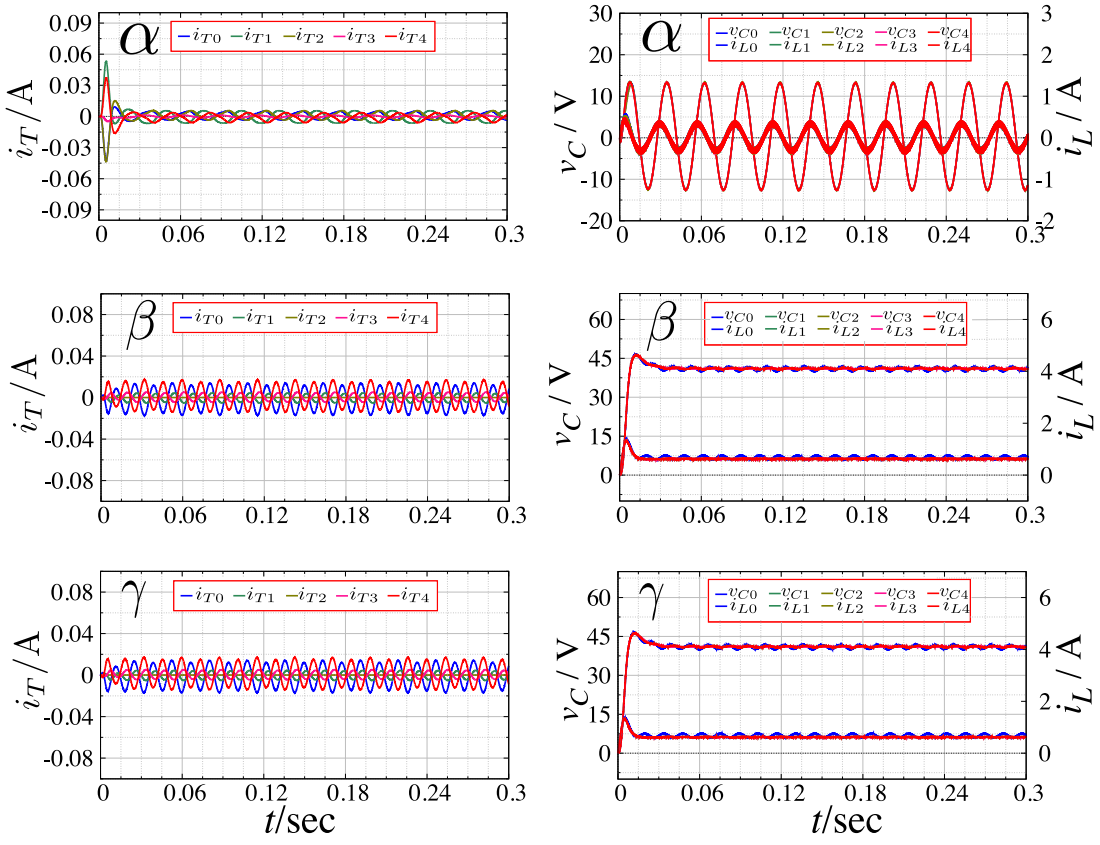

Figure 5.9: Numerical Simulation for balanced system with the applicaiton of feedback control through PBC.

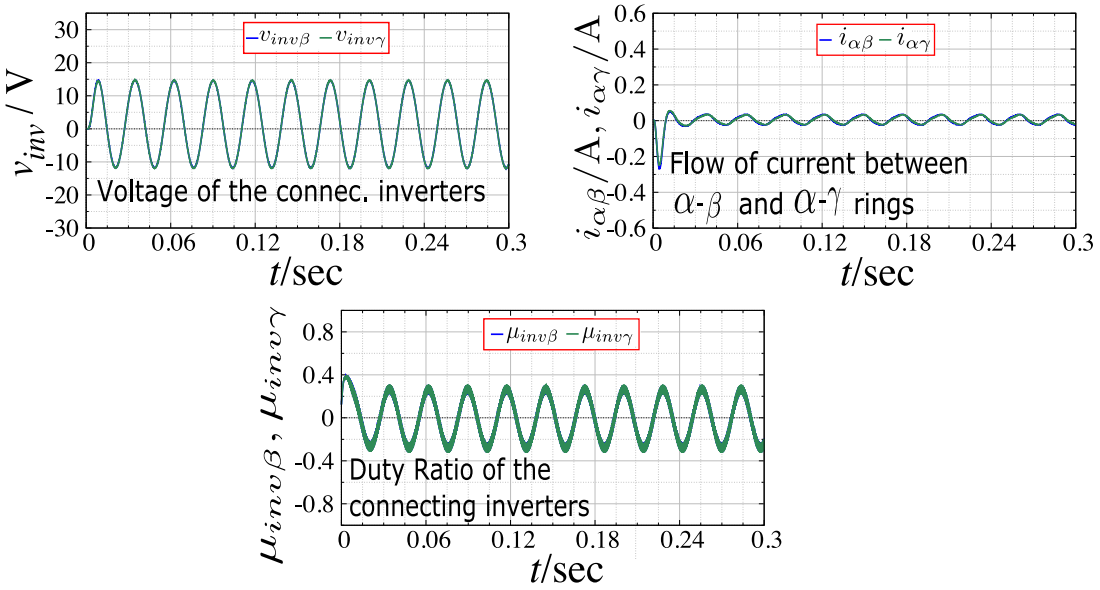

Figure 5.10: Numerical Simulation for balanced system with the applicaiton of feedback control throughPBC.

Figure 5.7 gives the result of numerical simulation for the distributed generation system without the application of PBC (open loop system). Here, the duty ratios for the rings $U_{\alpha \mathrm{n}}$, $U_{\mathrm{inv}\beta}$, $U_{\mathrm{inv}\gamma}$, $U_{\beta \mathrm{p}}$ and $U_{\gamma \mathrm{s}}$ are set at a constant value estimated at the steady state analysis. Any unforeseeable disturbance in the system will not be acted on but may affect the system output adversely. It is seen that all three rings settle on the desired output voltage after the transient.

The parameters for the β and γ ring have been set to be the same, creating symmetry and resulting in the output for the two DC rings to exactly equal. The duty ratio for the DC rings is constant, and sinusoidal for the α ring and the inverters as shown in Fig.5.7. The connection parameters for the inverters are given by Fig.5.8. Even beyond the transient, it is seen that current flows between the converter/inverter units in the rings ($i_{T\alpha \mathrm{n}}$, $i_{T\beta \mathrm{p}}$, $i_{T\gamma \mathrm{s}}$) as well as between the α-β and α-γ rings as indicated by $i_{\alpha\beta}$ and $i_{\alpha\gamma}$ given by Fig.5.8.

Next we look at simulations results when feedback control is applied through PBC. PBC results in an output dynamic feedback controller which induces a shaped closed loop energy and enhances the closed loop damping of the system. The damping has the condition $\mathbf{R} + \mathbf{R}_I > 0$. Then it was set and kept at $\mathbf{R}_k = 20$ for all the converter/inverter units. It is clearly seen that now the duty ratio is not constant, but a function of time, this confirms the application of feedback control through passivity. The output voltage shows a faster convergence to the desired value with damped oscillations for the transient as shown by Fig.5.9. The flow of current through the rings (i_T) as well as between the rings ($i_{\alpha\beta}$, $i_{\alpha\gamma}$) is reduced, allowing the system to attain stability by maintaining the passivity of entire network. The parameters for the connecting inverters are as shown in Fig.5.10

5.6.2 Simulations for system with disturbance

Imbalance occurs in the ring coupled system when converters in the ring and/or the dissipation between two neighbouring converters have different parameter values. In the following simulations we consider imbalance by varying input voltage values for the β and γ DC rings. Practically, as the DC rings represent a distributed network in remote villages, it is assumed that the input voltage from the solar arrays might change depending on the weather conditions. The simulated change in input voltage and the corresponding output of the open loop network is shown in Fig.5.11. Here, PBC is not applied, and the output is based on the open loop duty ratio calculated by the steady state analysis. Fig.5.12 shows the connection parameters for the same. As the input varies, the system shows the transient from one state to another creating imbalance, and a noticeable flow of current between the rings. The inverter output voltage for the β and γ rings varies according to the transient created by the changing input.

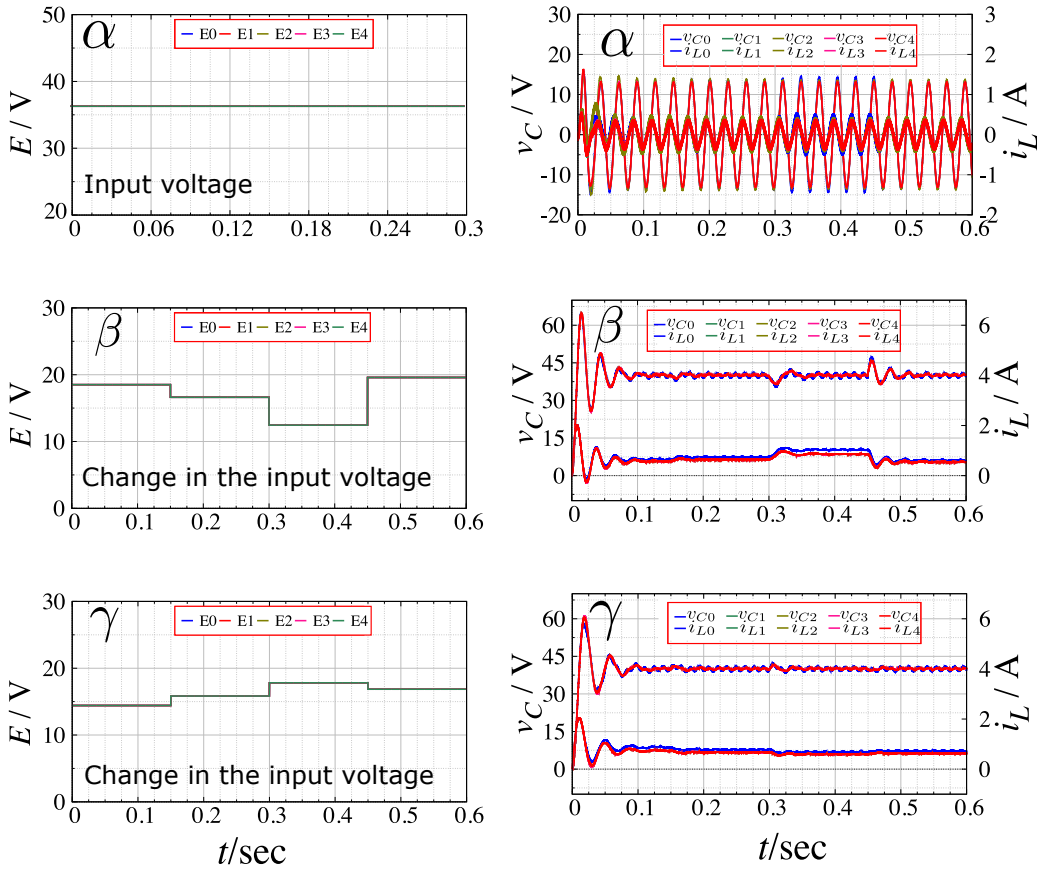

Figure 5.11: Numerical Simulation for varying inputs for the open loop system.

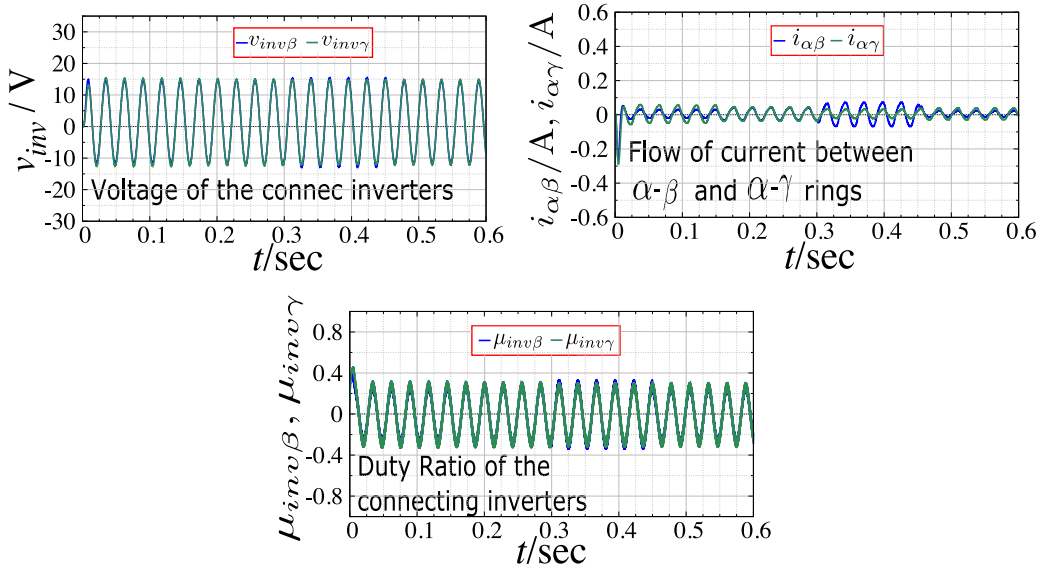

Figure 5.12: Numerical Simulation for varying inputs for the open loop system.

For the same change in input voltage, the application of PBC is as shown in Fig.5.13. The output voltage is seen to be devoid transient disturbances. The DC as well as the AC outputs are seen to be much closer to the desired values as compared to the original system. Fig.5.14 shows the duty ratio of connecting inverters, the output voltage and the flow of current between the rings as PBC is applied. As passivity is invariant under negative feedback interconnection, the connection of two passive systems is a passive system. Thus, PBC is applied to the entire network by ensuring the passivity of individual converter/inverter units, ensuring the passivation of the whole network. The results allude to this fact. The flow of the line current through the ring, at any point of time is zero, indicating that the entire system retains passivity. This is true even when there is flow of energy between individual converters/inverters.

5.7 Discussions

The engineering of a hybrid distributed generation system has to be consistent with a suitable and affordable extension of the network on the same portability grade. For this reason, the addition of different generation units as integral part of the system needs to be an undemanding and straightforward task [10, 78]. In the hybrid distributed generation network presented in this chapter, the numerical simulations have been carried out for a limited number of generation units per ring and limited number of DC rings connected to the main AC ring. The extension of this model to a practical system applicable to small villages must be discussed. As is shown in Eqs.(5.1)-(5.3), Eq.(5.4)-(5.6) and Eq.(5.7)-(5.9), the mathematical design facilitates the inclusion of further generator units. The same goes for the number of DC rings connected to the 'main' ring. The system design presented does not cause a loss of generality. The control equations have also been laid out to include an arbitrary number of units as well as DC rings.

The structure matrix **J** of the PCH modelling presents two highly desirable outcomes: not only is it necessary for system control but can also act as an adjacency matrix for analysis of vital system components and performances. The adjacency matrix (given by Figs.5.3-5.5) reveals the dynamic connection between all nodes of the network at a glance. For expansion it will be able to incorporate new node connections in the ring as well as jump connections between rings. Thus, the adjacency matrix provides valuable indicators of the distributed generation grid when expanded by adding a large number of units. Within this network representation framework, further analysis can be conducted to understand the robustness properties [79,80]. Here, robustness implies the ability of the distributed generation grid to be resilient to external disturbances one of which is failure to operate smoothly subject to expansion [81]. The vulnerable nodes in the network can be detected, thus making expansion achievable with keeping the safety. Here, the numerical results are in congruence with the centrality analysis presented in Sec. 5.3. The degree centrality graph presented in Fig. 5.6 predicted the most significant nodes to be the voltages to be $v_{C\alpha 0}$, $v_{C\alpha 2}$, $v_{C\beta 0}$, and $v_{C\gamma 0}$. This is confirmed from the numerical results of the original system (without control) when the input voltage is varied as shown in

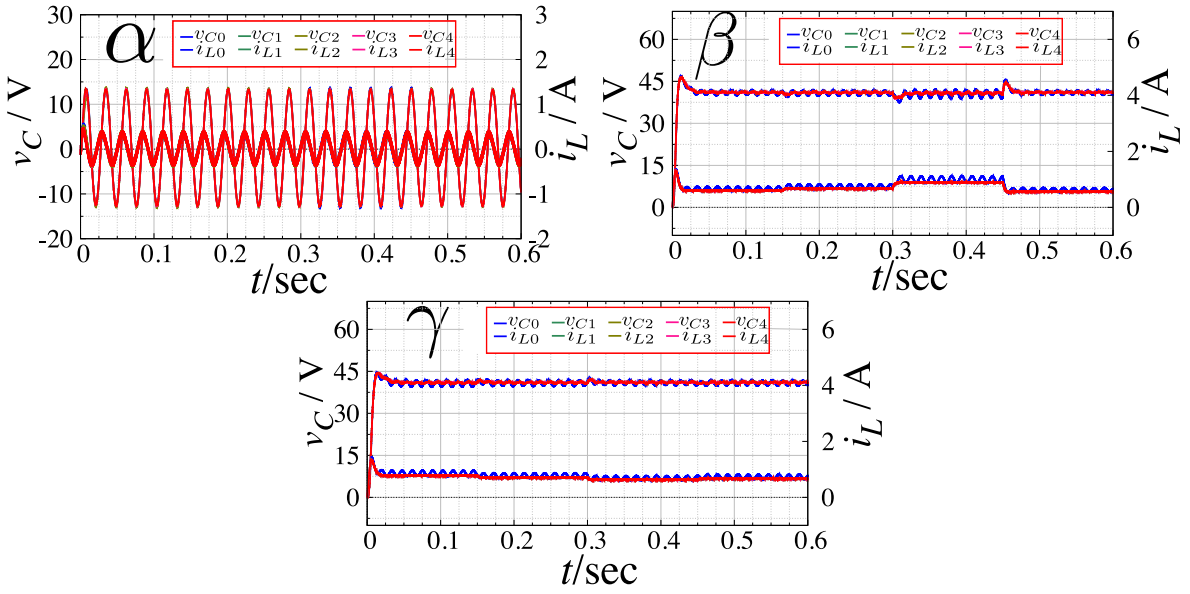

Figure 5.13: Numerical Simulation for varying inputs system with applicaiton of PBC.

Fig. 5.11. For an unbalanced system, the states of the connecting converters α_0, α_2, β_0, and γ_0 are the only ones that vary from the desired trajectory. For the same conditions, PBC exhibits accelerated convergence to the desired state.

The aim of the network is to have multiple consumers connected together, with all

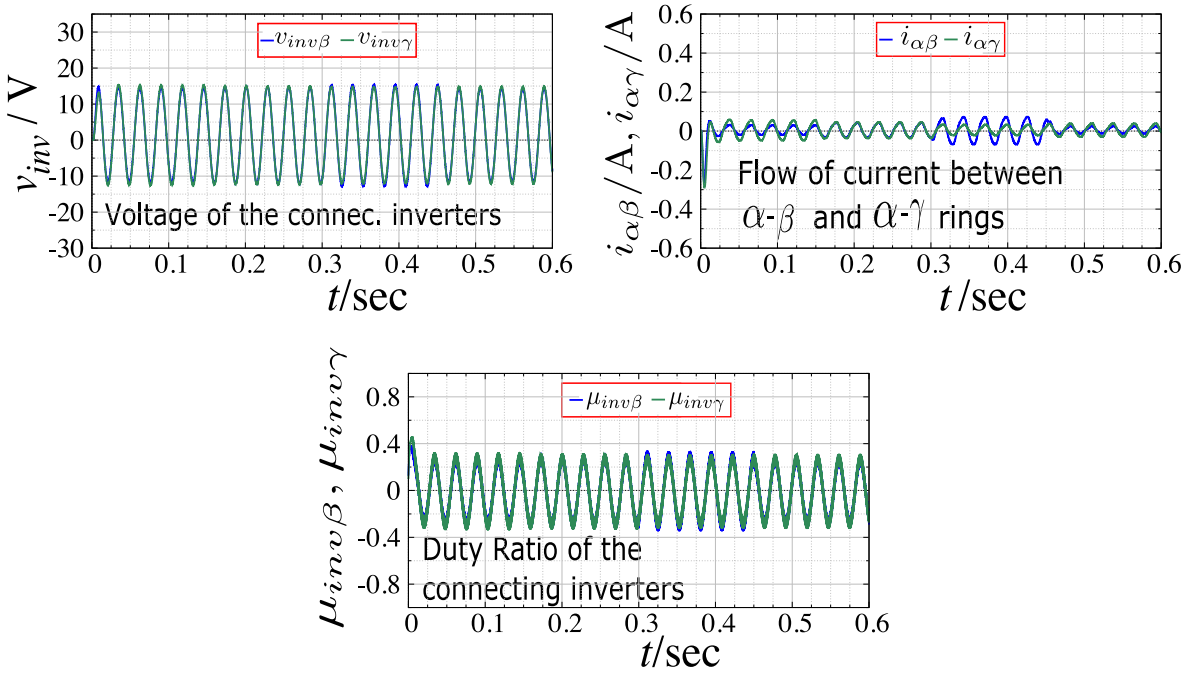

Figure 5.14: Numerical Simulation for varying inputs system with applicaiton of PBC.

units operating synchronously with equal output voltages. It is assumed that the consumers are scattered over a large area with varying distances between each other. The proposed hybrid network design considers the dissipation with a transmission line model. It enables incorporation of variable dissipation parameters potentially determined by the distance between the units. PCHM with its well ordered matrix structure allows effortless modification in the system parameters. It is well known that discrepancy in the output phase or frequency of the inverters in the AC-ring can cause undersirable interference effects throughout the AC-ring with rippling effects through the DC-rings as well. The issue of grid synchronization for the AC-ring, though not explored in this chapter, can be considered with the same strategy as presented in Chapter 4, with the application of PLLs in congruence with PBC. The synchronization of the outputs of the connecting inverters to that of the inverters in the AC-ring has to be underlined.

Based on the numerical simulations, it is clear that the AC as well as DC output with nonlinear PBC shows improved convergence time during transient operation. Nonlinear PBC takes into account the energy dynamics, and the physical structure of the original converter/inverter as well as its closed loop formulation. In Sec. 5.5 it was mathematically proven that the entire network achieves Lyapunov stability with the application of nonlinear PBC. Moreover, the system converges exponentially to the desired state with the addition of damping. The numerical results show coherence with the analytical solutions. For same input inductor and output capacitor values, the original system produces an under-damped transient response as opposed to the system with PBC, which shows a damped response.

Nonlinear controllers have shown to be exceptionally good at trajectory tracking as compared to their linear counterparts [82, 83]. It has been shown in comparitive studies that dependance on linearization objective renders the system fragile, making it less attractive in applications [82]. With the nonlinear PBC, the exogenous system described in Eqs.(5.25)-(5.33) is responsible for tracking the error based on the desired energy function. The controller anticipates the energy dynamics as well as the physical structure of the system, enhancing robustness and resilience to fluctuations during transient. The controller follows a time variant desired state-trajectory created by the exogenous system forcing the duty ratio of each of the converter/inverter to change as a function of time and is significant for the systems transient response. As the nonlinear exogenous system modifies the duty ratio based on the dynamic energy structure to track the desired state trajectory, the system rapidly converges to the steady state as shown in Fig. 5.9.

5.8 Conclusion

In this chapter we introduced a hybrid DC-AC distributed generation network, presented its mathematical formulation and proposed a method to stabilize the entire network based on the energy characteristics of its individual components with passivity-based control. PBC, with energy shaping and damping injection was discussed for the quadratic function of errors as the desired storage function. It was shown that with nonlinear passivity-based

control it was possible to stabilize a distributed generation system with DC as well as AC network components.

The application of passivity-based control was confirmed with numerical simulations. It was shown that by minimizing the desired storage function, it was possible to attain the user-defined desired output voltage by regulation of the duty cycle through feedback of the inductor current of the multiple power electronic inverters/converters in the network. Comparison to the dynamic behaviour of the original system suggests the successful application of PBC during transient operation. Numerical simulations were performed for a balanced case as well as under varying input to the network. The state variables of inductor current and capacitor output voltage as well as the current through the dissipation within each ring component of the network were obtained. The flow of current between the rings and the operation of the connecting inverters was investigated for both the original system as well as feedback control through PBC. The results indicate that the application of PBC significantly improves the system response time and drives the system to a stable equilibrium in an exponential time.

Chapter 6

Application of PBC for Multiple Equilibria

This chapter discusses the current-voltage (IV) characteristics of a solar array-DC/DC converter system. It is seen that systems consisting of power electronic devices and solar arrays show instabilities as well as chaotic behaviour [84, 85]. The energy function is modified to resonate the nonlinear properties shown by the system consisting of solar array and DC/DC converters [86]. PBC is applied with this modified energy function, by proving the function to be a Lyapunov function. Numerical simulations are performed to show the implementation of PBC for a ring coupled converter system with an energy function with multiple equilibria. The multiple equlibria can alter the state of the system within the nature of the system characteristics with a small perturbation.

6.1 Dual Equilibrium Storage Function

6.1.1 Solar Array-DC/DC Converter systems

For power generation using solar arrays, dispersed generation systems will have input power from solar cells. DC/DC converters are employed to convert the solar power into desirable DC voltage [87]. Thus, the system will comprise of both solar arrays and DC/DC converters. Considering the ring coupled converter system discussed in Chap.3, and focusing on solar arrays as the DC inputs (E_{n}) to this system, it is necessary to look at the characteristics of a solar array-DC/DC converter system.

Here, we consider the simplified model of a stand-alone generation system, i.e solar arrays as inputs connected to DC/DC converters neglecting the connection of batteries, further regulators etc for studying the dynamic behaviour of the system. For application in DC stand-alone grid systems, the point-of-load converters, i.e converters near the loads, when regulated tightly act as constant power loads when receiving sufficient input [85,88]. These CPL characteristics of the DC/DC converters connected in stand-alone systems combined with the well known characteristics of solar arrays, give rise to some interesting

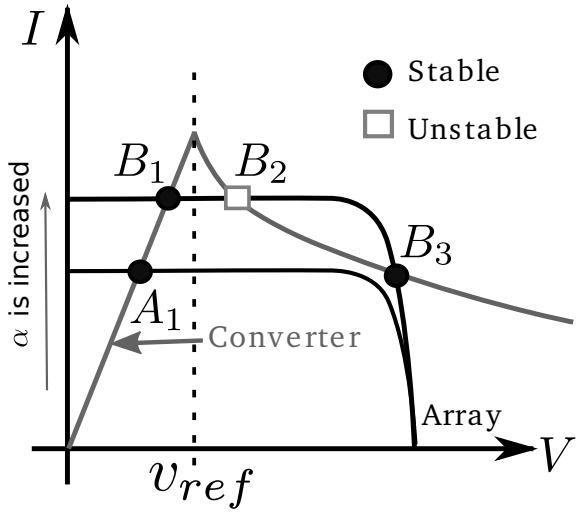

Figure 6.1: Bifurcation occurs if intensity of illumination is changed

non-linear behaviour [89].

We assume that the DC/DC converter is lossless and operating in a continuous conduction mode, and has a constant resistance as the load. As the solar array voltage input varies, the DC/DC converter operates in two separate regions. For sufficient voltage from the solar array, the characteristics are that of a constant-power hyperbola. If the output voltage from the solar array is insufficient, the output of the DC/DC converter will become unregulated to show constant resistance characteristics [30, 90, 91]. The current-voltage (I-V) characteristics of a DC/DC converter connected to a solar array are given by Fig.6.1 [30,92]. The position of these equilibrium points depends on the load resistance of the converter (Fig.6.2) or the intensity of illumination for the array (Fig.6.1) [30].

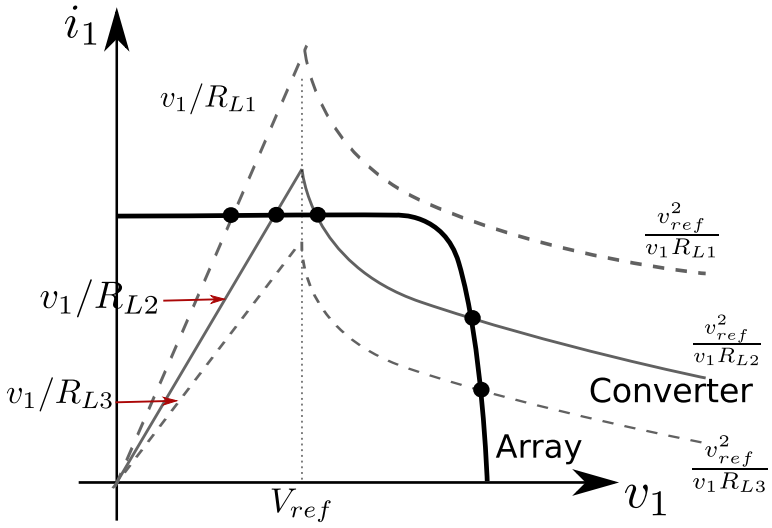

Figure 6.2: Bifurcation occurs with change in load resistance

When the load resistance is varied, the characteristics of the solar array- DC/DC converter system are given by Fig.6.2. The system shows bifurcation as the load resistance is changed, creating three equilibria under certain load resistances. Here, it can be seen that for lower loads the system exhibits one stable equilibrium which lies in the desirable region, and for higher loads a stable equilibrium in the undesirable part. For Fig.6.1, the three equilibria have been analysed as two stable equilibria and one unstable equilibrium in between them [92]. As the solar output voltage varies, the input to the converter varies and the DC/DC converter operates in two modes: desirable and undesirable. Desirable mode is denoted by $V > v_{ref}$. In the region where $V < v_{ref}$ is undesirable with insufficient output from the solar array. The first equilibrium is in the region where $V < v_{ref}$ and falls in the undesirable mode. The second equilibrium is unstable. The third equilibrium is in the region where $V > v_{ref}$, i.e. the desirable mode. This is a stable equilibrium and also corresponds to the equilibrium at which maximum power can be extracted from the system [92].

The Figure 6.1 also shows IV characteristics with respect to the intensity of illumination on the solar array. When the coefficient of illumination (α) decreases to a certain value, there exists an equilibrium point. The stability of this equilibrium point (A_1) is determined by examining the eigenvalues of the jacobian matrix. For lower values of α, the real part of the eigen values is negative, thus making this a stable point. As the intensity of illumination is increased, for a particular value of α, this equilibrium point diverges into three equilibrium points (B_1, B_2, B_3). The stability analysis shows that B_1 and B_3 are stable but B_2 is an unstable equilibrium point [30]. The change in the number of equilibria by changing α is a stationary bifurcation. (A bifurcation is a qualitative change in the system behavior as a particular parameter of the system is varied [93].)

Passivity-based control is a method of control which brings the system to the desired equilibrium by manipulating the energy characteristics of the system. It employs energy shaping, and damping injection to achieve asymptotic stability. Energy shaping implies the introduction of a new energy function with a minimum at the desired equilibrium. This principle can be extended by modifying the energy function to take into consideration the stability characteristics of the system of solar arrays and DC/DC converters. PBC employing a storage function which is altered to have multiple equilibria is used for the control of such a system. The use of PBC compels us to focus on the energy characteristics of the system, and analyze the dynamic behavior in light of the new storage function.

6.2 Design of Multistable Storage Function

The IV characteristics of a solar array-DC/DC converter system were given in Section 6.1.1. The bifurcation characteristics are a fatal demerit to the system. However, on the other hand, the multiple equilibria can alter the state of the system within the nature of the system characteristics with a small perturbation. For such a system, the energy function for the application of PBC can be designed to have similar characteristics. Conventionally, PBC has always seen the energy function to have a unique equilibrium as was done for

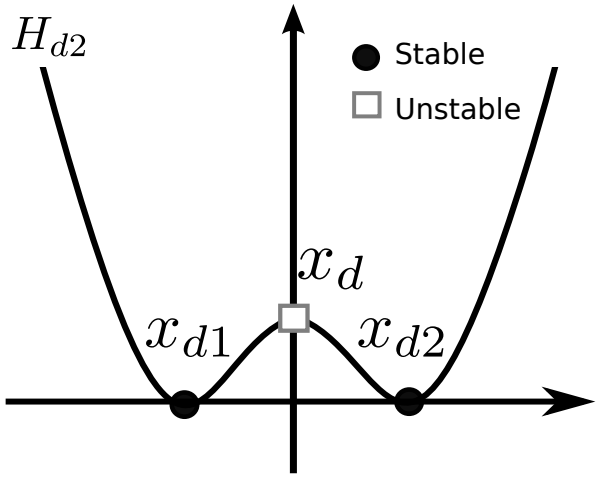

Figure 6.3: Energy function for dual equilibrium

the control of stand-alone power systems in the previous chapters. This method can be extended by designing the energy function to have multiple equilibria depending on the system in question. This method can enable the energy function to adapt to the natural characteristics of the system within the framework of PBC.

Such behavior is modeled by using a new storage function, H_{d2}, represented by Fig 6.3. This function has structure similar to Fig. 6.1 with two stable and one unstable equilibrium. PBC can shape the energy function to keep the structure with three equilibria. The shaping physically implies addition of a damping term. The new storage function is given by Eq. (6.1).

$$H_{d2} = \frac{1}{2}((\boldsymbol{x} - \boldsymbol{x}_{d1})^{\mathrm{T}}\mathbf{D}(\boldsymbol{x} - \boldsymbol{x}_{d2}))^2 \tag{6.1}$$

The modified function is represented by Fig. 6.3. Qualitively the function has structure similar to Fig. 6.1 with two stable and one unstable equilibrium. This function with its multiple equilibria, as opposed to the previous single equilibrium function, can be referred as a multistable function. The application of PBC with this dual equilibrium function will help to retain the system of solar array and DC/DC converter within its natural characteristics.

Here $\boldsymbol{x}_{d1}$ and $\boldsymbol{x}_{d2}$ are the two stable equilibria corresponding to B_1 and B_3 respectively. $\mathbf{D}$ as given in Eq. (3.5) is a diagonal matrix of the inductances and capacitances in the system, $\boldsymbol{x}$ is a column matrix of the states of the system.

6.3 PBC for Multistable function

In the case for a solar array-DC/DC converter system, where the the input voltage from the solar array is sufficient, it is desirable that the system settles on the equilibrium point B3. The system will retain the constant power load condition and it is possible to

draw an increased amount of power. In this section, firstly, we demonstrate the application of PBC with a multistorage function to a stand-alone ring coupled system. Secondly, we compare the results of the open loop system to the one where feedback nonlinear control with PBC is applied to numerically examine the choice of the equilibrium for different conditions of changing load and input voltage within the bifurcation range.

In Chap. 3, for the application of PBC, it was shown that the function is Lyapunov stable. We will proceed to do the same for the multistable storage function. To prove the function is Lyapunov stable, the derivative of the function must be given, and it should be shown that it is negative. Then, PCHM will be employed to confirm passivity of the system. Lastly, the design of control equations will allow the application of PBC.

6.3.1 Lyapunov Stability of Multistable Storage Function

Recalling equations for a ring coupled converter system with PCHM from Chap. 3 the system is represented as Eq. (6.2).

$$\mathbf{D}\dot{\boldsymbol{x}}(t) = [\mathbf{J}(\mu) - \mathbf{R}]\frac{\partial H}{\partial x} + \mathbf{E} \tag{6.2}$$

The energy of the system is the sum of energy of all the storage elements present in the system. This represents the Hamiltonian for the system. It is given by Eq. (6.3) considering $\boldsymbol{x}$ and $\mathbf{D}$ as defined in Chap. 3.

$$H = \frac{1}{2}\boldsymbol{x}^{\mathrm{T}}\mathbf{D}\boldsymbol{x} \tag{6.3}$$

To show that a function is Lyapunov stable, it needs to be shown that the derivative of that function is negative. Confirming $\dot{H}_{d2} \leq -kH_{d2}$ for the function H_{d2}, it is proved to be a candidate of Lyapunov function. Eq. (6.4) gives the derivative of the multistorage function.

$$\dot{H}_{d2} = ((\boldsymbol{x} - \boldsymbol{x}_{d1})^{\mathrm{T}}\mathbf{D}(\boldsymbol{x} - \boldsymbol{x}_{d2})) \times \frac{\mathrm{d}}{\mathrm{d}t}((\boldsymbol{x} - \boldsymbol{x}_{d1})^{\mathrm{T}}\mathbf{D}(\boldsymbol{x} - \boldsymbol{x}_{d2})) \tag{6.4}$$

Let,

$$A = \frac{\mathrm{d}}{\mathrm{d}t}((\boldsymbol{x} - \boldsymbol{x}_{d1})^{\mathrm{T}}\mathbf{D}(\boldsymbol{x} - \boldsymbol{x}_{d2})). \tag{6.5}$$

Here, consider $(\boldsymbol{x} - \boldsymbol{x}_{d1}) = \boldsymbol{e}_1$ and $(\boldsymbol{x} - \boldsymbol{x}_{d2}) = \boldsymbol{e}_2$. The derivative of A is given in Eq. (6.6). Thus, Eq. (6.7) equation holds.

$$A = \frac{\mathrm{d}}{\mathrm{d}t}(\boldsymbol{e}_1^T\mathbf{D}\boldsymbol{e}_2) \tag{6.6}$$

$$A = \boldsymbol{e}_1^{\mathrm{T}}\mathbf{D}\dot{\boldsymbol{e}}_2 + \boldsymbol{e}_2^T\mathbf{D}\dot{\boldsymbol{e}}_1 \tag{6.7}$$

Let $\boldsymbol{x}_d$ be the center between $\boldsymbol{x}_{d1}$ and $\boldsymbol{x}_{d2}$, such that if $\boldsymbol{e} = (\boldsymbol{x} - \boldsymbol{x_d})$ then $\boldsymbol{e}_1 = (\boldsymbol{e} - \boldsymbol{a})$ and $\boldsymbol{e}_2 = (\boldsymbol{e} + \boldsymbol{a})$. Then, Eq. (6.7) is rewritten in terms of $\boldsymbol{e}$ and $\boldsymbol{a}$ and given by Eq.(6.8).

$$A = 2(\boldsymbol{e}^{\mathrm{T}}\mathbf{D}\dot{\boldsymbol{e}} - \boldsymbol{a}^{\mathrm{T}}\mathbf{D}\dot{\boldsymbol{a}}) \tag{6.8}$$

Consider the substitution given in Eqs. (6.9) and (6.10).

$$\mathbf{D}\dot{\boldsymbol{x}}_{\boldsymbol{d}} = \mathbf{J}\boldsymbol{x}_d - \mathbf{R}\boldsymbol{x}_d + \mathbf{E} + \mathbf{R}_I(\boldsymbol{x} - \boldsymbol{x}_d) \tag{6.9}$$

$$\mathbf{D}\dot{\boldsymbol{a}} = \mathbf{J}\boldsymbol{a} - (\mathbf{R} + \mathbf{R}_I)\boldsymbol{a} \tag{6.10}$$

From PCHM it is known that $\mathbf{J}$ is a skew symmetric matrix. Thus, $\boldsymbol{e}^T\mathbf{J}\boldsymbol{e} = 0$ and $\boldsymbol{a}^T\mathbf{J}\boldsymbol{a} = 0$. Substituting Eqs. (6.9) and (6.10) in Eq. (6.8), the final expression for A is obtained.

$$A = -2(\boldsymbol{e}^{\mathrm{T}}(\mathbf{R} + \mathbf{R}_I)\boldsymbol{e} - \boldsymbol{a}^{\mathrm{T}}(\mathbf{R} + \mathbf{R}_I)\boldsymbol{a})$$

$$A = -2((\boldsymbol{e} - \boldsymbol{a})^{\mathrm{T}}(\mathbf{R} + \mathbf{R}_I)(\boldsymbol{e} + \boldsymbol{a})) \tag{6.11}$$

Substituting the values of $\boldsymbol{e}$ and $\boldsymbol{a}$ back in this equation and writing it in terms of $(\boldsymbol{x} - \boldsymbol{x}_{d1})$ and $(\boldsymbol{x} - \boldsymbol{x}_{d2})$ it is written as Eq. (6.12).

$$A = -((\boldsymbol{x} - \boldsymbol{x}_{d1})^{\mathrm{T}}2(\mathbf{R} + \mathbf{R_I})(\boldsymbol{x} - \boldsymbol{x}_{d2})) \tag{6.12}$$

Substituting Eq. (6.12) into the original equation for $\dot{H}_{d2}$ (Eq. (6.4)), we obtain Eq. (6.13).

$$\dot{H}_{d2} = -((\boldsymbol{x} - \boldsymbol{x}_{d1})^{\mathrm{T}}\sqrt{2\mathbf{D}(\mathbf{R} + \mathbf{R}_I)}(\boldsymbol{x} - \boldsymbol{x}_{d2}))^2 \tag{6.13}$$

Eq. (6.13) definitely implies that $\dot{H}_{d2} \leq -kH_{d2}$ with $k > 0$. As a sufficient condition, the dissipation matching condition $\mathbf{R} + \mathbf{R}_I > 0$ is requested. With these conditions, it is confirmed that $\dot{H}_{d2} \leq -kH_{d2}$ with $k > 0$. Thus H_{d2} becomes a candidate of Lyapunov function.

6.3.2 Control Equations

From the above discussions, the conditions given in Eqs. (6.10) and (6.9) are necessary for the function to be a candidate of Lyapunov function. The control equations for PBC are formulated from these equations. Two conditions, one for $\boldsymbol{x}_{d1}$ and one for $\boldsymbol{x}_{d2}$ are constructed. Adding Eqs. (6.9) and (6.10), we obtain Eq. (6.14).

$$\mathbf{D}(\dot{\boldsymbol{x}}_d + \dot{\boldsymbol{a}}) = \mathbf{J}(\boldsymbol{x}_d - \boldsymbol{a}) - \mathbf{R}(\boldsymbol{x}_d + \boldsymbol{a}) - \mathbf{E} + \mathbf{R}_I(\boldsymbol{x} - (\boldsymbol{x}_d + \boldsymbol{a})) \tag{6.14}$$

Taking $\boldsymbol{x}_{d1} = \boldsymbol{x}_d + \boldsymbol{a}$ into consideration, Eq. (6.15) holds.

$$\mathbf{D}\dot{\boldsymbol{x}}_{d1}(t) = (\mathbf{J} + \mathbf{R})\boldsymbol{x}_{d1}(t) + \mathbf{E} + \mathbf{R}_I(\boldsymbol{x} - \boldsymbol{x}_{d1}(t)) \tag{6.15}$$

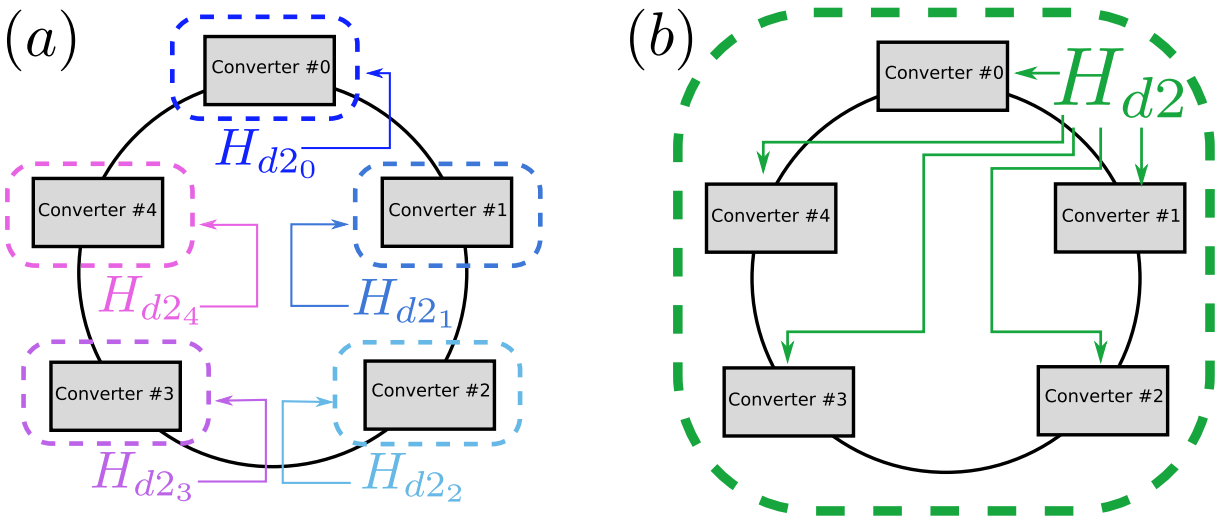

Figure 6.4: Two ways to apply control: (a) Each converter follows its own desired energy function (b) All the converters settle on the same equilibrium point corresponding to the energy of the whole system

Similarly subtracting Eq. (6.10) from Eq. (6.9), we obtain Eq. (6.16).

$$\mathbf{D}(\dot{\boldsymbol{x}}_d - \dot{\boldsymbol{a}}) = \mathbf{J}(\boldsymbol{x}_d - \boldsymbol{a}) - \mathbf{R}(\boldsymbol{x}_d - \boldsymbol{a}) - \mathbf{E} + \mathbf{R}_I(\boldsymbol{x} - (\boldsymbol{x}_d - \boldsymbol{a})) \tag{6.16}$$

Taking into consideration that $\boldsymbol{x}_{d2} = \boldsymbol{x}_d - \boldsymbol{a}$, Eq. (6.17) holds.

$$\mathbf{D}\dot{\boldsymbol{x}}_{d2}(t) = (\mathbf{J} - \mathbf{R})\boldsymbol{x}_{d2}(t) + \mathbf{E} + \mathbf{R}_I(\boldsymbol{x} - \boldsymbol{x}_{d2}(t)) \tag{6.17}$$

Thus, the control equations for the multi storage function are obtained by Eqs. (6.15) and (6.17).

6.3.3 Application of Control

The control equations obtained in Eqs. (6.15) and (6.17) denote the control rule. Implementing this control rule, the system recovers stability according to the function shown in Fig. 6.3. As was in Chap. 3, PBC is a feedback technique. Feedback is applied by solving the control equations for μ_{n}. As the control is applied, μ_{n} becomes a function of time and thus for all purposes should be considered as μ_{n} here on. Due to the zero dynamics discussed in Sec. 2.2, the feedback is acquired by measuring the current $i_{L\mathrm{n}}$.

Feedback to the duty cycle is obtained in two ways. One way is by setting each converter to follow its own desired energy function as shown in Fig. 6.4 (a). This individual energy function given by Eq.(6.18) is for converter #0. Here, $\boldsymbol{x}_0$ is the state vector, and $\boldsymbol{x}_{d1_0}$, $\boldsymbol{x}_{d2_0}$ the desired stable equilibria for converter #0. This implies that each converter has the freedom to chose either stable equilibrium at $\boldsymbol{x}_{d1}$ or $\boldsymbol{x}_{d2}$ without influence from neighbours.

$$H_{d2_0} = \frac{1}{2}((\boldsymbol{x}_0 - \boldsymbol{x}_{d1_0})^{\mathrm{T}}\mathbf{D}_0(\boldsymbol{x}_0 - \boldsymbol{x}_{d2_0}))^2 \tag{6.18}$$

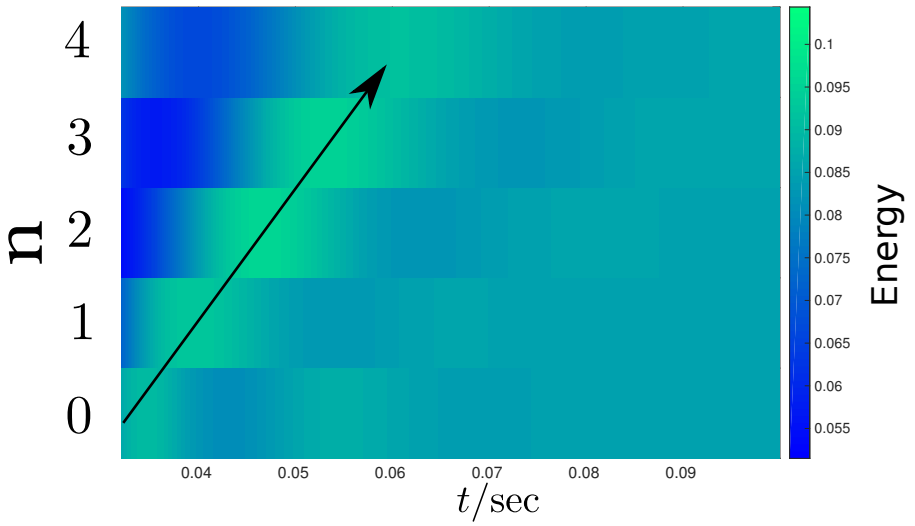

Figure 6.5: Control applied based on energy of whole system This case shows where converters are forced to settle at same equilibrium. Initial conditions: $E_0 = 24$ V, $E_1 = 21$ V, $E_2 = 18$ V, $E_3 = 15$ V, and $E_4 = 12$ V

The second way is by considering the energy of the whole system. Here, the storage function (H_{d2}) is minimized to attain stability as shown in Fig. 6.4 (b). It is ensured that the output voltage in the ring is constant, and all the converters in the system settle on

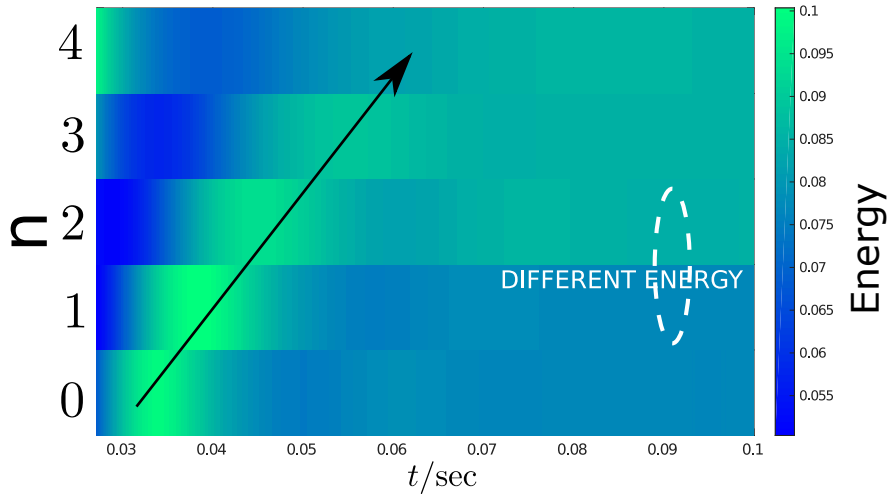

Figure 6.6: Control applied based on energy of single system Converters settle on different equilibrium according to individual energy. Initial conditions: $E_0 = 24$ V, $E_1 = 21$ V, $E_2 = 18$ V, $E_3 = 15$ V, and $E_4 = 12$ V

the same equilibrium without regard to the individual energy.

6.4 Numerical Simulations

The control equations given by Eqs. (6.15) and (6.17) were solved using a ode45 solver in MATLAB. As PBC is applied, the choice of the equilibrium corresponds to the energy of the system. The ring coupled converter system described in Chap. 3 and shown in Fig. 3.2 is considered. The parameters other than mentioned in the figure are according to Table. 3.1 For the following simulations $\boldsymbol{x}_{d1}$ was set at 20 V and $\boldsymbol{x}_{d2}$ was set at 24 V.

6.4.1 Flow of Energy through the Ring

Figures 6.5 and 6.6 show the flow of energy between the converters in the transient. In Fig. 6.5 the control was performed on the energy of the whole system. Fig. 6.6 shows the case in which the control is applied individually depending on the energy of each converter given by Eq. (6.18). For ease of visibility, the plot starts after the initial peak at 0.03 sec. In Fig. 6.5 all the converters settle at $\boldsymbol{x}_{d1} = 39$ V. Converter #0 has the highest input in the ring and thus the highest energy. It shows a peak transient first then converter #1 and so on. The energy flows through the ring until all the converters have the same energy and thus the same output voltage. Fig. 6.6 shows the dynamic behaviour for the same inputs as Fig. 6.5. The converters do not settle at the same equilibrium. Converter #0 and converter #1 settle at $\boldsymbol{x}_{d1} = 39$ V while the other three settle at $\boldsymbol{x}_{d2} = 41$ V. The final energy of all the converters is not the same, and thus a constant current flows through the dissipation.

These simulations show that given different inputs for the converters, the flow of energy occurs in the ring until all converters have same energy levels. This gives us an insight into the energy characteristics of coupled converters. We were also able to show that the energy of the converters remains different when they settle at different equilibria. The difference in the energy, and the constant flow of dissipation beyond the transient are an interesting observation for PBC.

6.4.2 Application of PBC

The application of PBC is applied as described by Fig.6.4 (b.).

Numerical results were obtained for conditions of varying input voltage and load resistance. Comparison between the simulation results of the open loop system and the system where PBC has been applied shows that with PBC, the system output voltage consistently equilibriates at a higher value than without PBC. These results are shown in Fig.6.7. First, keeping the output resistance constant at $R_{2\mathrm{n}} = 50$ V, the input is varied from $E_{\mathrm{n}} = 12$ V to $E_{\mathrm{n}} = 20$ V. Here, the final output voltage of the system is plotted on the y-axis. Then, keeping the input constant at $E_{\mathrm{n}} = 14$ V and $E_{\mathrm{n}} = 14$ V

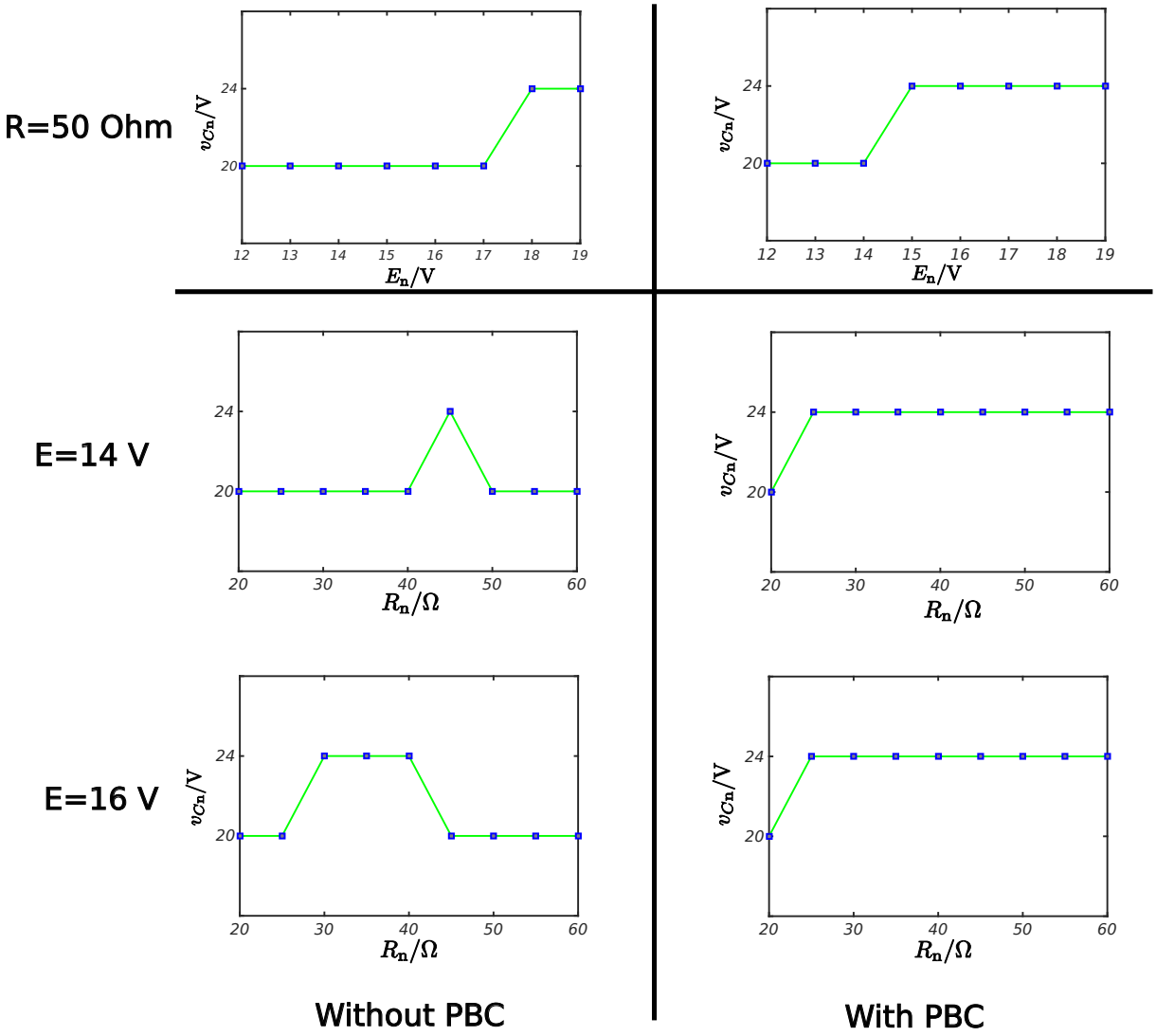

Figure 6.7: Comparison of open loop system to system with PBC for changing conditions of input voltage and load resistance. The other parameters are: $L_{\mathrm{n}} = 16$ mH $C_{\mathrm{n}} = 50$ μF $R_{1\mathrm{n}} = 10$ Ω $L_{T\mathrm{n}} = 5$ mH

respectively, the load resistance is varied. When PBC is applied, the system settles on a higher equilibrium as the load resistance increases. The same trend is seen in the open loop system but then, if the resistance is increased further, the system moves back to the lower equilibrium. This suggests unpredictability of the system output without the application of PBC. Therefore, the application of PBC,in addition, allows for more consistent predictability of the system's output voltage which is an important design consideration for systems with bifurcation properties like the solar array-DC/DC converter system.

The transient behaviour of the system, for both with and without PBC, is shown in Fig.6.8. Here the input inductor current and output voltage are plotted on the energy

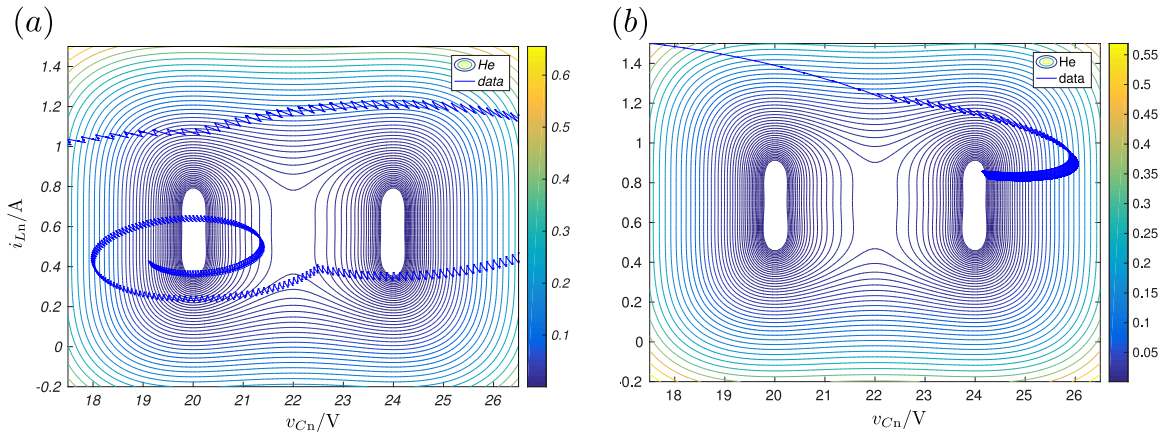

Figure 6.8: Transient behaviour of the system: (a) Without control (b) With PBC. System parameters are same as shown in Fig.6.7 with $E_n = 15$ V and $R_{2n} = 50\ \Omega$

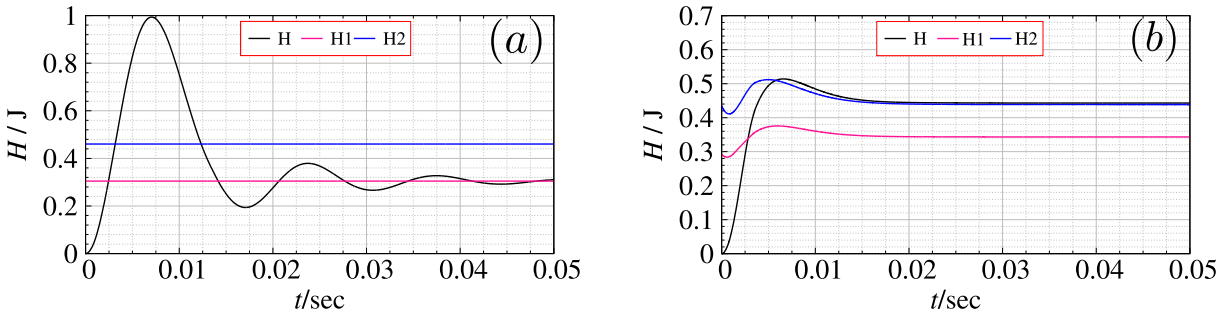

Figure 6.9: The system: (a) Without control (b) With PBC. System parameters are same as shown in Fig.6.7 with $E_n = 15$ V and $R_{2n} = 50\ \Omega$. Here, H is the energy of the system and

plots of the multistable energy function with two stable equilibria. It can be seen that the system oscillates in the transient while finally settling on the lower equilibrium for the open loop system without control. With dampened transient oscillations, the system quickly settles at 24 V. The energy of the system can be seen with respect to time in Fig.6.9. In Fig.6.9 (a) it is seen that the energy corresponding to the two equilibria are constant with respect to time. Thus, as the energy of the system also oscillates and settles on one equilibrium. For the same parameters, the energy corresponding to the equilibria is a function of time. This minimizes the unpredictability and makes it possible to drive the system to the higher equilibrium point for a variety of cases.

6.5 Conclusion

In this chapter the energy shaping properties of PBC were taken a step further by designing the energy function to suit the physical characteristics of the system. The solar

array-DC/DC converter system shows bifurcation characteristics with respect to the input voltage and load resistance. Studying the nature of the solar array-DC/DC converter system, the desired energy function, which is usually a paraboloid with a single equilibrium point to a quartic function with three equilibria. In the new double well potential function, there are two stable equilibria and an unstable equilibrium between them, corresponding to the characteristics of the solar array-DC/DC converter system. It was proved that this function is a candidate of Lyapunov function. This implies that PBC can be applied and consequently control equations were obtained.

Firstly, the method of application of control was discussed. It was shown that PBC can be applied to the stand-alone distributed generation system in two distinct ways. The first one is where the control is applied so that the converters follow their own energy function and thus possess the freedom to choose either of the stable equilibrium without influence from its neighbours. If the coupled converters in the system settle on different equilibria, it causes a flow of energy in the system. The second method is when the control is applied by considering the energy function of the entire system. It causes all the converters to choose the same equilibrium point corresponding to the energy of the entire system. The simulation results for the different methods of application of PBC give an insight in the behaviour of the stand-alone distributed system with solar array and DC/DC converters.

Finally, it was shown with numerical simulations that for different conditions of varying input voltage and load resistance, PBC helps the system to choose the equilibrium with higher power. It is thus possible to maintain the system on the higher equilibrium, and thus showing constant power characteristics. The transient behaviour is studied by plotting the current and voltage on the energy curves of the newly designed multiple equilibrium system.

Chapter 7

Conclusion

7.1 Conclusion

The aim of this thesis is to give a detailed design framework for stand-alone systems with DC inputs, stabilized with PBC. For this purpose, three types of dispersed generation stand alone power systems were designed, modelled and their behaviour was analysed with numerical simulations. Passivity-based control was employed to stabilize the entire network to the desired state, including the output voltage and inductor currents by consideration for the energy characteristics of the system. The method of the control rule was adjusted to suit the design of the stand-alone network under consideration.

Chapter 2 explained the basics of the operation and modelling of DC/DC converters. Port-controlled Hamilton modelling was applied to the simple case of a DC/DC boost converter. After consideration of the structural dynamics, it was found that the feedback applied through the input inductor retains the stability of the DC/DC boost converter. Finally, the application of nonlinear PBC was discussed by proving Lyapunov stability of the newly designed storage function.

Chapter 3 introduced the design of a DC stand alone system posessing individual units of DC inputs with a boost converter and a load, which were connected in a ring formulation. Here, PBC was achieved for coupled converters after successful modelling of the network as a PCHS. Numerical analysis of the structure resulted in the recognition of the different equilibria of the system for feedback through voltage and current. The stability of the feedback through current is determined with numerical analysis and was used in the following chapters to apply PBC to ring-connected converter/inverter systems. The numerical simulations of the DC output network were carried out to show the successful application of PBC. The results showed an improved transient response, and a faster convergence in conditions of disturbance.

Chapter 4 focussed on a practical approach of having AC outputs with DC inputs in the stand-alone generation system described in Chapter 3. Here, the steady state of the output is sinusoidal and had to be analysed analytically. After successful application of PBC to get a sinusoidal output voltage for all inverters, the synchronization was tackled. It

was shown that the any phase difference between the coupled inverters causes interference in the output voltage and renders the system unstable. PLLs were employed along with PBC to maintain the phase and frequency synchronization of the output voltage for all cases of phase difference between the inverters. It was also shown that the synchronization is maintained for a linear change in the frequency of the output voltage.

Chapter 5 combined the strategies implemented in Chapters 3 and 4 to construct a network with both DC and AC outputs. The idea of this design comes from the emerging concept of stand-alone power systems for remote rural areas. The design incorporates DC stand-alone grid for small villages, connected to larger remote towns requiring a functional AC connection. Inverters are employed to connect the DC-grids to a main AC-grid. Network modelling is carried out for all elements considered as one big system. Instead of attempting to control several individual rings separately, this allows for the control and stability of all the elements through the energy exchange between them. PBC was shown to stabilize the hybrid system to the desired DC and AC output voltages through rigorous numerical simulations.

Finally, Chapter 6 looks considers a reshaping of the conventional energy shaping-damping injection PBC. This chapter aimed at modifying the traditional storage function for PBC from the quadratic parabola to a quartic double well function. The double well storage function was chosen to suit the bifurcation characteristics of the stand-alone solar array-DC/DC converter system. The application of PBC through this quartic function is verified. The results showed that PBC is able to maintain the entire ring coupled converter network at an equilibrium with higher power compared with the original system for conditions of varying inputs and load resistances.

7.2 Future Directions

The discussion in this dissertation gave a basic design framework for the dispersed generation stand-alone power system. Chapter 5 gave a detailed design for a dispersed generation system particularly suited for remote rural areas in developing countries. Towards the actual realization of this design, a few more steps need to be performed after obtaining the mathematical model and numerical simulation results given in Chapter 5. Firstly, the energy storage elements have been neglected in this dissertation to obtain the basic model of the network for the application of PBC. Consideration of the energy storage system is an important next step towards the all round development of the dispersed generation described in this dissertation.

One of the main obstacles for the realization of successful dispersed generation systems is that of scalability. As the number of DER are increasing, the question of scaling and integration of these numerous DER has been underlined. The scalability of stand-alone systems and the integration of these systems to the utility grid is an important topic for discussion. In Chapter 5, a preliminary network analysis of the AC-DC network with multiple rings was performed to recognize and evaluate the vulnerable areas in the network. The adjacency matrix is a useful tool for making the network more scalable.

Further exploration of the network features of the stand alone system is necessary to obtain a better assessment of the system scalability. For grid integration, along with scalability, the role of PBC must be examined.

This dissertation provided the necessary numerical simulations performed on MATLAB. The simulations were performed using the PWM techniques provided the SIMULINK environment in MATLAB. For the further development of the stand-alone network described in this dissertation, it is desirable to have an experimental set up to analyse the control method.

Chapter 5 explored the possibility of the application of PBC with a storage function corresponding to the systems natural characteristics rather than the conventional quadratic parabolic energy function. Preliminary analysis and complementing numerical simulations were provided for a limited number of cases. It is an interesting aspect that demands to be explored further. Furthermore, it is desirable to provide a theoretical justification for the results provided in Chapter 5. The energy function can be further modified to align to the system characteristics of various other systems as well.

Appendix A

An inconsistency in the frequency or phase of the output voltages causes an interference effect. This effect is not desirable as the output voltage amplitude becomes unstable, instead of a pure sinusoidal waveform. Frequency as well as phase synchronization can be achieved with the help of a phase locked loop.

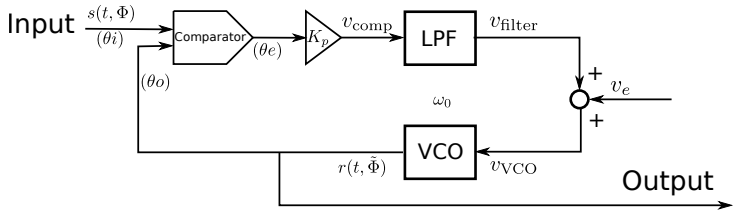

Figure 7.1: Block diagram of a phase locked loop

A phase locked loop is a circuit that generates an output signal, whose phase is the same as that of the input signal [58]. A PLL generally consists of a phase detector or a comparator, a VCO and a low pass filter [59, 60]. The phase detector(PD) produces an error signal that is proportional to the phase error between the input signal and the output of the VCO. The low pass filter supresses noise and the unwanted PD outputs, thus determining the dynamics of the PLL. The VCO produces a signal with frequency proportional to the control voltage (v_{VCO}). The closed loop forces the VCO to lock the phase of the output to that of the input signal. The output of the VCO is the output of the PLL. The block diagram of a phase locked loop is shown in Fig.7.1.

The input signal to the PLL is the sinusoidal signal for the PWM of the reference inverter. Let the input signal be given by $s(t,\Phi) = A\sin(\omega_d t + \theta_i(t))$, where A is the amplitude and $\phi = \omega_d t + \theta_i(t)$ is the phase of the input signal. ω_d is the centre frequency of the VCO. $\theta_i(t)$ incorporates the error in the input frequency, $\delta\omega = \omega_i - \omega_d$ from the centre frequency of the VCO. Let the output of the VCO be $r(t,\tilde{\Phi}) = V_0\cos(\omega_d t + \theta_o(t))$, with V_0 as the amplitude and $\tilde{\Phi} = \omega_d t + \theta_o(t)$ as the phase.

With $s(t,\Phi)$ and $r(t,\tilde{\Phi})$ as the inputs to the PD, the output voltage of the PD can be given by Eq.(7.1).

$$v_{\text{comp}} = K_p A\sin(\theta_e) \tag{7.1}$$

Here, K_p is the gain from the PD and $\theta_e = \theta_i - \theta_o$ is the phase error. v_{comp} is the input of the LPF. If the transfer function of the LPF in the frequency domain is given as $F(s)$,

then the output voltage of the filter can be obtained by Eq.(7.2). The LPF is considered ideal without any harmonics.

$$v_{\text{filter}} = \mathcal{L}^{-1}[F(s)V_{\text{comp}}(s)] \tag{7.2}$$

Here, $\mathcal{L}^{-1}$ denotes the Laplace inverse and $V_{\text{comp}}(s)$ is the Laplace transform of v_{comp}. The instantaneous output frequency of the VCO, given by $\omega_{\text{VCO}}(t)$, is proportional to the control input of the VCO. Then, Eq.7.3 can be obtained.

$$\omega_{\text{VCO}}(t) = \omega_d + K_C v_{\text{VCO}} \tag{7.3}$$

The instantaneous frequency of of the output of the VCO is given by the derivative of $\tilde{\Phi}$. Thus, the following set of equations hold, where v_e is the external control voltage.

$$\omega_{\text{VCO}}(t) = \frac{d\tilde{\Phi}}{dt} \tag{7.4}$$

$$\frac{d\theta_o}{dt} = K_C v_{\text{VCO}} \tag{7.5}$$

$$v_{\text{VCO}} = v_{\text{filter}} + v_e \tag{7.6}$$

Thus, the phase of the output voltage, $\tilde{\Phi}$ is locked with the phase of the input, and the output signal can be used as a sinusoidal reference to the PWM of the adjoining inverter. The loop equation for $\theta_o(t)$ is given by Eq.(7.7)

$$\frac{d\theta_o}{dt} = K_C[\mathcal{L}^{-1}[F(s)V_{\text{comp}}(s)]K_p A\sin(\theta_e) + v_e] \tag{7.7}$$

Bibliography

[1] J. A. Turner, "A realizable renewable energy future," *Science*, vol. 285, no. 5428, pp. 687–689, 1999.

[2] J. Twidell and T. Weir, *Renewable energy resources*. Routledge, 2015.

[3] I. Dincer, "Renewable energy and sustainable development: a crucial review," *Renewable and sustainable energy reviews*, vol. 4, no. 2, pp. 157–175, 2000.

[4] T. Adefarati and R. C. Bansal, "Reliability, economic and environmental analysis of a microgrid system in the presence of renewable energy resources," *Applied energy*, vol. 236, pp. 1089–1114, 2019.

[5] O. Ellabban, H. Abu-Rub, and F. Blaabjerg, "Renewable energy resources: Current status, future prospects and their enabling technology," *Renewable and Sustainable Energy Reviews*, vol. 39, pp. 748–764, 2014.

[6] R. E. Sims, H.-H. Rogner, and K. Gregory, "Carbon emission and mitigation cost comparisons between fossil fuel, nuclear and renewable energy resources for electricity generation," *Energy policy*, vol. 31, no. 13, pp. 1315–1326, 2003.

[7] J. Turkson and N. Wohlgemuth, "Power sector reform and distributed generation in sub-saharan africa," *Energy Policy*, vol. 29, no. 2, pp. 135–145, 2001.

[8] J. N. Brass, S. Carley, L. M. MacLean, and E. Baldwin, "Power for development: A review of distributed generation projects in the developing world," *Annual Review of Environment and Resources*, vol. 37, pp. 107–136, 2012.

[9] A. Thornton and C. R. Monroy, "Distributed power generation in the united states," *Renewable and Sustainable Energy Reviews*, vol. 15, no. 9, pp. 4809–4817, 2011.

[10] L. S. Thomas Ackermann, Goran Andersson, "Distributed generation: a definition," *Electric Power System Research*, vol. 57, no. 3, pp. 195–204, 2001.

[11] G. Pepermans, J. Driesen, D. Haeseldonckx, R. Belmans, and W. D'haeseleer, "Distributed generation: definition, benefits and issues," *Energy policy*, vol. 33, no. 6, pp. 787–798, 2005.

[12] H. Zerriffi, *Rural electrification: strategies for distributed generation*. Springer Science & Business Media, 2010.

[13] S. Goel and R. Sharma, "Performance evaluation of stand alone, grid connected and hybrid renewable energy systems for rural application: A comparative review," *Renewable and Sustainable Energy Reviews*, vol. 78, pp. 1378–1389, 2017.

[14] R. K. Akikur, R. Saidur, H. W. Ping, and K. R. Ullah, "Comparative study of stand-alone and hybrid solar energy systems suitable for off-grid rural electrification: A review," *Renewable and sustainable energy reviews*, vol. 27, pp. 738–752, 2013.

[15] B. K. Blyden and W.-J. Lee, "Modified microgrid concept for rural electrification in africa," in *2006 IEEE Power Engineering Society General Meeting*, pp. 5–pp, IEEE, 2006.

[16] R. Banerjee, "Comparison of options for distributed generation in india," *Energy Policy*, vol. 34, no. 1, pp. 101–111, 2006.

[17] K. Narula, Y. Nagai, and S. Pachauri, "The role of decentralized distributed generation in achieving universal rural electrification in south asia by 2030," *Energy Policy*, vol. 47, pp. 345–357, 2012.

[18] e. a. Arulampalam, "Control of power electronic interfaces in distributed generation microgrids," *International Journal of Electronics*, vol. 91, no. 9, pp. 503–523, 2004.

[19] V. Salas, E. Olias, A. Barrado, and A. Lazaro, "Review of the maximum power point tracking algorithms for stand-alone photovoltaic systems," *Solar energy materials and solar cells*, vol. 90, no. 11, pp. 1555–1578, 2006.

[20] M. N. Marwali, J.-W. Jung, and A. Keyhani, "Control of distributed generation systems-part ii: Load sharing control," *IEEE Transactions on power electronics*, vol. 19, no. 6, pp. 1551–1561, 2004.

[21] A. Camacho, M. Castilla, J. Miret, R. Guzman, and A. Borrell, "Reactive power control for distributed generation power plants to comply with voltage limits during grid faults," *IEEE Transactions on Power Electronics*, vol. 29, no. 11, pp. 6224–6234, 2014.

[22] H. Sira-Ramírez and R. Silva-Ortigoza, *Control design techniques in power electronics devices*. Springer Science & Business Media, 2006.

[23] H. Sira-Ramirez, R. Perez-Moreno, R. Ortega, and M. Garcia-Esteban, "Passivity-based controllers for the stabilization of dc-to-dc power converters," *Automatica*, vol. 33, no. 4, pp. 499–513, 1997.

[24] R. Ortega, J. A. L. Perez, P. J. Nicklasson, and H. Sira-Ramirez, *Passivity-based control of Euler-Lagrange systems: mechanical, electrical and electromechanical applications*. Springer Science & Business Media, 2013.

[25] I. D. Landau and R. Horowitz, "Synthesis of adaptive controllers for robot manipulators using a passive feedback systems approach," in *Proceedings. 1988 IEEE International Conference on Robotics and Automation*, pp. 1028–1033, IEEE, 1988.

[26] M. Takegaki and S. Arimoto, "A new feedback method for dynamic control of manipulators," 1981.

[27] P. L. Jie Bao, *Process - The Passive Systems Approach*. Springer-Verlag, 2007.

[28] R. Ortega, A. van der Schaft, B. Maschke, and G. Escobar, "Energy-shaping of port-controlled hamiltonian systems by interconnection," in *Decision and Control, 1999. Proceedings of the 38th IEEE Conference on*, vol. 2, pp. 1646–1651, IEEE, 1999.

[29] T. Hikihara and Y. Murakami, "Regulation of parallel converters with respect to stored energy and passivity characteristics," *IEICE transactions on fundamentals of electronics, communications and computer sciences*, vol. 94, no. 3, pp. 1010–1014, 2011.

[30] Y. H. Lim and D. C. Hamill, "Nonlinear phenomena in a model spacecraft power system," in *COM. P. EL. 98. Record 6th Workshop on Computer in Power Electronics (Cat. No. 98TH8358)*, pp. 169–175, IEEE, 1998.

[31] J. M. Guerrero, F. Blaabjerg, T. Zhelev, K. Hemmes, E. Monmasson, S. Jemei, M. P. Comech, R. Granadino, and J. I. Frau, "Distributed generation: Toward a new energy paradigm," *IEEE Industrial Electronics Magazine*, vol. 4, no. 1, pp. 52–64, 2010.

[32] C. S. Sinha and T. C. Kandpal, "Decentralized v grid electricity for rural india: the economic factors," *Energy Policy*, vol. 19, no. 5, pp. 441–448, 1991.

[33] A. Sinha, S. Neogi, R. Lahiri, S. Chowdhury, S. Chowdhury, and N. Chakraborty, "Smart grid initiative for power distribution utility in india," in *2011 IEEE Power and Energy Society General Meeting*, pp. 1–8, IEEE, 2011.

[34] N. Research, "Global der deployment forecast database," 2017.

[35] NERL, "Distributed generation renewable energy estimate of costs."

[36] I. (2019), "Innovation landscape brief: Market integration of distributed energy resources," *International Renewable Energy Agency, Abu Dhabi*.

[37] O. Ulleberg, "Stand-alone power systems for the future: optimal design, operation & control of solar-hydrogen energy systems," *NTNU, Trondheim, Norvège*, p. 225, 1998.

[38] M. I. S. O. (MISO), "Transmission cost estimation guide 2020," 2020.

[39] V. M. Popov and R. Georgescu, "Hyperstability of control systems," 1973.

[40] J. C. Willems, "Dissipative dynamical systems part i: General theory," *Archive for rational mechanics and analysis*, vol. 45, no. 5, pp. 321–351, 1972.

[41] B. M. R. Ortega, A. J. Van Der Schaft, "Putting energy back in control," *IEEE Control Systems*, vol. 21, no. 2, pp. 18–33, 2001.

[42] A. M. Lyapunov, "The general problem of the stability of motion," *International Journal of Control*, vol. 55, no. 3, pp. 531–534, 1992.

[43] H. K. Khalil and J. Grizzle, *Nonlinear systems*, vol. 3. Prentice hall New Jersey, 1996.

[44] H. Sira-Ramirez and R. Ortega, "Passivity-based controllers for the stabilization of dc-to-dc power converters," in *Decision and Control, 1995., Proceedings of the 34th IEEE Conference on*, vol. 4, pp. 3471–3476, IEEE, 1995.

[45] S. A. Morikazu Takegaki, "A new feedback method for dynamic control of manipulators," *Journal of Dynamic Systems, Measurement, and Control*, vol. 103, no. 2, 1980.

[46] K. Fujimoto and T. Sugie, "Canonical transformation and stabilization of generalized hamiltonian systems," *Systems & Control Letters*, vol. 42, no. 3, pp. 217–227, 2001.

[47] A. Van Der Schaft, "Port-hamiltonian systems: network modeling and control of nonlinear physical systems," in *Advanced dynamics and control of structures and machines*, pp. 127–167, Springer, 2004.

[48] B. Maschke and A. Van Der Schaft, "Port-controlled hamiltonian systems: modelling origins and systemtheoretic properties," *IFAC Proceedings Volumes*, vol. 25, no. 13, pp. 359–365, 1992.

[49] G. Escobar, A. J. Van Der Schaft, and R. Ortega, "A hamiltonian viewpoint in the modeling of switching power converters," *Automatica*, vol. 35, no. 3, pp. 445–452, 1999.

[50] M. H. Rashid, *Power electronics: circuits, devices, and applications*. Pearson Education India, 2009.

[51] J. G. Kassakian, M. F. Schlecht, and G. C. Verghese, *Principles of power electronics*, vol. 1991. Addison-Wesley Reading, USA, 1991.

[52] Y. Takatsuji, Y. Susuki, and T. Hikihara, "Hybrid controller for safe microgrid operation," *Nonlinear Theory and Its Applications, IEICE*, vol. 2, no. 3, pp. 347–362, 2011.

[53] M. Farzaneh, S. Farokhi, and W. Chisholm, *Electrical design of overhead power transmission lines*. McGraw-Hill Education, 2012.

[54] A. Isidori, "The zero dynamics of a nonlinear system: From the origin to the latest progresses of a long successful story," *European Journal of Control*, vol. 19, no. 5, pp. 369–378, 2013.

[55] Y. Miladi, M. Feki, and N. Derbel, "Optimal control of a single-phase h-bridge dc–ac inverter," *International Journal of Circuit Theory and Applications*, vol. 44, no. 3, pp. 744–758, 2016.

[56] M. Zhu and F. L. Luo, "Transient analysis of multi-state dc–dc converters using system energy characteristics," *International Journal of Circuit Theory and Applications*, vol. 36, no. 3, pp. 327–344, 2008.

[57] F. Blaabjerg, R. Teodorescu, M. Liserre, and A. V. Timbus, "Overview of control and grid synchronization for distributed power generation systems," *IEEE Transactions on industrial electronics*, vol. 53, no. 5, pp. 1398–1409, 2006.

[58] G.-C. Hsieh and J. C. Hung, "Phase-locked loop techniques. a survey," *IEEE Transactions on industrial electronics*, vol. 43, no. 6, pp. 609–615, 1996.

[59] R. E. Best, *Phase locked loops: design, simulation, and applications*. McGraw-Hill Professional, 2007.

[60] M. Karimi-Ghartema, *Enhanced phase-locked loop structures for power and energy applications*. John Wiley & Sons, 2014.

[61] J. G. Kassakian, M. F. Schlecht, and G. C. Verghese, *Principles of power electronics*. Graphis, 2000.

[62] W. El-Khattam and M. M. Salama, "Distributed generation technologies, definitions and benefits," *Electric power systems research*, vol. 71, no. 2, pp. 119–128, 2004.

[63] I. Mitra, T. Degner, and M. Braun, "Distributed generation and microgrids for small island electrification in developing countries: a review," *Solar Energy Society of India*, vol. 18, no. 1, pp. 6–20, 2008.

[64] R. Bhoyar and S. Bharatkar, "Potential of microsources, renewable energy sources and application of microgrids in rural areas of maharashtra state india," *Energy Procedia*, vol. 14, 2012.

[65] F. Beck and E. E. Martinot, "Renewable energy policies and barriers, forthcoming in encyclopedia of energy, cutler j. cleveland, ed," 2004.

[66] N.-K. C. Nair and L. Zhang, "Smartgrid: Future networks for new zealand power systems incorporating distributed generation," *Energy Policy*, vol. 37, no. 9, pp. 3418–3427, 2009.

[67] B. Banerjee and S. M. Islam, "Reliability based optimum location of distributed generation," *International Journal of Electrical Power & Energy Systems*, vol. 33, no. 8, pp. 1470–1478, 2011.

[68] A. Chauhan and R. Saini, "Renewable energy based off-grid rural electrification in uttarakhand state of india.," *Renewable and Sustainable Energy Reviews*, vol. 51, pp. 662–681, 2015.

[69] J. G. Castellanos, M. Walker, D. Poggio, M. Pourkashanian, and W. Nimmo, "Modelling an off-grid integrated renewable energy system for rural electrification in india using photovoltaics and anaerobic digestion," *Renewable Energy*, vol. 74, pp. 390–398, 2015.

[70] N. Agarwal, A. Kumar, *et al.*, "Optimization of grid independent hybrid pv–diesel–battery system for power generation in remote villages of uttar pradesh, india," *Energy for Sustainable Development*, vol. 17, no. 3, pp. 210–219, 2013.

[71] R. Sen and S. C. Bhattacharyya, "Off-grid electricity generation with renewable energy technologies in india: An application of homer," *Renewable Energy*, vol. 62, pp. 388–398, 2014.

[72] M. Cucuzzella, K. C. Kosaraju, and J. M. A. Scherpen, "Distributed passivity-based control of dc microgrids," in *2019 American Control Conference (ACC)*, pp. 652–657, 2019.

[73] M. A. Hassan and Y. He, "Constant power load stabilization in dc microgrid systems using passivity-based control with nonlinear disturbance observer," *IEEE Access*, vol. 8, pp. 92393–92406, 2020.

[74] S. Amirkhan, M. Radmehr, M. Rezanejad, and S. Khormali, "An improved passivity-based control strategy for providing an accurate coordination in a ac/dc hybrid microgrid," *Journal of the Franklin Institute*, vol. 356, no. 13, pp. 6875–6898, 2019.

[75] R. Manohar and T. Hikihara, "Dynamic behaviour of a ring coupled boost converter system with passivity-based control," *Nonlinear Theory and Its Applications, IEICE*, vol. 11, no. 1, pp. 109–122, 2020.

[76] A.-L. Barabási *et al.*, *Network science*. Cambridge university press, 2016.

[77] G. A. Pagani and M. Aiello, "The power grid as a complex network: a survey," *Physica A: Statistical Mechanics and its Applications*, vol. 392, no. 11, pp. 2688–2700, 2013.

[78] A. Zangeneh, S. Jadid, and A. Rahimi-Kian, "Uncertainty based distributed generation expansion planning in electricity markets," *Electrical Engineering*, vol. 91, no. 7, pp. 369–382, 2010.

[79] Y. Mao, F. Liu, and S. Mei, "On the topological characteristics of power grids with distributed generation," in *Proceedings of the 29th Chinese Control Conference*, pp. 4714–4720, IEEE, 2010.

[80] C. Liu, Q. Xu, Z. Chen, and C. L. Bak, "Vulnerability evaluation of power system integrated with large-scale distributed generation based on complex network theory," in *2012 47th International Universities Power Engineering Conference (UPEC)*, pp. 1–5, IEEE, 2012.

[81] L. Cuadra, S. Salcedo-Sanz, J. Del Ser, S. Jiménez-Fernández, and Z. W. Geem, "A critical review of robustness in power grids using complex networks concepts," *Energies*, vol. 8, no. 9, pp. 9211–9265, 2015.

[82] K.-C. Kim, R. Ortega, A. Charara, and J.-P. Vilain, "Theoretical and experimental comparison of two nonlinear controllers for current-fed induction motors," *IEEE Transactions on Control Systems Technology*, vol. 5, no. 3, pp. 338–348, 1997.

[83] H. Rodríguez, A. J. van der Schaft, and R. Ortega, "On stabilization of nonlinear distributed parameter port-controlled hamiltonian systems via energy shaping," in *Proceedings of the 40th IEEE Conference on Decision and Control (Cat. No. 01CH37228)*, vol. 1, pp. 131–136, IEEE, 2001.

[84] J. H. Deane and D. C. Hamill, "Instability, subharmonics and chaos in power electronic systems," in *20th Annual IEEE Power Electronics Specialists Conference*, pp. 34–42, IEEE, 1989.

[85] C. K. Tse and M. Di Bernardo, "Complex behavior in switching power converters," *Proceedings of the IEEE*, vol. 90, no. 5, pp. 768–781, 2002.

[86] J. Beane and D. Hamil, "Chaotic behaviours in current-mode controlled dc-dc converter," *IEE Electronics Letters*, vol. 27, no. 13, p. 1172, 1991.

[87] S. R. Wenham, *Applied photovoltaics*. Routledge, 2012.

[88] M. M. Al-Hindawi, A. Abusorrah, Y. Al-Turki, D. Giaouris, K. Mandal, and S. Banerjee, "Nonlinear dynamics and bifurcation analysis of a boost converter for battery charging in photovoltaic applications," *International Journal of Bifurcation and Chaos*, vol. 24, no. 11, p. 1450142, 2014.

[89] M. Zhioua, A. El Aroudi, S. Belghith, J. M. Bosque-Moncusí, R. Giral, K. Al Hosani, and M. Al-Numay, "Modeling, dynamics, bifurcation behavior and stability analysis of a dc–dc boost converter in photovoltaic systems," *International Journal of Bifurcation and Chaos*, vol. 26, no. 10, p. 1650166, 2016.

[90] V. Grigore, J. Hatonen, J. Kyyra, and T. Suntio, "Dynamics of a buck converter with a constant power load," pp. 72 – 78 vol.1, 06 1998.

[91] S. Singh and D. Fulwani, "Voltage regulation and stabilization of dc/dc buck converter under constant power loading," 12 2014.

[92] H. Bae, J. Lee, S. Park, and B. H. Cho, "Large-signal stability analysis of solar array power system," *IEEE Transactions on Aerospace and Electronic Systems*, vol. 44, no. 2, 2008.

[93] S. H. Strogatz, *Nonlinear dynamics and chaos: with applications to physics, biology, chemistry, and engineering*. Hachette UK, 2014.